UNIVERSITY OF
KWAZULU-NATAL

INYUVESI
YAKWAZULU-NATALI

ARTEMISIA AFRA CRUDE AQUEOUS LEAF EXTRACT INDUCES OXIDATIVE STRESS AND INFLAMMATION IN HUMAN COLON ADENOCARCINOMA CELLS VIA THE UPREGULATION OF THE TNF-α, p38 AND STAT3 PATHWAY

By

Slindelo Mposula

BSc (Biochemistry, Chemistry and Chemical Technology), BMedSc Hons (Medical Biochemistry) (UKZN)

Submitted in fulfilment of the requirements for the degree of

Master of Medical Science

Discipline of Medical Biochemistry

School of Laboratory Medicine and Medical Sciences

College of Health Sciences

University of KwaZulu-Natal

Durban

2022

PLAGIARISM DECLARATION

I, **Slindelo Mposula**, Student Number: **215007900** declare that

i. The research reported in this dissertation, except where otherwise indicated, is my original work.

ii. This dissertation has not been submitted for any degree or examination at any other university

iii. This dissertation does not contain other person's data, pictures, graphs or other information, unless specifically acknowledged as being sourced from other persons.

iv. This dissertation does not contain other person's writing, unless specifically acknowledged as being sourced from other researchers. Where other written sources have been quoted then:

   a. Their words have been re-written, but the general information attributed to them has been referenced.

   b. Where their exact words have been used, their writing has been placed inside quotation marks, and referenced.

v. Where I have reproduced a publication of which I am an author, co-author or editor, I have indicated in detail which part of the publication was actually written by myself alone and have fully referenced such publications.

vi. This dissertation does not contain text, graphics or tables copied and pasted from the internet, unless specifically acknowledged, and the source being in the dissertation and in the Reference sections.

Signed:  **Date:** 28 August 2022

Signed: 

Dr RB Khan

ACKNOWLEDGEMENTS

Firstly, all praises and thanks be to God the Father, my savior and King Jesus and my friend the Holy Spirit, for being with me throughout this quest and guiding me to the path of wisdom and knowledge.

I would also like to acknowledge: **My family**, I am thankful for the patience, support and financial relief from my dad (**John Mlangeni)** and mom **(Zurich Mposula)** who are my biggest supporters. I am also grateful to the **Mposula clan** who contributed to the man i am today. **Dr Rene Khan** There are no words to describe your role throughout in developing a scientist in me. You have been an office mom before being a supervisor and a Guru before being my lecturer. You are awesome and cool as the youth of today says.

To Angela: Words cannot describe the role you played in this project especial during data collection period. This project would not be a success if you did not assist with your technical skills**. Dr Preggie:** You are the lighthouse and beacon of hope when one is in the dark and cannot find the light, you shine bright such that you are noticed**.**

Professor Anil Chuturgoon: I am grateful to have met a scientist who deeply cares about people such as Prof who inspired a scientist in me, helped to guide and shape my academic path.

Mr Simphiwe Mcoyi, Miss Nrateng Tsotetsi, Miss Philile Mkhulisi, Miss Fulu, Mrs Marcilyn, Mr Sifundo Nxele and the rest of master's class of 2019/2020 thank you for being my family and having my back all the times.

This project would have not been a success if **Mncedisi**, **Lindokuhle Mposula** and **Sboniso, and soon to be Dr Zinhle** and the rest of my church assembly have not provided spiritual support and assistance where needed. For that I would like to acknowledge their roles and importance in continuing doing the work of our good Lord.

I would like to acknowledge **Moses Kotane Institute (MKI)** for financial assistance along with the Department of Medical Biochemistry for supervision and technical support. I would also like to thank **College of Health Science** for financial assistance required to purchase the consumables required for this study.

Staff and **postgraduate students** of Medical Biochemist for their support and technical assistance throughout this thesis

TABLE OF CONTENTS

LIST OF ABBREVIATIONS vii
LIST OF FIGURES xii
LIST OF TABLES xiii
ABSTRACT xiv
CHAPTER 1 : INTRODUCTION 1
1.1 Background 1
1.2 Problem statement 3
1.3 Significance/implications 4
1.4 Research question 4
1.5 Null hypothesis 4
1.6 Hypothesis 4
1.7 Aim 4
1.8 Objectives 4
CHAPTER 2 : LITERATURE REVIEW 6
2.1 *Artemisia afra* (Jacq.ex. wild) 6
2.1.1 Classification and appearance 6
2.1.2 Distribution 7
2.1.3 Traditional medicinal uses 8
2.1.4 Side effects of A. afra 9
2.1.5 Phytochemistry 9
2.1.6 Pharmacological activities 11
2.2 Cancer 12
2.2.1 Colorectal cancer 12
2.3 Inflammation 16
2.3.1 Tumour necrosis factor alpha (TNF-α) 17
2.3.2 Cell signaling cascade – MAPK 18
2.3.3 Nuclear factor kappa -light-chain-enhancer of activated B cells (NF-κB) 19
2.3.4 Signal transducer and activator of transcription 3 (STAT3) 20
2.3.5 Inducible nitric oxide synthases (iNOS) 21
2.4 Oxidative stress 22
2.4.1 Electron transport chain as a source of ROS 22
2.4.2 Antioxidant response 24

2.4.3 Consequences of oxidative stress 26
2.4.5 Cellular repair pathway 27
2.5 Apoptosis 27
2.5.1 Intrinsic pathway: mitochondrial mediated 28
2.5.2 Extrinsic "Death-receptor mediated apoptosis" 29
2.5.3 Execution of cell death 30
CHAPTER 3 : MATERIALS AND METHODS 32
3.1 Materials 32
3.2 Cell culture 32
3.3 Extraction and *A. afra* preparation 32
3.4 3-4, 5-dimethylthiazol-2-yl)-2, 5- diphenyl tetrazolium bromide (MTT) assay 33
3.4.1 Principle 33
3.4.2 Protocol 33
3.5 Lactate dehydrogenase assay 34
3.5.1 Principle 34
3.5.2 Protocol 35
3.6 Luminometry 35
3.6.1 ATP quantification 36
3.6.2 Caspase quantification 37
3.6.3 GSH quantification 38
3.6.4. Phosphatidylserine (PS) quantification 39
3.6.5 JC-10 assay 40
3.7 TBARS assay 41
3.7.1 Principle 41
3.7.2 Protocol 42
3.8 Nitrate assay 43
3.8.1 Principle 43
3.8.2 Protocol 44
3.9 Single cell Gel Electrophoresis (SCGE) or "Comet" assay 44
3.9.1 Principle 44
3.9.2 Protocol 45
3.10 Quantitative Polymerase Chain Reaction (qPCR) Assay 46
3.10.1 Principle 46

3.10.2 Protocol....47
3.11 Western blotting....49
3.11.1 Principle....49
3.11.2 Protocol....50
3.12 Statistical analysis....52
CHAPTER 4 : RESULTS....53
4.1 Cell viability....53
4.2 Mitochondrial integrity....54
4.2.1 ATP assay....54
4.2.2 Mitochondrial membrane potential....55
4.3 Lactate dehydrogenase membrane integrity assay....56
4.4 Free radical production....56
4.4.1 TBARS assay....56
4.4.2 Nitrate and Nitrite....57
4.5 Antioxidant response....58
4.5.1 GSH assay....58
4.5.2 Antioxidant enzyme defense....58
4.5.3 Oxidative damage repair....59
4.6 Death parameters analysis....60
4.6.1 Caspase analysis....60
4.6.2 Annexin-V fluorescence assay....62
4.6.3 Expression of apoptotic and anti-apoptotic proteins....62
4.7 MAPK pathway....63
4.8 HSP response....65
4.9 Comet assay....66
4.10 Inflammatory response invoked by the treatment with *A. afra*....66
4.11 Proliferation marker c-Myc and pRb....67
CHAPTER 5 : DISCUSSION....69
CHAPTER 6 : CONCLUSION....79
REFERENCES....80
APPENDICES....93
APPENDIX A....93
APPENDIX B....94

APPENDIX C 95
APPENDIX D 96
Appendix E 97
Appendix F 97

LIST OF ABBREVIATIONS

Ab	Antibody
A. afra	*Artemisia afra*
ADP	Adenosine diphosphate
AIDS	Acquired immunodeficiency syndrome
AIF	Apoptosis inducing factor
Apaf-1	Apoptotic-protease-activating-factor-1
APS	Ammonium persulphate
ATP	Adenosine triphosphate
ARE	Antioxidant response element
Bax	Bcl-2-associated X
BCA	Bicinchoninic acid
Bcl-2	B-cell lymphoma/leukemia-2
BH	Bcl-2 homology
BHT	Butylated hydroxytoluene
Bid	BH3 interacting-domain death agonist
BIR	Baculovirus inhibitor of apoptosis repeat
BSA	Bovine serum albumin
Ca (Ca^{2+})	Calcium (Calcium cation)
CAD	Caspase-activated DNase
CAT	Catalase
CCM	Complete culture medium
Cd (Cd^{2+})	Cadmium (Cadmium cation)
c-IAP	Cellular inhibitor of apoptosis protein
CO_2	Carbon dioxide
CoQ	Coenzyme Q
Cu (Cu^{2+})	Copper (Cupric ion)
CYP	Cytochrome P450
c-Myc	Cellular Myc
dH_2O	Distilled water

CRC	Colorectal carcinoma
Cyt c	Cytochrome c
DISC	Death inducing signaling complex
DMSO	Dimethyl sulphoxide
DNA	Deoxyribonucleic acid
Ds	Double stranded
ECL	Enhanced chemiluminescence
EDTA	Ethylenediaminetetraacetic acid
EMEM	Eagle's minimum essential medium
ER	Endoplasmic reticulum
ERK	Extracellular-regulated-signal kinase
ETC	Electron transport chain
FADD	Fas associated protein with death domain
$FADH_2$	Flavin adenine dinucleotide hydroquinone
FasL	Fas ligand
FCS	Foetal calf serum
GERD	Gastroesophageal reflux disease
GPx	Glutathione peroxidase
GSH	Reduced glutathione
GSSG	Oxidised glutathione
GST	GSH-S-transferase
H^+	Hydrogen ion/ proton
H Hour	Hour
H_2O_2	Hydrogen peroxide
HIV	Human immunodeficiency virus
H_3PO_4	Phosphoric acid
HCl	Hydrochloric acid
$HO_2^{\bullet}$	Hydroperoxyl radical
HOCl	Hypochlorous acid
HRP	Horseradish peroxidase
HSP	Heatshock protein

IAP	Inhibitor of apoptosis protein
IBM	IAP-binding motif
IC_{50}	Median Inhibition Concentration
IC_{20}	20% inhibitory concentration
iCAD	Inhibitor of caspase-activated DNase
IMM	Inner mitochondrial membrane
IMS	Intermembrane space
iNOS	Inducible nitric oxide synthase
INT	Iodonitrotetrazolium
JNK	Jun N-terminal kinase
JC-10	Tetraethylbenzimidazolylcarbocyanine iodide
kDa	Kilodalton
LDH	Lactate dehydrogenase
LMPA	Low melting point agarose
MAPK	Mitogen-activated protein kinase
M	Meter
mm	Millimeter
Min	Minutes
MIC	Minimum inhibitory concentration
Mt	Mitochondrial
MTB	*Mycobacterium tuberculosis*
MPTP	Mitochondrial permeability transition pore
MTT	3-(4,5-Dimethyl-2-thiazolyl)-2,5-diphenyl-2H-tetrazolium
NaCl	Sodium chloride
NAD (NAD^+)	Nicotinamide adenine dinucleotide
NADH	Nicotinamide adenine dinucleotide hydride (reduced)
NADPH	Nicotinamide adenine dinucleotide phosphate (reduced)
NaOH	Sodium hydroxide
NIAP	Normal-molecular-weight IAP
NF-κB	Nuclear factor kappa-light-chain-enhancer of activated B cells
NRF2	Nuclear factor-erythroid factor 2-related factor
$^{\bullet}OH$	Hydroxyl radical

$O_2^{\bullet-}$	Primary superoxide anion radical
OD	Optical density
OGG1	8-oxoguanine glycosylase
OMM	Outer mitochondrial membrane
ONOO	Peroxynitrite
$ONOOCO_2$	Nitrosoperoxycarbonate
PA	Picolinic acid
PARP-1	Poly (ADP-ribose) polymerase-1
Pb (Pb^{2+})	Lead
PBS	Phosphate buffer saline
PFA	Paraformaldehyde
PSF	Penicillin-streptomycin-fungizone
PUMA	p53-upregulated modulator of apoptosis
qPCR	quantitative polymerase chain reaction
RB	Retinoblastoma
RBD	Relative band density
RLU	Relative light unit
RNS	Reactive nitrogen species
$RO_2^{\bullet}$	Peroxyl radical
ROS	Reactive oxygen species
RT	Room temperature
SA	South Africa
SCC	Squamous cell carcinoma
SCGE	Single cell gel electrophoresis
SD	Standard deviation
SDS-PAGE	Sodium dodecyl sulphate - polyacrylamide gel electrophoresis
Smac/DIABLO	Second mitochondria-derived activator of caspases/ direct inhibitor of apoptosis-binding protein with low pI
SOD	Superoxide dismutase
TB	*Tuberculosis*
TBA	Thiobarbituric acid
TBARS	Thiobarbituric acid reactive substances

TCA	Tricarboxylic acid
TEMED	Tetramethylene diamine
TNF-α	Tumour necrosis factor-α
TNF-R1	Tumour necrosis factor receptor-1
TRAIL-R	Tumour necrosis factor related apoptosis inducing ligand receptors
TTBS	Tris-buffered saline containing 0.5% Tween20
VDAC	Voltage-dependent anion channel
XIAP	X-linked mammalian inhibitor of apoptosis protein
Zn (Zn^{2+})	Zinc
%	Percentage

LIST OF FIGURES

CHAPTER 2

Figure 2.1: Characteristic features of *A. afra* (Jacq: ex. wild) 7
Figure 2.2: Geographical distribution of *A. afra* across South Africa 8
Figure 2.3: Phytochemicals isolated from *A. afra*. 10
Figure 2.4: Structural overview of the human colon 13
Figure 2.5: Incidence and mortality associated with colorectal cancer. 15
Figure 2.6: A proposed model for regulation of proinflammatory responses when there is an imbalance in oxidative stress causing ROS production 17
Figure 2.7: Overview of MAPK signaling. 19
Figure 2.8: The signalling pathway that mediates NF-κB inflammatory effects 20
Figure 2.9: STAT3 in inflammation 21
Figure 2.10: Schematic diagram show factors that induce oxidative stress and the associated cytotoxic effects 22
Figure 2.11: Formation of ATP through the electron transport chain and oxidative phosphorylation 23
Figure 2.12: A mechanism of how antioxidants detoxify ROS produced 25
Figure 2.13: Overview of the apoptotic pathways. 29
Figure 3.1: Principle of the MTT assay. 33
Figure 3.2: Quantification principle for extracellular LDH. 35
Figure 3.3: ATP quantification using the Cell Titre-Glo® assay. 36
Figure 3.4: The luminescent principle for quantification of caspase activity 37
Figure 3.5: Luminescence-based principle for GSH concentration 38
Figure 3.6: Differentiation of apoptotic and necrotic cells using the RealTime-GloTM Annexin V Apoptosis and Necrosis Assay 39
Figure 3.7: Determination of mitochondrial membrane potential using the JC-10 cationic dye. 40
Figure 3.9: Nitrate reduction pathway resulting in the formation of chromophoric azo-derivative that is measured spectrophotometrically 43
Figure 3.10: Principle of the SCGE assay: 45
Figure 3.11: The qPCR procedure from mRNA extraction to amplified gene product 47
Figure 3.12: Western blotting procedure showing protein separation, transfer and immunoblotting. 50
Figure 4.1: Cell viability of Caco-2 and Hek293 cells treated with *A. afra* extract for 48 hours. 54
Figure 4.2: The intracellular ATP levels in treated Caco-2 cells 55
Figure 4.3: The Δψm in treated and untreated Caco-2 cells. 55
Figure 4.4: A spectrophotometric study of extracellular LDH levels in A. afra-treated and untreated Caco-2 cells. 56
Figure 4.5: The MDA concentration in A. afra-treated Caco-2 cells. 57
Figure 4.6: The concentration of nitrate and nitrite in Caco-2 treated cells. 57
Figure 4.7: Antioxidant response to *A. afra* in Caco-2 cells 58
Figure 4.8: Antioxidant enzyme response in A. afra-treated and untreated Caco-2 cells 59
Figure 4.9: Gene expression of OGG1 in Caco-2 cells treated with A. afra extract. The OGG1 gene expression 60
Figure 4.10: Crude aqueous leaf extract of A. afra dramatically decreased caspase activity. 61
Figure 4.11: Annexin-V affinity for phosphatidylserine in *A. afra*-treated and untreated Caco-2 cells 62
Figure 4.12: The *A. afra* extract modulated protein expression of apoptosis-associated proteins 63
Figure 4.13: The protein expression of MAPK after *A. afra* treatment. 64
Figure 4.14: The heatshock response to *A. afra* treatment. 65
Figure 4.15: DNA fragmentation in Caco-2 cells treated with *A. afra* extract. 66
Figure 4.16: Inflammatory markers in Caco-2 cells after treatment with the IC_{50} of *A. afra*. 67
Figure 4.17: Expression of proliferation markers c-Myc and p-pRb/pRb in Caco-2 cells treated with *A. afra* extract. 68
Figure 5.1: Mechanistic overview of the biochemical effects of *A. afra* on membrane and mitochondrial integrity, oxidative stress, stress response and inflammation in human cancerous Human epithelial Caco-2 cells 78

LIST OF TABLES

CHAPTER 3

Table 3.1: Annealing temperatures of target genes…….……...49

ABSTRACT

Introduction: *Artemisia afra* (*A. afra*) is a widely used medicinal plant located in the southern African region. It is traditionally used to alleviate medical conditions such as coughs. Literature indicates a protective role by improving antioxidant capacity and reducing cell proliferation, which suggests anti-cancer potential. Colorectal carcinoma (CRC) is a global public health crisis and the second common cause of cancer-related fatalities. Current cancer treatment is deemed effective but not easily accessible and expensive in the southern African region. Therefore, the need for naturally derived anti-cancer agents remains to be investigated for accessible and affordable treatment. This study investigates the antiproliferative and antioxidant effects of *A. afra* crude aqueous leaf extract in the Caco-2 cell line.

Materials and Methods: Caco-2 cells were treated with a range of *A. afra* concentrations (0-5000 µg/ml) for 48 hours. An IC_{50} was derived from the MTT assay and all subsequent assays compared the IC_{50}-treatement to an untreated control. Mitochondrial integrity was luminometrically assessed by measuring JC-10 fluorescence and ATP. Free radical production (TBARS, NOS) and membrane damage (LDH cytotoxicity), together with GSH quantitation were used to infer the presence of oxidative stress; antioxidant enzymes (SOD2, GPx-1, catalase, Nrf2) were also detected by western blotting. Apoptotic induction was verified by measuring phosphatidylserine externalisation, quantifying caspase activities and detecting pro- and anti-apoptotic proteins (Bax, Bcl2, cIAP, xIAP) by western blotting. Single strand DNA fragmentation was evaluated via the comet assay. Additionally, relative expression of DNA repair, inflammation and stress markers were determined using western blotting and qPCR.

Results: Crude aqueous leaf extract of *A. afra* induced a dose-dependent reduction in cell viability, yielding an IC_{50} of 250 µg/ml. Decreased mitochondrial integrity ($p = 0.697$) was associated with significant depletion of intracellular ATP ($p = 0.0043$) and increased ROS production as validated by increased lipid peroxidation ($p = 0.1638$) and DNA oxidation (amplified OGG1). In addition, increased iNOS contributed to the production of RNS. *Artemisia afra* induced an antioxidant response that elevated Nrf2 at the mRNA and protein level, causing increased GSH ($p = 0.0001$), GPx-1 ($p = 0.5067$) and catalase, but SOD2 was decreased. Heightened levels of heatshock proteins (HSP27 and HSP70) correlate with increased ROS and upregulated phosphorylated p38 protein, but ERK and JNK protein expression was downregulated. Significant downregulation caspase-8 ($p = 0.0252$), caspase-9 ($p = 0.0099$) and caspases-3/7 ($p = 0.0232$) was associated with reduced Annexin-V) and extracellular LDH. In addition, the Bax/Bcl-2 ratio ($p = 0.0033$) and protein expression of inhibitors of apoptosis protein such as cIAP-1 and xIAP indicated reduced apoptotic activity in this study. Comet tail analysis indicated intact DNA, in congruence with decreased OGG1. Both TNF-α ($p =$

0.2323) and STAT-3 were upregulated, but NF-κB was decreased. In addition, cellular Myc and phosphorylated retinoblastoma were upregulated.

Conclusion: The crude aqueous leaf extract of *A. afra* induced mitochondrial toxicity and ROS production. Despite a heightened antioxidant defense, ROS-mediated upregulation of TNF-α, p38 and STAT3 promoted cell proliferation and inhibited apoptosis in Caco-2 cells. Taken together, *A. afra* is a cytotoxic and genotoxic agent that may induce cancer in human colorectal cells.

Keywords: *Artemisia afra*, Caco-2 cells, oxidative stress, apoptosis, inflammation, cell proliferation

CHAPTER 1 : INTRODUCTION

1.1 Background

The global use of medicinal plants from which most therapeutic agents are derived is entirely popular as most of Africa's population depends on it for primary health care (Organization, 2019). In southern Africa, approximately 80% of the population relies on plant-based medicine to relieve various animal and human infections (Mahomoodally, 2013, Organization, 2019). Increased growth in population, inadequate supply of medicine, high cost of treatment, adverse side effects associated with several synthetic therapeutic agents and the occurrence of drug resistance have prompted an increase in the use of medicinal plants to treat various ailments such as *tuberculosis* (TB), human immunodeficiency viruses (HIV/AIDS), diabetes and cancer (Hussein and El-Anssary, 2018). One of the advantages of using medicinal plants is the plethora of potential therapeutic phytochemicals contained within the plants (Abdel-Aziz *et al.*, 2016). Studies report that approximately 15% of the world's plants have been examined for therapeutic efficacy (McGaw and Eloff, 2008). The active use of traditional medicine in healthcare presents side effects, which are not as severe or debilitating as those inflicted by synthetic medicine, but they may present adverse effects if misused. Therefore, the need for cytotoxicity screening of traditional medicinal remedies is of significant priority (Rabe and Van Staden, 1997, Mahmood *et al.*, 2019).

Artemisia afra (*A. afra)* is a medicinal plant that belongs to the Asteraceae family. It is widely distributed throughout southern Africa, especially within the Cape region and some parts of East Africa (Van Wyk *et al.*, 1997, Liu *et al.*, 2009, Du Toit and Van der Kooy, 2019a). Decoctions of *A. afra* are expansively used within these tribal communities as a treatment to relieve common ailments such as coughs, colds, fever, loss of appetite, headache, earache, diabetes and parasitic intestinal worms (Hilliard, 1977, Van Wyk *et al.*, 1997, Mukinda, 2005, Liu *et al.*, 2009, Du Toit and Van der Kooy, 2019a). Past studies have identified *A. afra* to exhibit significant biological activities such as antimicrobial, antiviral, anti-bacterial, anti-plasmodial, anti-inflammatory and anticancer activities, prompting research into its role as a possible treatment for *Mycobacterium tuberculosis* (MTB), diabetes, cardiovascular diseases, HIV-AIDS and cancer (Liu *et al.*, 2009, Du Toit and Van der Kooy, 2019b). There is also evidence of cytotoxicity that results in mitochondrial-mediated caspase-dependent apoptosis, which suggests anticancer potential in Hela and U937 cells (Spies *et al.*, 2013).

Inflammation is a physiological process that protects tissues from infection and helps them heal after they've been injured (Yan *et al.*, 2015). Chronic inflammation, on the other hand, can lead to a number

of inflammatory illnesses such as cancer (Yan *et al.*, 2015). Indeed, tumour necrosis alpha (TNF-α) is a pro-inflammatory cytokine that plays a role in apoptosis and cell survival, two processes that are intimately linked to the progression of cancer. When TNF-α binds to its cognate receptor, TNF receptor 1 (TNFR1), its activation triggers signalling through several pathways that promote cell survival, including the p38 mitogen-activated protein kinase (MAPK) pathway through signal transducer and activator of transcription 3 (STAT3). Activated STAT3 dimers translocate to the nucleus and bind to specific DNA sequences to directly regulate expression of anti-apoptotic and pro-survival genes (Cheng *et al.*, 2017, Cruceriu *et al.*, 2020). Anti-apoptotic proteins include Bcl-2 and Bcl-xl which act to prevent intrinsic/mitochondrial apoptosis by blocking mitochondrial outer membrane permeabilisation (MOMP). Thus, apoptosome formation does not occur, caspase-9 and caspases-3/7 are not activated and apoptosis is not executed (Cope and Tomei, 1991, Renault *et al.*, 2013). Cell proliferation and survival may be stimulated through transcription of c-Myc and cyclin D1, amongst others. A weak activation of the c-Jun N-terminal kinase (JNK) MAPK pathway has been noted in different breast cancer cell lines (Cheng *et al.*, 2017, Cruceriu *et al.*, 2020).

Reactive oxygen species (ROS) can cause oxidative stress, a condition that occurs when oxidants overwhelm the body's antioxidant systems. Inflammation may be induced by ROS and oxidative stress, a condition that arises when oxidants overwhelm antioxidant systems in the body (Huang and Groves, 2018). Antioxidants are essential free radical scavengers, the molecules implicated as the body's primary cause of oxidative stress. It is anticipated that oxidative stress contributes significantly to the causation of several diseases, including cancer (Thanan *et al.*, 2015). The role of oxidative stress in cancer pathophysiology occurs primarily through DNA damage induced by oxidation of DNA bases. In addition, protein carbonylation and lipid peroxidation are also associated hallmarks of oxidative stress (Gaschler and Stockwell, 2017).

The production of ROS may take place through non-enzymatic or enzymatic reactions (Pizzino *et al.*, 2017a). Some endogenous sources of free radicals include oxidative phosphorylation in mitochondria for the production of adenosine triphosphate (ATP), NADH-oxidase and peroxidases. The superoxide radical ($O_2^{\bullet-}$) produced in these reactions is necessary for the production of hydrogen peroxide (H_2O_2), which is a substrate for the non-enzymatic Fenton reaction that uses cations such as Fe^{3+} to produce the potent hydroxyl radical ($^{\bullet}OH$) (Thanan *et al.*, 2015). The arginine nitric oxide (NO) radical is synthesised by the nitric oxide synthase (NOS) system (Thanan *et al.*, 2015, Lin *et al.*, 2016). Exogenous sources of free radicals include environmental variables such as emissions and xenobiotic metabolism (Pizzino *et al.*, 2017b). Physiological levels of free radicals are beneficial for processes such as cell signaling and are maintained at physiological concentrations by antioxidants

such as reduced glutathione (GSH), superoxide dismutase (SOD), catalase and glutathione peroxidase (Gpx-1) (Naregal *et al.*, 2017). The nuclear factor-erythroid 2 related factor 2 (Nrf2) is a master regulator of antioxidant response elements (AREs); it is activated to transcribe antioxidants and cytoprotective genes (Ikwegbue *et al.*, 2018). Stress response proteins such as heat shock protein (HSP70 and HSP27) protect proteins from damage and inhibit apoptosis.

It has been noted that ROS are a double-edged sword causing both oxidative stress and inflammation that may predispose to the development of cancer. One such cancer is colorectal cancer (CRC), the 3rd most common cancer worldwide and ranked as the 2nd most common cause of cancer-related mortalities (Rawla *et al.*, 2019, Mathur *et al.*, 2020). The fourth most diagnosed cancer is CRC within South Africa's borders and the sixth most lethal cause of mortalities (Brand *et al.*, 2018). Men remain more susceptible to CRC; CRC is the second most common cancer in men, whereas it is the fourth most common in women. Ethnic differences also play a role in how CRC affects individuals in the southern African region (McCabe *et al.*, 2019). Current treatment for CRC may include surgery, ablation, chemotherapy and radiation therapy, which are expensive and inaccessible to patients living in rural areas (Miller *et al.*, 1981, Mokdad *et al.*, 2015, Daher *et al.*, 2018). The five-year survival rate of CRC varies given the CRC stage at diagnosis; 93.2% for stage I, 72.2-84.7% for stage II, 52.3-83.4% for stage III and 8.1% stage IV (Brand *et al.*, 2018).

Given the involvement of inflammation and oxidative stress in the development of CRC, it is reasonable to suggest that amelioration of these detrimental processes may be a viable treatment option. Indeed, several studies have yielded promising *in vitro* activity of phytochemicals against cancer cells. Administration of *A. afra* is associated with anti-inflammatory, antioxidant and anti-cancer effects. Therefore, this study evaluated the antioxidant and anti-proliferative potential of *A. afra* in colorectal cancer (Caco-2) cells.

1.2 Problem statement

Cancer incidence and mortality are increasing in South Africa (Motsuku *et al.*, 2021). Colorectal cancer presents a challenge in therapeutics due to low efficacy and limited available treatment options (Organization, 2015, Mak *et al.*, 2018). In addition, traditional cancer remedies present with debilitating side effects that often result in patients not being able to complete treatment and increases the risk of becoming drug-resistant (Sak, 2012, Xiang *et al.*, 2019). The medicinal plant *A. afra* is used by South African traditional healers and has demonstrated potential as an anticancer agent (Liu *et al.*, 2009, Mothibe and Sibanda, 2019, Du Toit and Van der Kooy, 2019a). To date, there is no information available on the biochemical effect of *A. afra* crude aqueous leaf extract on human Caco-

2 cells. Therefore, the purpose of this study is to investigate the biochemical mechanisms of *A. afra* in human colon adenocarcinoma Caco-2 cells.

1.3 Significance/implications

An alternative treatment with fewer side effects and improved treatment efficacy will alleviate the high morbidity and mortality associated with colorectal cancer. Traditional medicines are easily obtainable and locally sourced making them cost-effective for poor communities. They also have been used by traditional healers with no known side effects. It is with great hope that the results produced from this study may provide a basis for developing cost-effective, easily obtainable, potently effective anti-CRC treatment, which may also be used to combat other forms of cancer. This will also provide a clear biochemical pathway for the first time, which will provide groundwork for drug discovery. Hence, specific proteins may be targeted to produce desired result.

1.4 Research question

Does the *A. afra* crude aqueous leaf extract exert cytotoxic effects or protective antioxidant, antiproliferative, and anti-inflammatory effects?

1.5 Null hypothesis

The crude aqueous leaf extract of *A. afra* does not have antioxidant, antiproliferative and anti-inflammatory effects in Caco-2 cells following acute exposure.

1.6 Hypothesis

The crude aqueous leaf extract of *A. afra* extracts induces antioxidant, antiproliferative and anti-inflammatory effects on in Caco-2 cells following acute exposure.

1.7 Aim

The aim of this study is to determine the antioxidant, antiproliferative and anti-inflammatory effects of a crude aqueous extract from *A. afra* leaves on human Caco-2 cells.

1.8 Objectives

The crude aqueous leaf extract of *A. afra* will be used to measure the cell viability and metabolic activity of Caco-2 cells using the methylthiazol tetrazolium (MTT) assay. The half-maximum inhibitory concentration (IC_{50}) obtained will be used to

- determine the metabolic effect of *A. afra* by measuring mitochondrial membrane potential and quantifying intracellular ATP using luminometry.
- assess the effect of *A. afra* on apoptosis by
    - luminometrically quantifying caspases-3/7, caspase-8, and caspase-9 activity and phosphatidylserine externalisation (Annexin-V).
    - detecting protein expression markers of apoptosis (Bcl-2, Bax, cIAP and xIAP) via western blotting.
- evaluate the antioxidant potential of *A. afra* by
    - quantifying ROS-induced lipid peroxidation and reactive nitrogen species (RNS) using the TBARS and NOS assays respectively.
    - examining membrane integrity through the lactate dehydrogenase assay, and DNA integrity via the comet assay and 8-oxoguanine glycosylase (OGG1) mRNA levels.
    - analysing the antioxidant response including GSH quantification by luminometry and antioxidant enzyme detection by western blotting (Nrf2, SOD2, Gpx1, and catalase).
- investigating the anti-inflammatory potential of *A. afra* by
    - quantification of targeted proteins and genes such as iNOS, TNF-α, p38, NF-κB and STAT3 using the quantitative polymerase chain reaction (qPCR) assay.
    - considering expression of proliferative markers such as c-Myc and pRb.

CHAPTER 2 : LITERATURE REVIEW

2.1 *Artemisia afra* (Jacq.ex. wild)

2.1.1 Classification and appearance

Artemisia afra is a medicinal plant classified in the magnoliophyte division, magnoliophyte class (Asteridae subclass) and the Asterales order (Mukinda, 2005). It is an erect, multi-perennial woody aromatic shrub that is hairy, contains leafy ridged stems (Figure 2.1A-C) and grows up to 2 meters (m) in height depending on its geographical location (Liu *et al.*, 2009). The plant's leaves are characterised by an oval shape and are dark green on the adaxial surface. The underside of the leaves along with stem are covered with small white hairs resulting in the characteristic of overall grey colour with a soft texture (Figure 2.1A-C). The tubular floret of *A. afra* comprising yellow butter-coloured flowers occurs as an elongated panicle (Figure 2.1D) that blossoms in summer between January and June (Hilliard, 1977, Van Wyk *et al.*, 1997, Mukinda, 2005, Liu *et al.*, 2009, Du Toit and Van der Kooy, 2019a). The plant's fruit is 1 millimeter (mm) in length with silvery-white coating and characterised by a 3-angled curved shape. The indigenous *A. afra* emits an aromatic odour with a pungent smell and when crushed, it releases a sweet-smelling aroma. Interestingly, during winter the plant is noted to generate branches rapidly from the base. The plant can be cultivated easily from seeds, cuttings and rooted pieces, and it grows well in the wilderness and household environment (Hilliard, 1977, Van Wyk *et al.*, 1997, Mukinda, 2005, Liu *et al.*, 2009, Du Toit and Van der Kooy, 2019a).

Figure 2.1: Characteristic features of *A. afra* (Jacq: ex. wild); **(A)** young leaves, (**B**) leaves on a woody stem, (**C**) fully grown mature tree and (**D**) flowers (Van Wyk *et al.*, 1997).

2.1.2 Distribution

In South Africa, *A. afra* is located in Gauteng, Limpopo's northern regions and part of the Eastern and Western Cape (Figure 2.2) (Hilliard, 1977, Van Wyk *et al.*, 1997, Mukinda, 2005, Liu *et al.*, 2009, Du Toit and Van der Kooy, 2019a). The plant is also found in Swaziland and Lesotho. *Artemisia afra* plant has also been discovered in the range of mountains in Kenya, Tanzania, Uganda, and Ethiopia (northern region) (Hilliard, 1977, Van Wyk *et al.*, 1997, Mukinda, 2005, Liu *et al.*, 2009, Du Toit and Van der Kooy, 2019a). In KwaZulu-Natal, *A. afra* is found in abundance along the coast to the Drakensberg (Figure 2.2), where it is known as *umhlonyane* in isiZulu. It is usually located in mountainous areas, forest margins and near streams in these tribal communities (Hilliard, 1977, Van Wyk *et al.*, 1997, Mukinda, 2005, Liu *et al.*, 2009, Du Toit and Van der Kooy, 2019a).

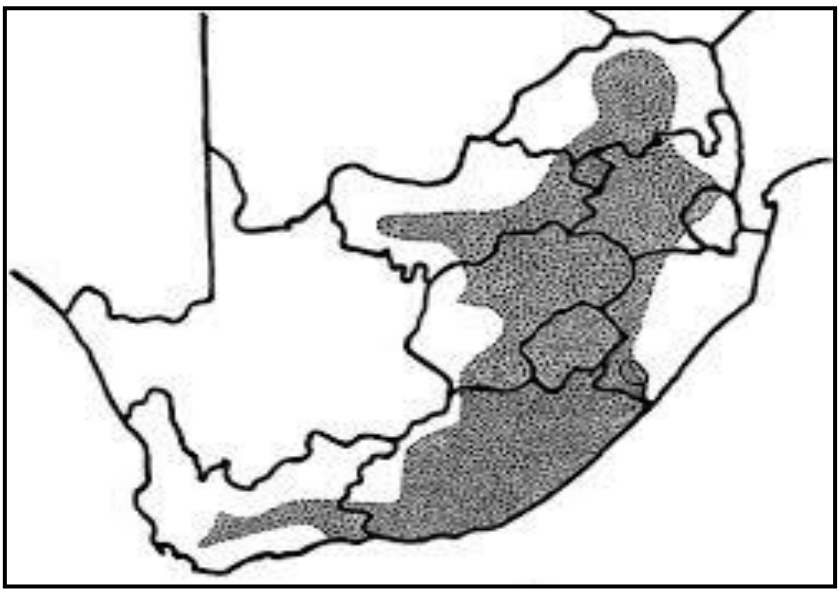

Figure 2.2: Geographical distribution of *A. afra* across South Africa (Van Wyk, 2011).

2.1.3 Traditional medicinal uses

Many *Artemisia* species, which are members of the Asteraceae family, have been studied for their medicinal potential. The decoctions containing extracts from stems, leaves and roots are utilised as an analgesic (colic, headache and earache), anthelmintic (intestinal worms and malaria) and to treat various diseases (Watt and Breyer-Brandwijk, 1962). In South Africa, *A. afra* is used to treat respiratory dysfunction including coughs, colds, fever, asthma and influenza, as well as gastrointestinal disorders, loss of appetite and diabetes (Watt and Breyer-Brandwijk, 1962, Mukinda, 2005, Thring and Weitz, 2006, Du Toit and Van der Kooy, 2019a).

Although the leaves and flowers of *A. afra* are the main focus in traditional medicine, the leaves are the most utilised component of the entire plant. This is possibly due to leaves being easily accessible. In addition, tribal communities believe that the healing properties are in the leaves (Watt and Breyer-Brandwijk, 1962, Mukinda, 2005, Thring and Weitz, 2006, Mahop and Mayet, 2007, Du Toit and Van der Kooy, 2019a). The leaves and stems, fresh or dried, are used in teas, decoctions and tinctures to make medicinal preparations. To prevent headaches, coughing, asthma, hay fever and sinusitis, the leaves and stems are boiled for the fumes to be inhaled (Watt and Breyer-Brandwijk, 1962, Mukinda, 2005, Thring and Weitz, 2006, Du Toit and Van der Kooy, 2019a). In the Eastern Cape province of South Africa, the plant leaf or root infusion is used to treat diabetes mellitus (Du Toit and Van der Kooy, 2019a).

When chewed, the bark of this aromatic perennial is reported to treat or prevent oral ailments *(Rasul et al., 2013)*. The filtrate from *A. afra* preparation is used as a topical ointment for sores, rashes, bites,

stings, hemorrhoids and measles. In addition, the filtrate may be used to treat fevers or as an eye rinse to alleviate red, irritated eyes. Enemas made from ground leaves and hot water are administered to children suffering from the adverse effects of intestinal worms or constipation (Watt and Breyer-Brandwijk, 1962, Mukinda, 2005, Liu *et al.*, 2009, Du Toit and Van der Kooy, 2019a).

Eardrops for earache prepared from *A. afra* also act as a mouthwash to ease pain from gumboils and oral ulcers. Coughs, colds, chest ailments, indigestion and stomach cramps are treated with an old remedy known as 'Wilde als brandy' (Liu *et al.*, 2009, Braünlich *et al.*, 2018a). Bronchitis, blocked nose, tight chest, asthma and chest colds are treated by inhaling the steam of boiled *A. afra* leaf infusion (Watt and Breyer-Brandwijk, 1962, Mukinda, 2005, Liu *et al.*, 2009, Du Toit and Van der Kooy, 2019a). A poultice of *A. afra* leaves is used to treat neuralgic pain, mumps, tired muscles and to relieve colic; drawing out of pimples is also treated in this way (Watt and Breyer-Brandwijk, 1962, Mukinda, 2005, Liu *et al.*, 2009, Du Toit and Van der Kooy, 2019a).

2.1.4 Side effects of A. afra

Ingestion of all *Artemisia* species should be avoided during pregnancy due to the thujone compound found in *A. afra*, which acts as an abortifacient and promotes menstruation. The effect of thujone is associated with gamma-aminobutyric acid (GABA) receptors and is thought to play a role in the inhibition of serotonin 5-HT3 receptors (Liu *et al.*, 2009, Du Toit and Van der Kooy, 2019a). In addition, patients presenting with a dry cough and severe kidney disease should also keep away from the use of any *Artemisia* species (Watt and Breyer-Brandwijk, 1962, Mukinda, 2005, Liu *et al.*, 2009, Du Toit and Van der Kooy, 2019a). Due to potential adverse side effects, the extract of *A. afra* should not be administered to children and patients suffering from duodenal ulceration or epilepsy. Prolonged ingestion or excessive use results in absinthism, which manifests as convulsive symptoms, sleeplessness, tremors, vertigo and fatty degeneration of the liver (Watt and Breyer-Brandwijk, 1962, Mukinda, 2005, Liu *et al.*, 2009, Du Toit and Van der Kooy, 2019a).

2.1.5 Phytochemistry

A vast number of active compounds have been identified and isolated from the oil, leaves, stem and roots of *A. afra.* There is also a high content of essential and volatile oils, depending on the plant's geographical location (Patil *et al.*, 2011). Anti-microbial and antioxidant effects have been attributed to the volatile oil. Other standard active compounds found in the plant include 1.8-cineole (eucalyptol), alpha-thujone, beta-thujone, camphor, borneol sesquiterpenoids such as chrysanthenyl acetate and devannone (Figure 2.3) (Silbernagel *et al.*, 1990, Afolayan and Sunmonu, 2013). There

are also several non-volatile constituents found in the plant, which include triterpenes (amyrin and friedelin), alkanes (ceryl cerotinate and N-nonacosane), flavonoids (methyl ethers of luteolin), coumarins (scopoletin) and polyacetylenes (Figure 2.3) (Viljoen *et al.*, 2006, Liu *et al.*, 2009, Du Toit and Van der Kooy, 2019a). A new isoalantoctone was isolated by Venable *et al.* (2016) following the study on the main types of polysaccharides that also reported the presence of pectin (Venables *et al.*, 2016, Braünlich *et al.*, 2018b, Du Toit and Van der Kooy, 2019a).

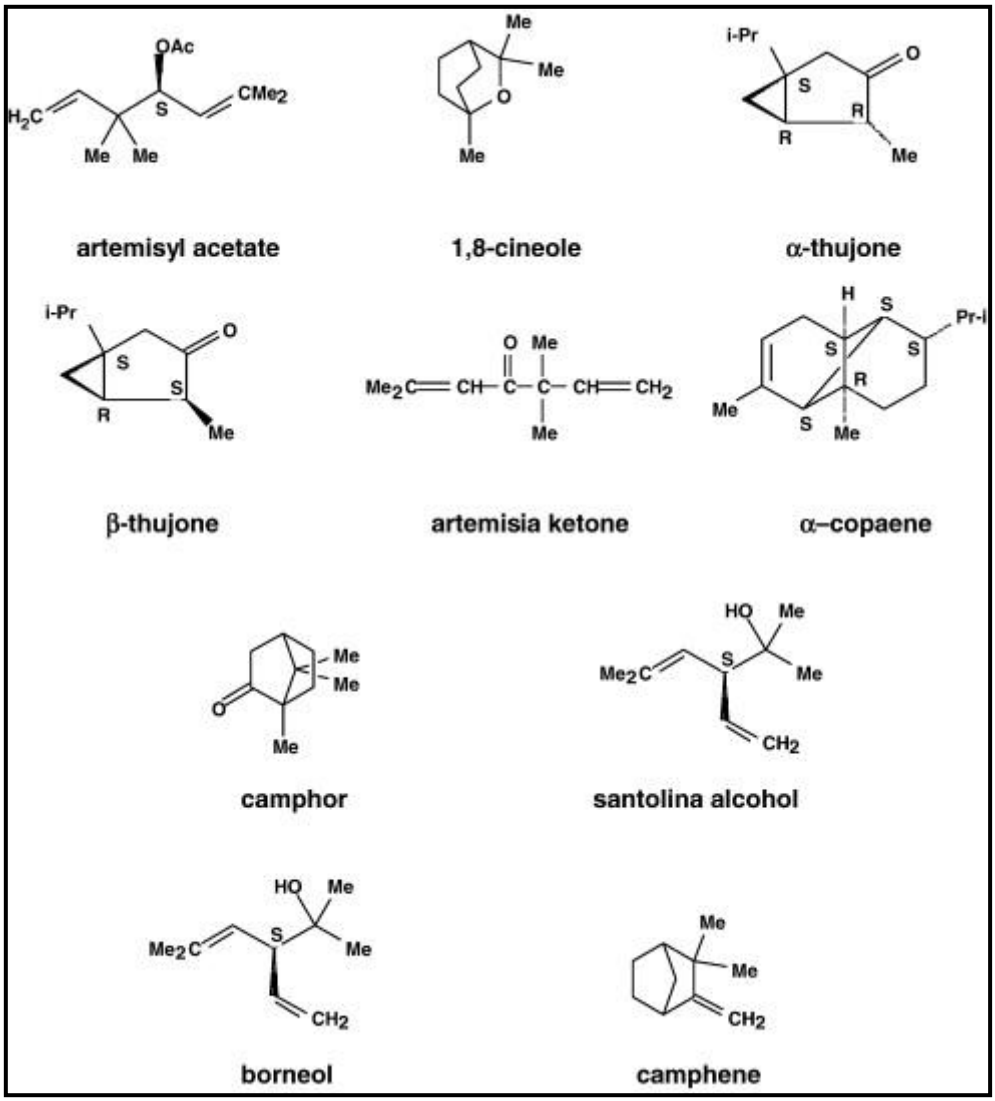

Figure 2.3: Phytochemicals isolated from *A. afra*. Two-dimensional chemical structures of isolated cytotoxic/antitumour compounds from *A. afra* species (Liu *et al.*, 2009).

The plant also contains monoterpenes, sesquiterpenes, triterpenoids and flavonoids (Liu *et al.*, 2009). The aerial part of the plant is also known to produce sesquiterpene lactones such as guaianolides and glucosides (Jakupovic *et al.*, 1988, Du Toit and Van der Kooy, 2019a, Moyo *et al.*, 2019b). In Zimbabwe, most of the plant's oil content consists of β-thujone, whereas in Kenya the oil is rich in 1,8-cineole, β-thujone and camphor. In South Africa, several compounds were identified such as α-pinene, β-pinene, terpineol, chrysanthenyl acetate, camphene, myrcene, and trans-β-

ocimene, thus demonstrating the effect of geographical distribution on phytochemical content (Liu *et al.*, 2009, Du Toit and Van der Kooy, 2019a).

2.1.6 Pharmacological activities

Antioxidant, anti-inflammatory, cardiovascular and spasmolytic activities are exhibited by pharmacological components of *A. afra* extracts. Sedative and antidepressant effects are associated with the central nervous system. In addition, *A. afra* is considered as folk medicine in Zimbabwe, where the extracted plant oil was screened for significant activity against *Aspergillus ochraceus*, *Aspergillus niger*, *Aspergillus parasiticus*, *Candida albicans*, *Alternaria alternate*, *Geotrichum candidum*, and *Penicillium citrinum* (Liu *et al.*, 2009, Du Toit and Van der Kooy, 2019b). The essential oil of *A. afra* showed high antimicrobial activity, with specific anti-mycobacterium potential against respiratory pathogens as observed against *Mycobacterium smegmatis* at a minimum inhibitory concentration (MIC) value of 1.57 mg/ml. *In vitro* antibacterial activity was also observed in the traditional extract of the South African *A. afra* plant (Mativandlela *et al.*, 2008, Liu *et al.*, 2009, Du Toit and Van der Kooy, 2019a). The *A. afra* extract has thus demonstrated antimicrobial and antifungal capabilities against gram-positive and negative bacteria, fungi and protozoa (Graven *et al.*, 1992, Suliman *et al.*, 2010).

The oil obtained from selected aromatic plants, including *Agathogsma betulina, Eucalyptus globulus* and *Osmitopsis asteriscordes* can be combined with *A. afr*a for therapeutic purposes (Suliman *et al.*, 2010, Du Toit and Van der Kooy, 2019b). The essential oil obtained from these plant concoctions demonstrated the ability to prevent lipid oxidation and elicit free radical scavenging, chelating metal ions and acts as a reducing agent (Liu *et al.*, 2009, Du Toit and Van der Kooy, 2019b). The oil of *A. afra* has antioxidant potential as elucidated by Burits and co-investigators (2001) in a study for non-enzymatic lipid peroxidation in liposomes (Burits *et al.*, 2001). In the study, *A. afra* acted as a non-specific donor of hydrogen atoms or electrons in the diphenyl picrylhydrazyl assay. Furthermore, it was effective as a hydroxyl radical scavenging agent in the deoxyribose degradation assay (Konishi *et al.*, 2002, Liu *et al.*, 2009).

Several compounds were isolated from the crude leaf extract of *A. afra*, but only a few were noted to have high antioxidant activity such scopoletin and betulinic acid. Sesquiterpenes have high antioxidant activity and are known to cause the generation of reactive oxygen species (ROS) in various cancer cell lines, making it a potential bioactive compound in cancer treatment (Liu *et al.*, 2009, More *et al.*, 2012, Du Toit and Van der Kooy, 2019b). Isoalantolactone is shown to protect against *Staphylococcus aureus* pneumonia. Phenolic compounds found in the *A. afra* were found to

exhibit protective activities against degenerative diseases such as cancer and cardiovascular diseases (Magalhães *et al.*, 2009, Du Toit and Van der Kooy, 2019a, Moyo *et al.*, 2019a). The phenolic groups of the plant are known to chelate metals by inhibiting lipoxygenase and scavenging free radicals (Martínez-Valverde *et al.*, 2000, Du Toit and Van der Kooy, 2019a).

Treatment of various inflammatory diseases such as rheumatism, fever and other inflammatory-related diseases involves the use of *A. afra* (Halliwell and Gutteridge, 1989, Naidoo *et al.*, 2008, Liu *et al.*, 2009, Du Toit and Van der Kooy, 2019a). Scopoletin isolated from *A. afra* exhibited cardiovascular and hypotensive effects, resulting in potential therapeutic options for cardiovascular diseases (Guantai and Addae-Mensah, 1999, Liu *et al.*, 2009, Du Toit and Van der Kooy, 2019a). The plant also possesses anti-convulsive and GABA-benzodiazepine receptor-binding activity due to active flavonoids as isoalantolactone within the plant, enabling sedative and CNS-acting activities (Liu *et al.*, 2009, Du Toit and Van der Kooy, 2019a). Two studies by Nielsen *et al*. (2004) and Liu *et al*. (2009) both indicated the use of ethanolic *A. afra* extract for the treatment of depression (Nielsen *et al.*, 2004, Liu *et al.*, 2009).

2.2 Cancer

Cancer is a broad group of diseases that begins when abnormal cells divide uncontrollably in almost any organ or tissue of the body, go beyond their natural limits to invade adjoining parts of the body and spread to other organs (Auyang, 2006, Edge *et al.*, 2010, Jiang *et al.*, 2015). There were 19.3 million cases in 2020, and the incidence rate is growing throughout the world due to socioeconomic burden, late diagnosis and poor prognosis (Bray *et al.*, 2018, Mathur *et al.*, 2020). Cancer is the second leading cause of death in the world with almost 10.0 million cancer-related deaths reported in 2020; the mortality rate also remains high in South Africa (Brand *et al.*, 2018, Mathur *et al.*, 2020).

2.2.1 Colorectal cancer

2.2.1.1 The colon

The colon (Figure 2.4) is part of the digestive system and is also referred to as the large intestine, which has 3 primary functions: absorbing water and electrolytes, producing and absorbing vitamins and forming propelling faeces toward the rectum for elimination (Sulaiman and Marciani, 2019). By the time indigestible materials have reached the colon, most nutrients and up to 90% of the water have been absorbed by the small intestine (Azzouz and Sharma, 2018, Sulaiman and Marciani, 2019). The undigested and unabsorbed nutrients are retained within the large intestine. The ascending colon's function is to remove the indigestible material's remaining water and nutrients before solidifying it

into a stool. Faecal material that will gradually be drained into the rectum are locally contained in the descending colon (Azzouz and Sharma, 2018). To raise the colon's pressure, the sigmoid colon contracts, allowing the stool to pass into the rectum. The rectum houses the faeces pending removal by defecation (Click and Regueiro, 2019).

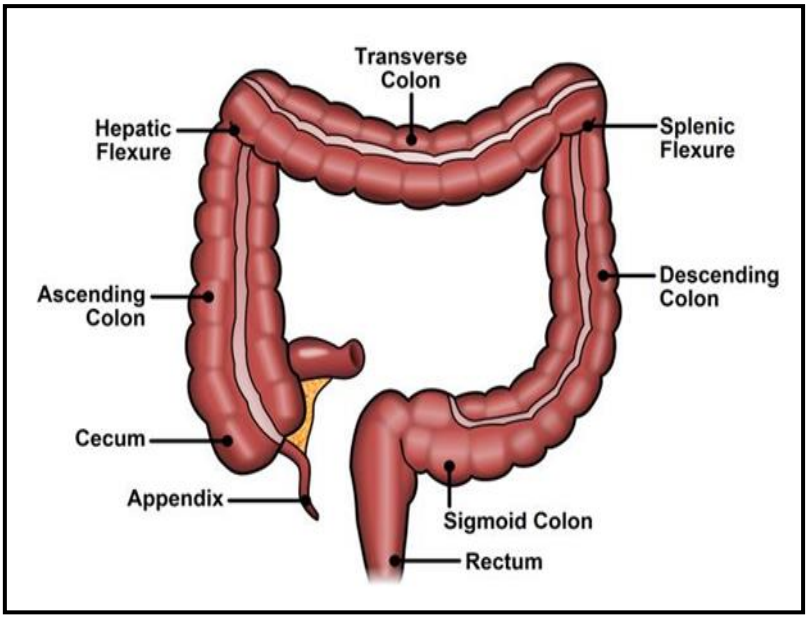

Figure 2.4: Structural overview of the human colon (www.Fascrs.org: The colon).

2.2.1.2 Consequences of the colon damage

The build-up of toxic agents or xenobiotics within the colon leads to intestinal damage, which may cause cell lining injury ultimately leading to the formation of small cancerous tumours. This may be due to DNA mutations that allow cancerous cell replication to occur (Cooper and Hausman, 2000). The cancerous tumours grow over time in the surface and block nutrients from entering the large intestine leading to pain and discomfort (Shadad *et al.*, 2013).

Colorectal carcinoma (CRC) is a malignant tumour that affects the colon and the rectum (Figure 2.4). It occurs as a result of inherited or acquired mutations within the large intestine (Armaghany *et al.*, 2012). There are vast types of tumours that include neuroendocrine neoplasm, haematomas, mesenchymal tumours and relatively unusual lymphomas. Adenocarcinomas account for 90% of carcinoma usually found in the colon and rectum (Gill *et al.*, 2001, Armaghany *et al.*, 2012). Adenocarcinoma is initiated by the growth of polyps on the inner lining of the colon and rectum. The polyps arise over time from the pre-cancerous colon that progressively grows and turns into cancer cells. The polyps have invasion and expansion properties due to their conformational morphological patterns (Gill *et al.*, 2001, McCabe *et al.*, 2019). In fact, approximately 90% of adenocarcinoma cancer metastasizes to the liver if diagnosis does not occur at an early stage (Valderrama-Treviño *et*

al., 2017). In addition, more than half of CRC patients have metastases and recurrent CRC disease (Ueda *et al.*, 1994, Chung *et al.*, 2017).

2.2.1.3 Incidence

There are over 1.9 million cases of CRC reported annually and 935000 deaths estimated to have occurred in 2020 alone (Bray *et al.*, 2018, Mathur *et al.*, 2020). On a global scale, CRC ranks third in cancer incidence and second in mortality (Figure 2.5A); this is a reflection of westernized nations where CRC is the second leading cause of death amongst cancer patients (Sung *et al.*, 2021). However, the global trend differs in Africa where CRC is ranked 5th in terms of cancers with high incidence and 4th for mortality rate (Figure 2.5B) (Sung *et al.*, 2021). It is also the 5th most diagnosed cancer with 108168 cases in 2020 and the 4th most lethal cause of mortalities within South Africa's borders (Figure 2.5C) (Sung *et al.*, 2021). Men are more susceptible to CRC; although CRC is currently the 3rd most common cancer in men and women, it accounts for 7.3% of cases in men and 6.3% of cases in women. Different ethnicities in South Africa are also impacted differently by CRC. The most affected are White (Caucasian (52-54%)), followed by Black (African (26-28%), Coloured (mixed ancestry (14-15%)) and Asian (Indian (4-7%)) populations (McCabe *et al.*, 2019, Motsuku *et al.*, 2021). There is a growing risk for Black South African males to be affected by CRC (Motsuku *et al.*, 2021).

2.2.1.4 Risk factors

There are various risk factors associated with the diagnosis of CRC, which includes a diet that is high in fat and low in fiber, excessive consumption of red meat or processed foods; family history: age, race, gender, and inherited gene mutation; and lifestyle with relation to lack of exercise, alcohol abuse and tobacco use. Other factors that contribute to CRC include alcohol consumption and cigarette smoking (Armaghany *et al.*, 2012, Hughes *et al.*, 2017). The pathogenesis of CRC remains complex despite the effectiveness of current CRC treatment (Hughes *et al.*, 2017).

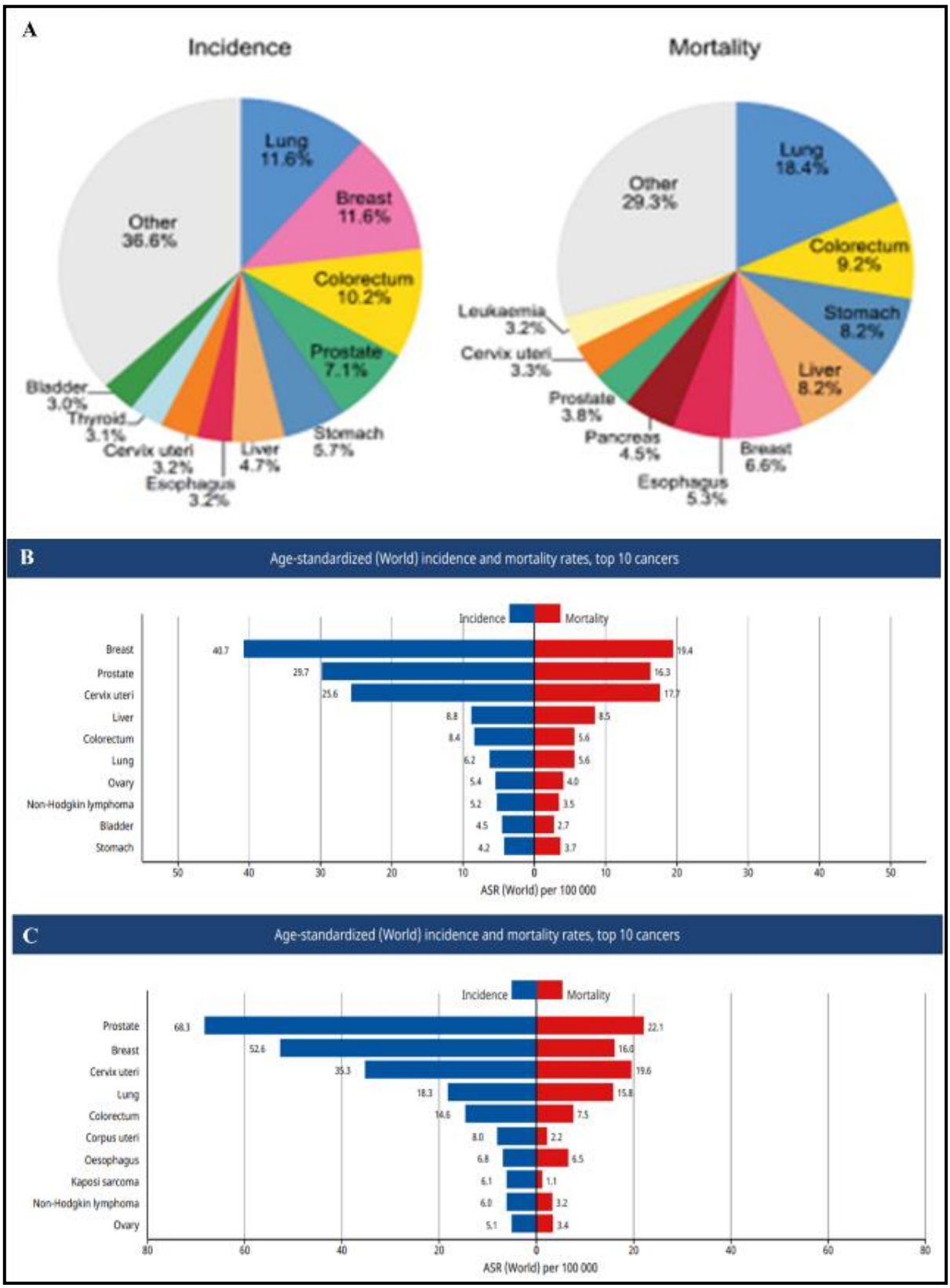

Figure 2.5: Incidence and mortality associated with colorectal cancer. (**A)** The percentage distribution of various cancer incidence and fatalities throughout the world, showing the contribution of the CRC to the global incidence and death rates associated with cancer. (**B**) Cancer incidence and mortality in Africa showing colorectal cancer ranked 5th and 4th, respectively. (**C**) The South African statistics shows incidence and mortality rate of colorectal cancer similar to the continent statistics [Data source**:** GLOBOCAN 2020 Graph production (Global, Africa and South Africa)**:** IARC (http://gco.iarc.fr/today) World Health Organisation].

2.2.1.5 Treatment

Depending on each patient's significant exposure and severity, care plans can be used in conjunction with first-line therapy such as radiation, surgery, chemotherapy and radiation (Chabner and Longo, 2011). Radiation has the limitation of killing healthy cells in the surrounding region, which has adverse side effects in the patient, such as weakened skin and intestinal cells and other undesirable implications (Moding *et al.*, 2013). Chemotherapeutics can destroy cancer cells by causing DNA damage or triggering multiple signaling pathways, such as cell cycle arrest, global translation inhibition and DNA repair (Skeel and Khleif, 2011). The critical issues associated with chemotherapy are cytotoxicity, drug resistance and adverse reactions. Localized malignant tumours are eligible for surgical removal and care, but metastatic cells pose a risk since the cancer may spread throughout the patient's body (Tohme *et al.*, 2017). Surgery remains the most effective method for both late and early diagnosis of CRC. The prevention of CRC typically relies on screening techniques to detect adenomatous polyps that are precursor lesions of colon cancer. In addition to these therapies, antiangiogenic agents are also used to treat and monitor cancer progression (Simon, 2016). However, due to current treatment being expensive and requiring well-equipped medical facilities, research is ongoing into the use of naturally occurring plants and their active compounds to treat CRC. Some are in clinical trials and remain to be approved if found to be safe (Greenwell and Rahman, 2015).

2.2.1.6 Human adenocarcinoma (Caco-2) cells

The Caco-2 cells were isolated from the human colon adenocarcinoma of a 72-year-old Caucasian male and shown to be a good prediction model for human intestinal absorption of drugs and other compounds as a human colon epithelial cancer cell line (Hidalgo *et al.*, 1989). As a result, Caco-2 cells are useful cell model system for investigations on drug design and development, endothelial carcinogenesis processes, xenobiotic metabolism, cytotoxicity, and genotoxicity. (Hidalgo *et al.*, 1989, Lea, 2015).

2.3 Inflammation

Inflammation is a complex biological response that serves as a defense mechanism to damage induced by injury or infection (Fiers, 1991, Chung *et al.*, 2017). Chronic inflammation in the microenvironment is required for the induction and progression of cancer (Grivennikov *et al.*, 2010). Indeed, it has been estimated that 15–20% of cancer types have direct origin from chronic inflammation in the same tissue or organ prior to the development of the malignancy (Greten and Grivennikov, 2019). The likelihood of getting cancer as a result of inflammation is often time-dependent and specific to the type of cancer. The inflammatory response is linked to cancers such as

prostate, breast and lung carcinoma. In addition, colitis-related cancer may be triggered by chronic inflammatory illnesses of the small and large intestines such as ulcerative colitis and Crohn's disease, and chronic inflammation is linked to the development of CRC (Lin *et al.*, 2015).

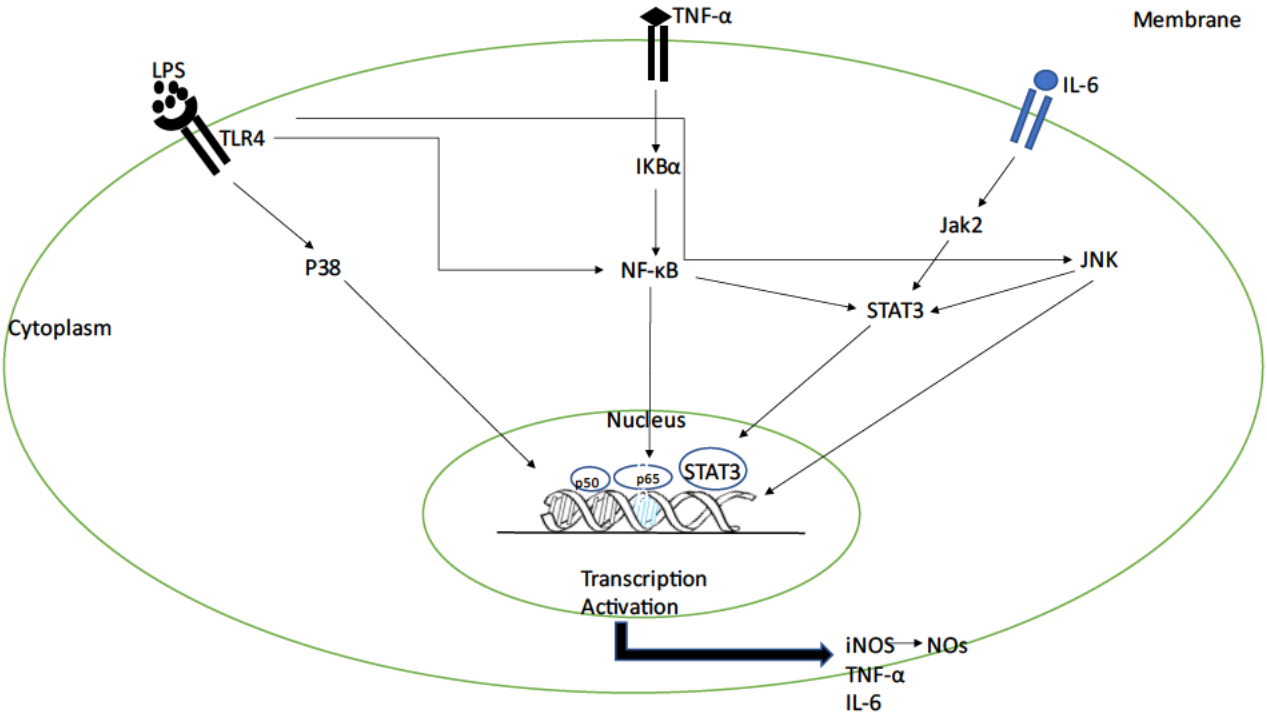

Figure 2.6: A proposed model for regulation of proinflammatory responses when there is an imbalance in oxidative stress causing ROS production (Prepared by the Author).

The inflammatory response is mediated by cytokines such as interleukin (IL) 1β (IL-1β), IL-6 and TNF-α. These chemical mediators are considered the primary cause of colorectal carcinogenesis. In addition, transcription factors such as nuclear factor kappa-light-chain-enhancer of activated B (NF-κB) and signal transducer and activator of transcription 3 (STAT3) are active in the majority of malignancies; cell survival, proliferation, angiogenesis, invasiveness and cytokine production are all regulated by these genes (Chung *et al.*, 2017). Inducible nitric oxide synthase (iNOS) is also a unique mediator of inflammation (Chung *et al.*, 2017) (Figure 2.6).

2.3.1 Tumour necrosis factor alpha (TNF-α)

Tumour necrosis factor alpha (TNF-α) is a pro-inflammatory cytokine that belongs to the TNF superfamily which includes a number of transmembrane proteins that share a homologous TNF domain (Albensi, 2019). The TNF-α effects are mediated by two receptors called TNFR1 and TNFR2. TNFR1 is expressed ubiquitously on most cell types, whereas TNFR2 is found largely in endothelial, epithelial and immune cell subsets. TNFR1 signaling increases apoptosis and is pro-inflammatory, whereas TNFR2 signaling stimulates cell proliferation and is anti-inflammatory (Makamure *et al.*,

2016, Chung *et al.*, 2017). TNF-α is produced by macrophages or monocytes during acute inflammation and is responsible for a variety of signaling events within cells that may culminate in the induction of cell death. This pro-inflammatory cytokine is a 157-amino-acid that stimulates the immune system in the presence of cancer, infection, endotoxins, bacteria, viruses, parasites or inflammatory agents (Figure 2.6) (Roitt and Delves, 1992, Makamure *et al.*, 2016). According to studies, the inflammatory response is linked to cancers such as prostate, breast, and lung carcinoma. Furthermore, TNF-α remains a major catalyst for cancer progression and metastasis and is associated with a poor prognosis because overexpression causes tumours to grow larger. In addition, TNF-α together with other growth hormones and cytokines has also been shown to increase ROS generation (Ueda *et al.*, 1994, Kulinsky, 2007).

2.3.2 Cell signaling cascade – MAPK

Mitogen-activated protein kinases are protein kinases that activate or deactivate their target by phosphorylating their own dual serine and threonine residues (auto phosphorylation) or those located on their substrates (Cargnello and Roux, 2011). They control key cellular functions such proliferation, stress responses, apoptosis, and immunological defense (Cargnello and Roux, 2011). The activation of a MAPK cascade happens in a module of consecutive phosphorylations, in which each MAPK is phosphorylated by an upstream MAPK following a previous stimulation. A MAPK module consists of a MAP3K that triggers a MAP2K, which activates a MAPK in turn (Soares-Silva *et al.*, 2016). In mammalian cells, the three well-known MAPK pathways are ERK1/2, c-JUN N-terminal kinase 1, 2, and 3 (JNK1/2/3), and the p38 MAPK pathways (Figure 2.6 and 2.7) (Cargnello and Roux, 2011). Stress and cytokines both activate p38 MAPK isoforms, which are involved in inflammatory responses (Raman *et al.*, 2007). The production of immunomodulatory cytokines such as TNF-α, IL-1, IL-10, and IL-12, which are triggered by the activation of the p38 MAPK, JNK, and ERK pathways, is one of numerous critical functions regulated by MAPKs. Radiation, environmental stressors, and growth hormones stimulate the JNK pathway, which regulates stress, inflammation, and apoptotic responses. Chemical stressors, hormones, and cytokines such as IL-1 and TNF-1,3 activate p38 MAPKs, which target many transcription factors (TFs), including NF-κB (Cargnello and Roux, 2011).

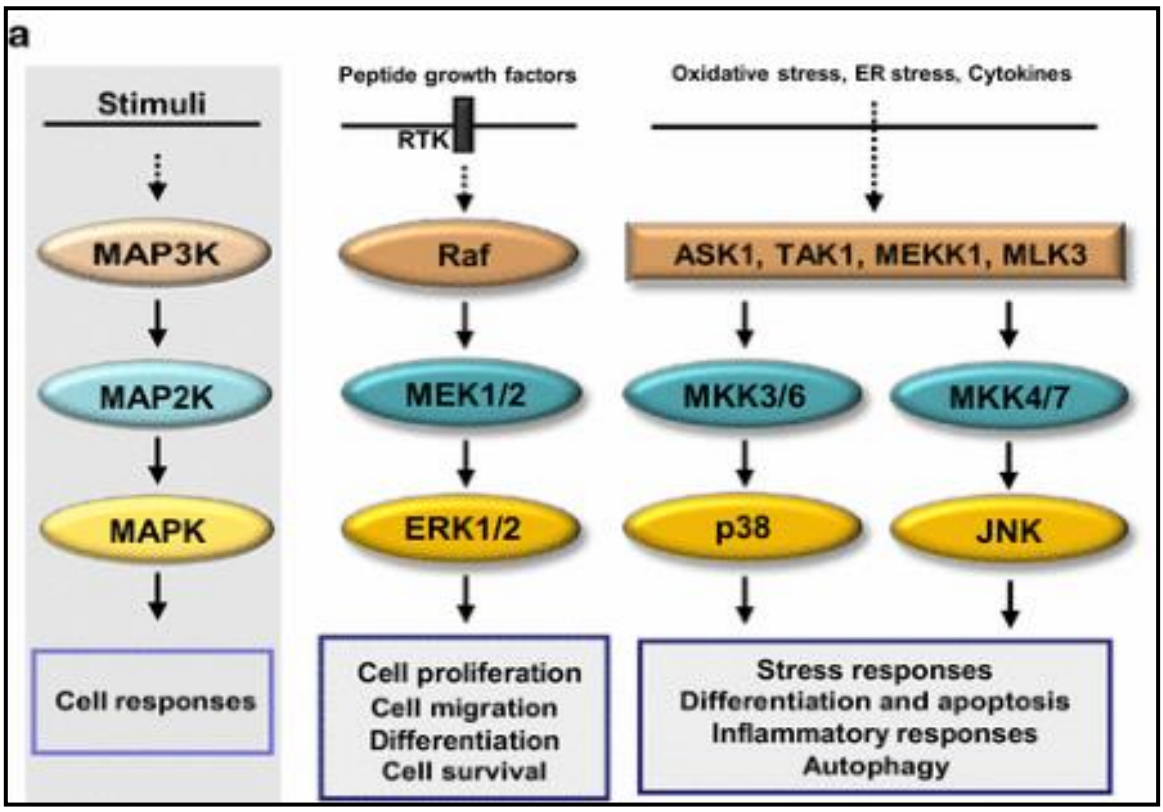

Figure 2.7: Overview of MAPK signaling. The MAPK's including p38, JNK, and ERK1/2 are involved in various cell responses (Soares-Silva *et al.*, 2016).

2.3.3 Nuclear factor kappa -light-chain-enhancer of activated B cells (NF-κB)

NF-κB is a transcription factor that regulates genes that control survival and cell proliferation in eukaryotic cells. Activated NF-κB is required for the expression of genes that keep the cell functioning and protects it from events that would otherwise cause programmed cell death (Beinke and Ley, 2004, Albensi, 2019). NF-κB is also implicated in the immune response and inflammation; many proinflammatory stimuli can activate NF-κB. Activation is principally by phosphorylation of the inhibitory kappa B proteins (I-κB) by IκB kinase (IKK), followed by ubiquitination and eventual degradation of IκBs as possible outcomes (Ben-Neriah and Karin, 2011, Liu *et al.*, 2017b). Free of IκB, NF-κB translocate to the nucleus where it stimulates the transcription of cytokines, chemokines and antiapoptotic genes (Figure 2.6 and 2.8). The regulation of cell survival as well as apoptosis is linked to NF-κB target genes, and most lymphoid and solid tumours have constitutively active NF-κB (Ben-Neriah and Karin, 2011). NF-κB activation is maintained in the majority of cancer cells as a response to external stimuli in the tumour microenvironment or by alterations in signaling molecules upstream of active NF-κB (Liu *et al.*, 2017b).

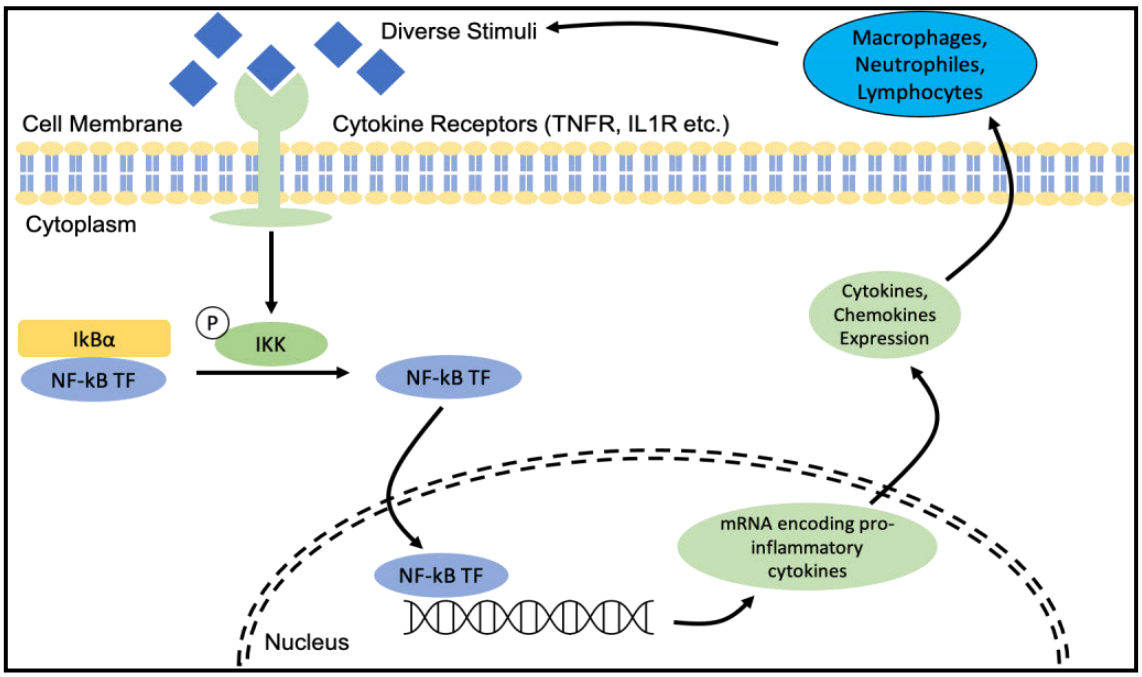

Figure 2.8: The signalling pathway that mediates NF-κB inflammatory effects. When attached to DNA, NF-κB promotes the production of pro-inflammatory cytokines. Immune cells will be drawn to the location by pro-inflammatory cytokines. The presence of immune cells also produces pro-inflammatory cytokines, which may bind to the cytokine receptors that activate NF-κB, resulting in a never-ending cycle of inflammation (Liu *et al.*, 2017a).

2.3.4 Signal transducer and activator of transcription 3 (STAT3)

The STAT proteins are implicated in cytokine signaling pathways that control cell growth, proliferation, and differentiation. Seven members of the STAT family identified include STAT1, STAT2, STAT3, STAT4, STAT5a, STAT5b, and STAT6 (Yu *et al.*, 2009). These proteins are unique in that they serve as transcription factors in the nucleus, while also transmitting signals through the cytoplasm. In particular, STAT3 has prompted a lot of attention among STAT members because of its position in oncogenic signaling pathways and its regulatory influence on the pro-inflammatory cytokines involved in hepatic damage and repair mechanisms (Bishayee, 2014). The internal and extrinsic mechanisms of STAT3 activation is linked to inflammation and cancer. The intrinsic pathway, also known as the oncogenic pathway, is activated in transformed cells by epigenetic or genetic alterations such as persistent activation or overexpression of cytokine receptors with accompanying Janus kinase (JAK) family of tyrosine kinases and growth factor receptors with intrinsic tyrosine kinase activity. (Schmidt-Arras and Rose-John, 2016). Extrinsic or environmental pathway inducers include cigarette smoking, stress, UV radiation, and carcinogens. When IL-6 binds to its corresponding receptor, the IL-6-STAT3 signaling pathways are activated (Figure 2.9). When the IL-6/IL-6R combination binds to the glycoprotein receptor GP130, signaling is initiated. The GP130 receptor dimerises, activating the tyrosine kinase JAK1 and triggering the activation of the STAT3 protein (Yu *et al.*, 2009). Furthermore, STAT3 promotes the expression of inflammatory

mediators such as cyclo-oxygenase 2, IL-10, and IL-6, the latter of which causes STAT3 to become even more activated, resulting in genetic alterations and the advancement of cancer-related inflammation(Yu *et al.*, 2009).

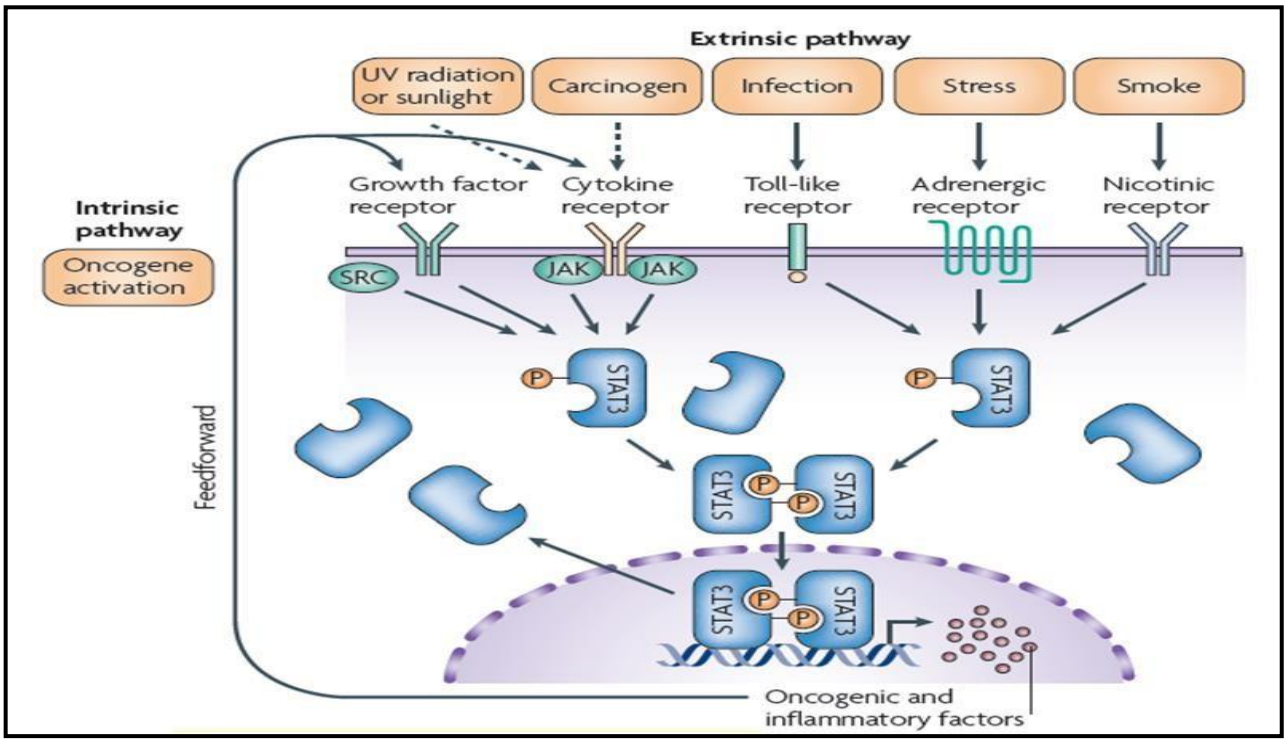

Figure 2.9: STAT3 in inflammation. Inflammation and cancer are linked by the intrinsic and extrinsic pathways of STAT3 activation (Yu *et al.*, 2009).

2.3.5 Inducible nitric oxide synthases (iNOS)

Nitric oxide synthases are a group of enzymes that catalyze the conversion of L-arginine to NO, a crucial free radical involved chemical in cellular signaling (Stuehr, 2004). The calcium-calmodulin-controlled isozymes endothelial NOS (eNOS) and neuronal NOS (nNOS) mediate NO synthesis in mammals (Anavi and Tirosh, 2020). However, iNOS stands out among the three NOS enzymes in mammalian systems because it produces more NO than the constitutive members nNOS or eNOS as an immune defense mechanism (Kröncke *et al.*, 1998). Several inflammatory mediators including cytokines (TNF-α; IL-1, interferon (IFN-γ), lipopolysaccharide (LPS) and others regulate the expression of the iNOS gene in macrophages (Figure 2.6), dendritic cells, neutrophils, epithelial cells of the gut and lung mucosa, smooth muscle cells and stromal cells of secondary lymphoid organs (Geller *et al.*, 1993). These cells use different transcriptional and post-transcriptional pathways that result in the induction of iNOS expression; the NF-κB and JAK-STAT pathways are the most significant intracellular signal transduction pathways (Figure 2.6 and 2.9) (Geller *et al.*, 1993, Kröncke *et al.*, 1998, Anavi and Tirosh, 2020). Hypoxia and oxidative stress are also involved in the regulation of iNOS expression. More recently, heat shock protein (HSP) 70 (HSP70) has been shown

to regulate iNOS expression. Many stages of carcinogenesis involve NO, including DNA damage, oncogene activation, inhibition of DNA repair enzymes and tumour suppressor genes, as well as apoptosis and metastasis (Torgovnick and Schumacher, 2015).

2.4 Oxidative stress

Oxidative stress is an imbalance between oxidant and antioxidant levels due to excess free radical formation in the cell, which overwhelms the antioxidant capacity of the body (Rahal *et al.*, 2014, Romani, 2018). The exogenous sources of reactive oxygen species (ROS) include the mitochondrial electron transport chain (ETC), NADPH-oxidase, xanthine oxidase, NO synthase and intracellular xenobiotic mechanisms (CYP_{450}) (Figure 2.10). When the concentration of ROS is not managed adequately through defense mechanisms such as antioxidant systems involving tocopherols, ascorbic acid and glutathione or key enzymes catalase (CAT), glutathione peroxidase (GPx) and superoxide dismutase (SOD) that are involved in free radical scavenging (Figure 2.12); the resulting oxidative stress disrupts redox signaling (Thanan *et al.*, 2015). This culminates in promotion of cell growth and inhibition of cell death. The activation of proliferation pathways with corresponding inhibition of repair mechanisms leads to the enhancement of DNA damage. This damage often results in cytotoxicity, genotoxicity and carcinogenesis (Poljsak *et al.*, 2013).

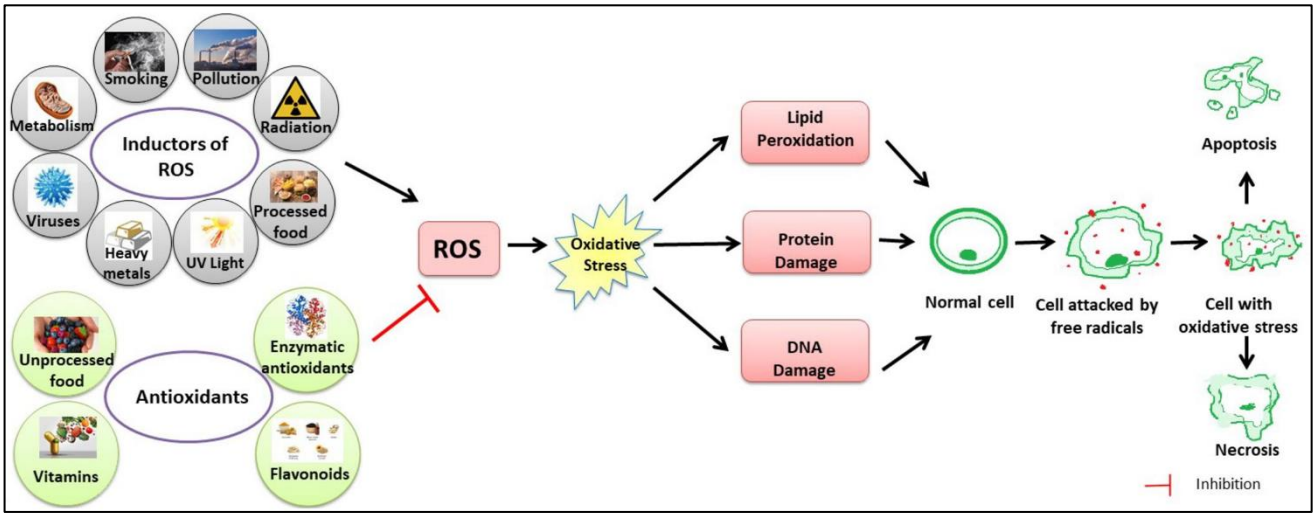

Figure 2.10: Schematic diagram show factors that induce oxidative stress and the associated cytotoxic effects (Sharifi-Rad *et al.*, 2020).

2.4.1 Electron transport chain as a source of ROS

Metabolism of molecular oxygen results in low ROS levels in aerobic cells, but exposure to toxic stimuli can generate excessive amount of ROS (Zorov *et al.*, 2014, Snezhkina *et al.*,

2019). Mitochondria function to generate energy in adenosine trisphosphate (ATP) within mammalian cells through oxidative phosphorylation, a process of electron transfer in the transport chain (Figure 2.11). The electron transport chain (ETC) is made up of series of complexes that are enzyme dependent including complex I (NADH-Q oxidoreductase), II (succinate-Q reductase), III (Q-cytochrome C oxidoreductase), IV (cytochrome c oxidase) and V (mitochondrial ATP synthase) ATP (Schieber and Chandel, 2014, Choi and Kim, 2019). However, nicotinamide adenine dinucleotide (NADH) is oxidised to NAD^+, making the complex supercharged due to the presence of electrons entering. This results in the accumulation of electrons in the intermembrane space (Ahmad and Kahwaji, 2018).

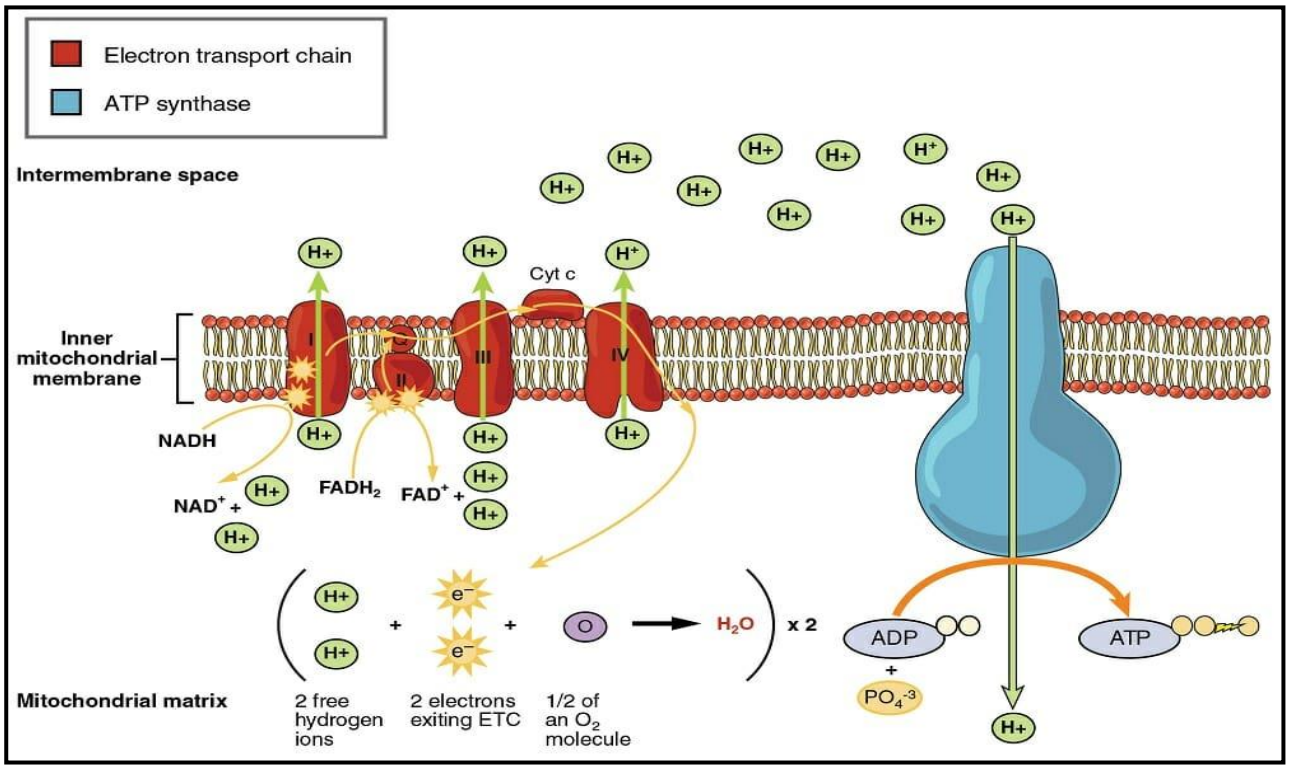

Figure 2.11: Formation of ATP through the electron transport chain and oxidative phosphorylation (*Image modified from "Oxidative phosphorylation: Figure 1", by OpenStax College, Biology (CC BY 3.0)).*

Complex 1 passes electron to coenzyme A and flavin adenine dinucleotide ($FADH_2$) becomes oxidized to FAD^+. Electrons are passed from complex II to coenzyme Q, resulting in the enzyme supercharging by creating enough energy potential to pump protons from the mitochondrial matrix through complex III to the intermembrane space. Complex III passes electrons to cytochrome c (cyt c) and supercharge complex IV and create gradient energy potential. Complex IV gives electrons to the electron acceptor oxygen, which is reduced to two molecules of water. ATP synthase uses the proton gradient in the intermembrane space by passing through to phosphorylation of ADP to ATP (Schieber and Chandel, 2014, Choi and Kim, 2019).

However, studies report that 1-3% of oxygen consumed is discharged from system due to incomplete reduction within complex I and II resulting in formation of superoxide anion radicals ($O_2^{\bullet-}$) (Turrens, 2003, Krumova and Cosa, 2016, Collin, 2019). The superoxide radical result in the formation of other forms of ROS species production as it a precursor. The dismutation of $O_2^{\bullet-}$ by SOD ends in production of hydrogen peroxide (H_2O_2) (Krumova and Cosa, 2016, Sharma *et al.*, 2012). Conversely, H_2O_2 is used in Fenton reaction (in the presence of Fe^{2+}) to produce hydroxyl radicals ($^{\bullet}OH$). The $^{\bullet}OH$ radical remains unremovable by enzymatic enzymes as the precursor that generate $^{\bullet}OH$ is eliminated when GSH-PX metabolises the reduced glutathione to its oxidised form (Reiter *et al.*, 1995). Other radicals formed are RNS including nitrogen dioxide (NO_2), peroxynitrite ($ONOO^-$) and nitrosoperoxycarbonate ($ONOOCO_2^-$). Bioavailability $^{\bullet}NO$ and activity are influenced by its swift response with the superoxide radical, which produces a basic and reactive peroxide, Peroxynitrite, which represents the fusion of the oxygen and $^{\bullet}NO$ pathways (Radi, 2018). Altered levels of NO result in cancer as it plays a role in cellular signaling and immune response (Lloyd *et al.*, 1997, Choi and Kim, 2019).

2.4.2 Antioxidant response

The antioxidant response element (ARE) is a regulatory element that mediates the transcriptional activation of antioxidant enzymes in cells exposed to oxidative stress. It is activated when a stress signal leads to Nrf2 translocation to the nucleus (Baird and Dinkova-Kostova, 2011, Jaiswal, 2004). The stress signals that affect cellular component include oxidative stress, reduction of antioxidant capacity of the cell (GSH), xenobiotics that affect homeostasis (redox cycle) and biotransformation (Nguyen *et al.*, 2009). The production of several enzymes that play a crucial role in protecting the cell oxidative stress induced by a toxic insult results from interactions of Nrf2 and the ARE (Ma, 2013). As a result of ROS-associated toxicity in the tissue, the cell manifest an antioxidant defense mechanism to protect itself. Several enzymes are involved including SOD, CAT, along with non-enzymatic compounds ascorbic acid and glutathione that maintain redox state and optimum detoxification of ROS (Weydert and Cullen, 2010). There are two types of SOD that are important in the detoxification of $O_2^{\bullet-}$ to H_2O_2**.** SOD1 is found in the cytoplasm and exists as dimer, thus a dinuclear metal cluster which consists of copper and zinc at the active site in each subunit of the dimer and SOD2 which is localised in the mitochondrial matrix and is a homotetrameric that accommodates one manganese per subunit (Candas and Li, 2014).

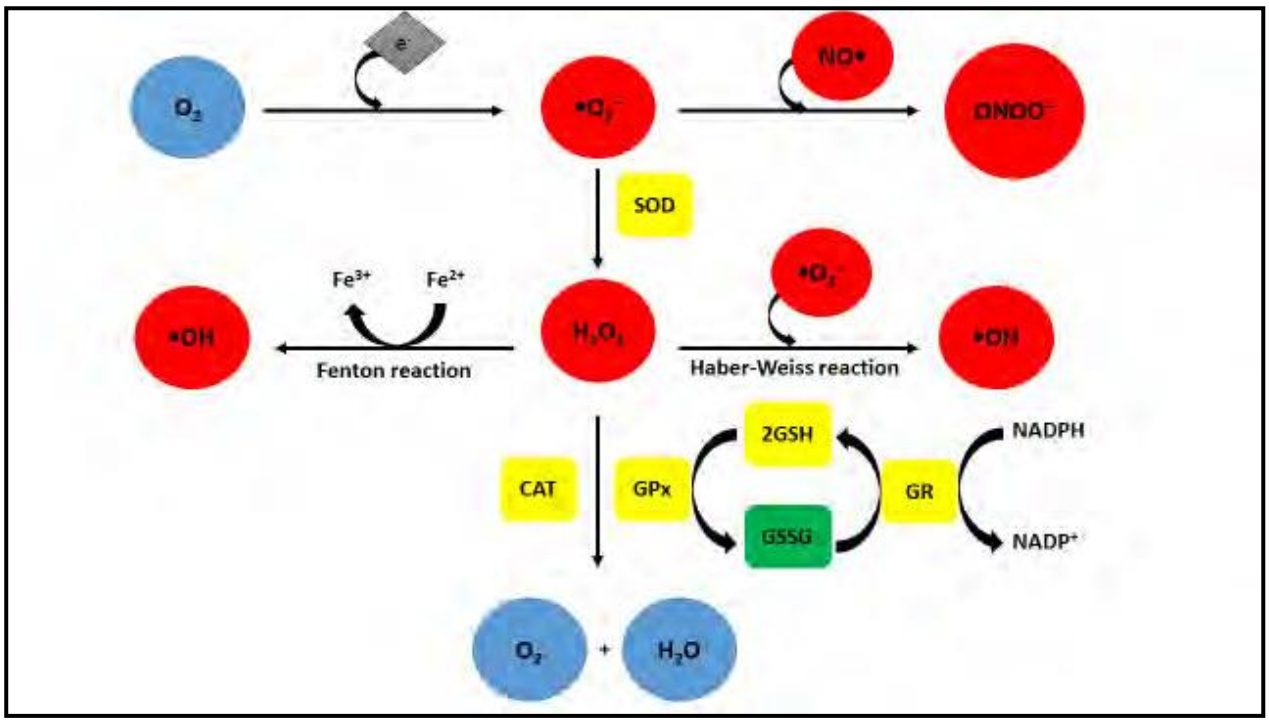

Figure 2.12: A mechanism of how antioxidants detoxify ROS produced *(Hermes-Lima, 2004)*. (Note: $NO^{\bullet}$ nitric oxide, $O_2^{\bullet-}$—superoxide radicals, ONOO—peroxynitrite, $^{\bullet}OH$- hydroxyl radicals, H_2O_2- hydrogen peroxide, CAT- catalase, SOD- superoxide dismutase, GSH- reduced glutathione, GSSG- glutathione disulphide, GR- glutathione reductase, GPx-1 glutathione peroxidase).

The products of detoxification by SOD is H_2O_2 and oxygen (Figure 2.12), thus H_2O_2 remain toxic to the cell and needs to be removed. Detoxification of H_2O_2 is carried out by two enzyme families, GPx-1 and CAT in mammalian cells (Davies, 2000, Weydert and Cullen, 2010). There are three fates for H_2O_2 (Figure 2.12); it can be detoxified by CAT, detoxified by GPx or form $^{\bullet}OH$ in the Fenton reaction. Catalase is found in high concentration in peroxisomes in several tissues where it catalyses the decomposition of H_2O_2 into water and gaseous oxygen. The enzyme's reactivity with H_2O_2 is facilitated by each subunit of the four polypeptide chains of CAT with a porphyrin haem (Gutteridge, 1995, Alfonso-Prieto *et al.*, 2012). GPx facilitates the mitigation of H_2O_2 and lipid hydroperoxide to water, where GSH act as an electron donor. However, the altering of GSH to its oxidised form to glutathione disulphide (GSSG) or glutathione reductase (GR) reprocess GSSG back to GSH which avert depletion and the reaction is regulated by NADPH-dependent (Zitka *et al.*, 2012, Milisav *et al.*, 2012). The GSH/GSSG ratio is a major determinant of the measure of oxidative stress (Lobo *et al.*, 2010, Zitka *et al.*, 2012). (ii) H_2O_2 can be detoxified through the Fenton reaction ends from hydrogen peroxide and an Iron (II) catalyst, forming hydroxyl radicals. This, in turn, causes DNA to respond (Collin, 2019). (iii) The combination of ROS should cause the metal-catalysed Haber-Weiss reaction to occur in the presence of iron ions, resulting in the formation of hydroxyl radicals (Kehrer, 2000).

2.4.3 Consequences of oxidative stress

Failure of antioxidant defense mechanism system causes oxidative modification of macromolecules that alter cellular processes' function and structure (Kurutas, 2015). Free radical-mediated damage to the cell's lipid component, induced by oxidative stress, may lead to lipid peroxidation. The oxidation of polyunsaturated fatty acids lipids into polar lipid hydroperoxide propagation of free radical reaction during lipid peroxidation often impairs the cell (Halliwell and Chirico, 1993, Betteridge, 2000).

Oxidised product that causes modification of DNA, protein and other macromolecules are products of lipid peroxidation. Malondialdehyde (MDA) and 4-hydroxy-2-nonenal (4-HNE) provides clear example of how MDA acts with nucleic acid bases for the formation of adducts, that are mutagenic (Halliwell and Chirico, 1993, Chan and Murin, 2011, Deavall *et al.*, 2012). Lipid peroxidation-induced oxidative damage to lipid component may alter cellular functions, thus increasing membrane permeability due to altered membrane fluidity, decreased membrane potential, and rapture of the membrane by inactivating membrane-bound receptors and enzymes (Zhang *et al.*, 2013, Ayala *et al.*, 2014).

The maintenance of overall cell homeostasis relies entirely on essential mitochondrial mechanisms. As a method of action, certain xenobiotics have been reported to specifically target the mitochondria, causing process dysregulation and generating mitochondrial toxicity (Liu and Wang, 2016, Tsai *et al.*, 2016). Although these mitochondria are still a toxicity target, mitochondrial malfunction has been linked to a variety of diseases, including Alzheimer's, Parkinson's, cardiomyopathy, cancer, and diabetes (Wang *et al.*, 2014). Reduced energy generation is the most-early consequence of mitochondrial malfunction. During dysfunction, however, there are significant increases in mitochondrial catalysed side processes. These include the formation of free radicals and the exothermic burning of oxygen, both of which cause cellular damage (Wang *et al.*, 2014). When the respiratory chain ATP synthase is inhibited and OXPHOS is uncoupled, primary toxicity might result. Interference with mitochondrial biogenesis, protein synthesis, gene expression, and membrane transporter inhibition are all examples of secondary mitochondrial toxicity (Wallace and Starkov, 2000). Interference with the ETC, which results in increased ROS generation, is the most common mechanism of mitochondrial toxicity. Oxidative stress is caused by an imbalance of ROS and antioxidants within cells. Reactive nitrogen species can interact with macromolecules like proteins and lipids, creating conformational changes that cause further stress (Kowaltowski and Vercesi, 1999, Picard *et al.*, 2011). Cell death occurs when oxidative stress is not alleviated. In other circumstances,

tampering with mitochondrial apoptotic pathways results in uncontrolled cell death, which has been seen in a variety of malignancies (Reed, 1999).

2.4.5 Cellular repair pathway

When cells are exposed to ROS oxidative DNA damage results in base lesions such as 8-oxoguanine. Various repair mechanisms may be implemented, and if that fails the cells induce cellular death (Davies, 2000). In the base excision repair (BER) pathway, the glycosylase (OGG1) removes the, highly mutagenic base, thus preventing mispairing with adenine residues, which result in a G:C to T:A transverse mutation. Thus, OGG1 prevents mutations that promote carcinogenesis brought on by ROS (Cooke *et al.*, 2003, Boldinova *et al.*, 2019). In the event of base lesion (8-oxoguanine) accumulation due to OGG1 downregulation, the probability of transformation that leads to carcinogenesis is high. A decrease in DNA-binding is caused by a reduced OGG1, which increases base mutations and serves as a marker for cancer susceptibility (Jaiswal *et al.*, 2001, Cooke *et al.*, 2003, Boldinova *et al.*, 2019).

2.5 Apoptosis

When the cellular defense mechanism fails, cell death is induced to target damaged cells for elimination. There are different kinds of cells death, including apoptosis or necrosis depending on the exposure time and severity of the toxic insult (Tsujimoto, 1997, Van Cruchten and Van Den Broeck, 2002). Apoptosis is a cell death program initiated by extracellular or intracellular signals that activate a cascade of events that culminates in the ordered degradation of the cell (Elmore, 2007, Kerr *et al.*, 1972, Green, 2019). Excessive apoptosis results in neurodegeneration, while inadequate apoptotic cell death may result in cancer, autoimmune or chronic inflammatory diseases (Saraste and Pulkki, 2000, Elmore, 2007, Zhang *et al.*, 2018).

A family of cysteine proteases is activated to carry out apoptosis (Figure 2.13). Caspases are inactive zymogens (procaspases) that require activation to facilitate proteolytic cleavage of cellular proteins. Caspases are classified into two groups, initiator and executioner caspases (Franco *et al.*, 2009, Salvesen, 2010, Danial and Hockenbery, 2018). Initiator caspases such as caspase-8 and caspase-9 become active through homodimerisation causing cleavage and activation of executioner caspases-3/7 that are responsible for the execution of cell death (Chang and Yang, 2000, Danial and Hockenbery, 2018).

Apoptosis occurs in two pathways, viz. extrinsic and apoptotic pathway. Both pathways ultimately lead to end stage cell death. The intrinsic pathway is mitochondrial dependent and requires various stimuli, including hypoxia, radiation, growth factor deprivation, DNA damage, and oxidative stress (Kerr *et al.*, 1972, Elmore, 2007, Green, 2019).

2.5.1 Intrinsic pathway: mitochondrial mediated

The intrinsic pathway (Figure 2.13) is orchestrated by the mitochondria. It is activated by various stimuli such as ROS-induced DNA damage that activate the tumour suppressor p53 protein regulator (Jin and El-Deiry, 2005, Deavall *et al.*, 2012, Green and Llambi, 2015). The p53 protein is a homotetrameric transcription factor located in the nucleus that functions by inducing the transcription of target genes involved in cell cycle arrest, DNA repair, and cell death (Cooke *et al.*, 2003, Achanta and Huang, 2004, Deavall *et al.*, 2012). In the intrinsic pathway, a stimulus received by a cell causes the reduced Bcl-2 function through p53-upregulated modulator of apoptosis (PUMA) and NOXA resulting in the activation and migration of Bax and Bak to the mitochondrial surface (Figure 2.13). These proteins are proapoptotic members of the Bcl-2 family which contain BH3 and BH4 domains (Harris and Thompson, 2000, Murphy *et al.*, 2000). Bax protein undergoes conformational modification, resulting in binding the protein on the outer mitochondrial surface (Shamas-Din *et al.*, 2013, Campbell and Tait, 2018).

Oligomerisation of Bax and Bak protein causes the mitochondria to release pro-apoptotic proteins and cytochrome c from its intermembrane space to the cytosol (Dewson *et al.*, 2009, Goldstein *et al.*, 2000, Renault *et al.*, 2013, Vringer and Tait, 2019). Among the pro-apoptotic proteins are SMAC/DIABLO, a second mitochondria activator of caspases; cytochrome c is the primary activator (Figure 2.13). Cytosolic cytochrome c binds to apoptotic protease activating factor 1 activating factor-1 (Apaf-1), initiating the recruitment of countless procaspase-9 to the caspase recruitment domain (CARD) of Apaf-1 resulting in the formation of the apoptosome complex (Baliga and Kumar, 2003). The apoptosome complex undergoes conformational changes that are activated by ATP hydrolysis and culminates in the cleavage of procaspase-9, which homodimerises to form active caspase-9 (Figure 2.13). The executioner caspases-3/7 are activated by caspase-9 to execute cell death (Wei *et al.*, 2001, Cory and Adams, 2002, Bratton and Salvesen, 2010, Yuan and Akey, 2013).

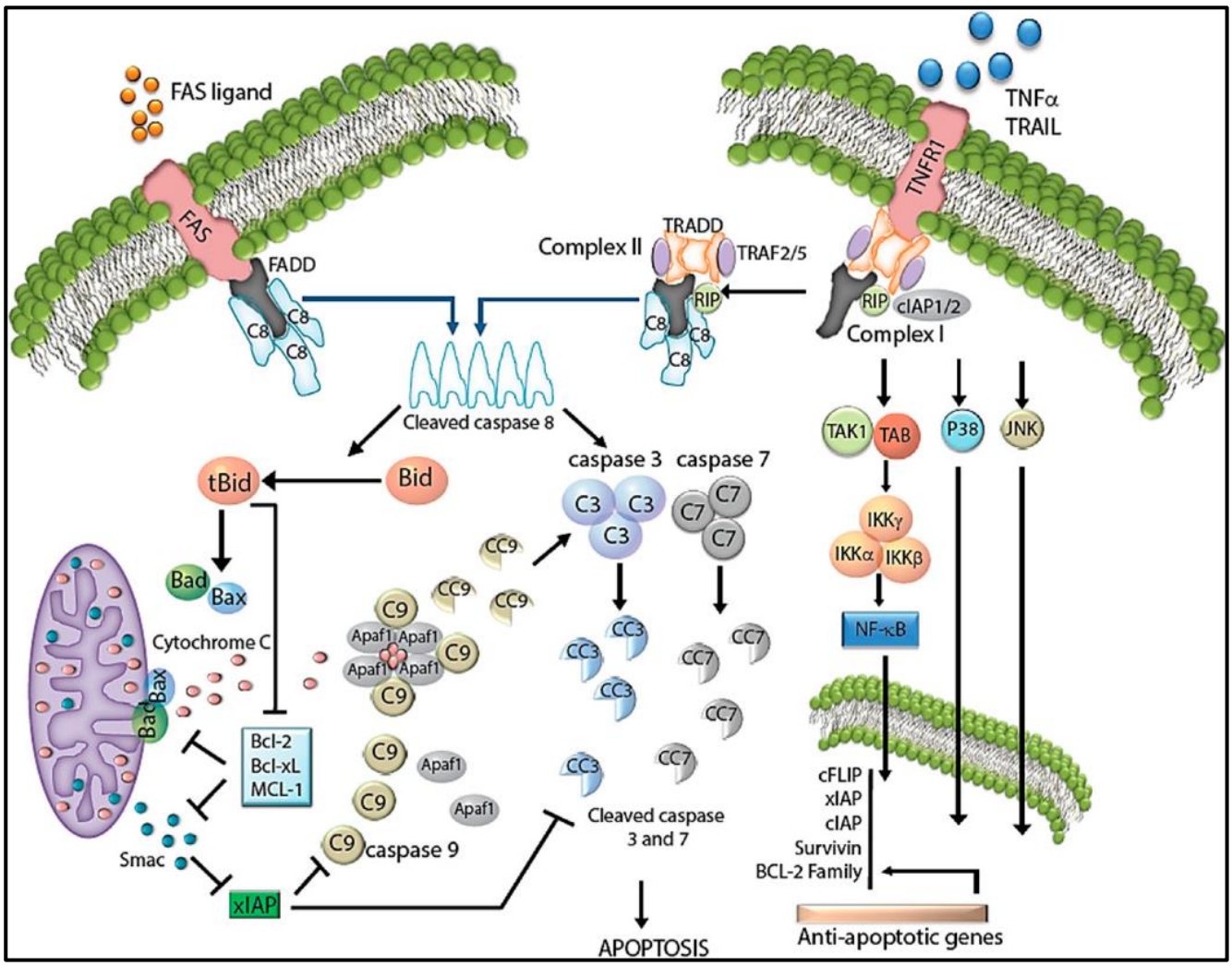

Figure 2.13: Overview of the apoptotic pathways. The death receptor pathway (extrinsic) and mitochondrial-mediated pathway (intrinsic) are linked by caspase-8 cleavage of Bid. The TNF-α death receptor pathway is also shown (Koff *et al*., 2015).

2.5.2 Extrinsic "Death-receptor mediated apoptosis"

The extrinsic pathway (Figure 2.13) transmits extracellular death signals to the intracellular machinery by induced interaction of the TNF superfamily and a specific associated ligand (Cope and Tomei, 1991, Schneider and Tschopp, 2000, Koff *et al.*, 2015). The TNF family include Fas (CD-95), TNF receptor 1 (TNFR1), TNF-related apoptosis-inducing ligand-receptor 1 and 2 (TRAIL1 / 2). The receptors are characterised by distinct motifs such as death domains (DD) and death effector domains (DED). Ligands from TNF family on the cell surface interact with CD-95 and TRAIL receptor to attract DD-containing molecules including Fas-associated death domain protein (FADD) and TNF receptor-associated death domain (TRADD) (Gibson, 2004). Engagement of FADD activates the pro-apoptotic pathway, while TRADD triggers anti-apoptotic signals. The DD/DED of FADD associate with procaspase-8 and procaspase-10 leading to the formation of the death-inducing signaling complex (DISC) in the cytoplasmic compartment (Gibson, 2004). Induced

proximity of these procaspases results in their cleavage and dimerisation to active caspase-8 and caspase-10. The initiator caspase-8 or caspase-10 cleave and activate downstream effector procaspases including caspase-3, caspase-6 and caspase-7 to execute cell death. (Lin *et al.*, 1999, Zhang *et al.*, 2009, Long and Ryan, 2012, Koff *et al.*, 2015). Alternatively, the initiators relay a signal to the mitochondria via the cleavage of the cytosolic BH3-only protein, Bid, to tBid leading to activation of the intrinsic pathway.

In contrast, TRADD binds to and forms a complex with protein including receptor interacting proteins 1 (RIP1), TNF receptor-associated factor 2 (TRAF2), TRAF5 and the inhibitor of apoptosis, protein -1 and -2 (cIAP1/2), this leads to the regulation of pro-survival signals including those mediated by NF-κB, JNK and p38 (Koff *et al.*, 2015). The enzyme cylindromatosis (CYLD) deubiquitinates RIP1 resulting in dissociation of RIP1 and TRADD from complex I leading to the formation of complex II through the binding of RIP1 and TRADD to FADD and caspase-8 or caspase-10 (Li-Weber, 2013, Koff *et al.*, 2015, Kupka *et al.*, 2016).

2.5.3 Execution of cell death

Activation of the execution phase of apoptosis occurs via the extrinsic and intrinsic pathways. The activation of cytoplasmic endonucleases and proteases is facilitated by caspases-3/7 (Festjens *et al.*, 2006, Julien *et al.*, 2017). The cleavage and activation of inhibitor of capsase-3-activated DNase (iCAD) by caspases-3/7 that leaves caspase-activated DNase (CAD) and in apoptotic cells facilitates fragmentation of DNA. Degradation of nuclear material such as lamin, cytoskeletal elements such as Golgi and actin microfilaments is also facilitated by caspases-3/7. Caspases-3/7 also cause cleavage and inactivation of the repair proteins poly (ADP-ribose) polymerase (PARP-1), and externalisation of phosphatidylserine for apoptotic cell recognition. Therefore, caspases-3/7 are vital to the execution of apoptosis since they cause reorganisation of the cytoskeletal structure and the disintegration of cellular contents into apoptotic vesicles (Hassan *et al.*, 2014).

2.6.3.1 Poly (ADP-ribose) polymerase (PARP-1)

Numerous repair proteins including PARP-1 are used when there is DNA damage (Surjana *et al.*, 2010, Nowsheen and Yang, 2012). In response to double or single stranded DNA breaks, PARP-1 binds to damaged DNA through the two-Zinc finger domain situated in the protein's amino terminal area. PARP-1 converts NAD^+ to nicotinamide and ADP-ribose. Elongation and branching of the protein on the glutaminic residue is facilitated where PARP-1 catalyses poly (ADP-ribose) binding. However, during apoptosis the executioner caspases-3/7 cleave PARP-1 at the tetrapeptide carboxyl

cleavage site [(Asp-Glu-Val-Asp) (DEVD)] localised between Gly215 and Asp214 to produce a 89kDa and 24kDa fragment. Zinc promotes the binding of PARP-1 to DNA strand break and inhibit PARP-1 cleavage. The conserved sites such as a Cys-285 and His-237 interact with catalytic function of caspases-3/7 to regulate the Zn inhibition, which allows for PARP-1 cleavage by caspases-3/7 to occur (Kaufmann *et al.*, 1993, Perry *et al.*, 1997, Erener *et al.*, 2012).

Colorectal carcinoma (CRC) continues to present a public health challenge in the southern African region where current cancer treatment is expensive and not easily accessible to the vast majority of patients. *Artemisia afra* is a widely used medicinal plant located in the southern African region that is accessible and affordable. Current literature suggests that *A. afra* possesses anti-cancer potential. This study investigates the anti-cancer potential of *A. afra* crude aqueous leaf extract by determining its antioxidant, anti-inflammatory and apoptotic effects in the Caco-2 cell line.

CHAPTER 3 : MATERIALS AND METHODS

3.1 Materials

The leaves of *A. afra* were secured from the Durban Market (KwaZulu-Natal, SA) and verified by the University of KwaZulu-Natal herbarium. All tissue culture reagents and plasticware were procured from Whitehead Scientific (Johannesburg, South Africa), except for foetal calf serum (FCS) that was obtained from ThermoFisher Scientific (Waltham, Massachusetts, United States). Promega kits and reagents used for luminometry, and Cell Signaling Technology (CST) antibodies were acquired from Anatech (Johannesburg, South Africa). The methylthiazol tetrazolium (MTT salt), phosphate buffered saline (PBS) tablets, bicinchoninic acid (BCA) assay kit, β-actin and acrylamide were bought from Sigma (Johannesburg, South Africa). The lactate dehydrogenase (LDH) cytotoxicity detection kit, protease and phosphatase inhibitors were obtained from Roche Diagnostics (Mannheim, Germany). Western blot reagents were purchased from Bio-Rad (Hercules, CA, USA). Reagents for qPCR were bought from Bio-Rad and the primer sequences were purchased from Inqaba Biotechnologies (Johannesburg, South Africa). All other reagents were obtained from Merck (Johannesburg, South Africa) unless stated otherwise.

3.2 Cell culture

Caco-2 and Hek293 cells were cultured in a 75 cm^2 culture flask reconstituted with 10 ml of complete culture medium [CCM; Dulbecco's Modified Eagle's Medium (DMEM), 10% foetal calf serum (FCS), 1% L-glutamine and 1% penicillin-streptomycin-fungizone and 25mM 4-(2-hydroxyethyl)-1-piperazineethanesulphonic acid) (HEPES) buffer]. The cells were allowed to attach and grow at 37°C with 5% CO_2 and were monitored with constant change of CCM until cell growth reached 90% confluence. Confluent flasks were trypsinised using 1 ml trypsin and counted using the trypan blue exclusion method (150 µl of CCM, 50 µl of trypan blue, 50 µl of cell suspension in a microfuge tube, and 10µl of this mixture was pipetted onto a haemocytometer) for sub-culturing or storage. Cell number was adjusted as required for each assay.

3.3 Extraction and *A. afra* preparation

The *A. afra Jacq.ex wild* plant was verified by University of KwaZulu-Natal Herbarium, Botany Department, Westville Campus. Plant leaves were dried at room temperature (RT) and crushed using a blender. The crude leaf aqueous extract was prepared by adding 20 g crushed leaves to 200 ml distilled water and boiled for 15 minutes. The supernatant was then filtered, transferred into 50 ml

tubes and centrifuged at 3220xg, 20°C, 30 minutes. The upper aqueous layer was aspirated, lyophilized and stored (4°C) until use. A 5000 µg/ml stock solution was prepared, filter sterilised using a 0.45 µM filter (Milipore) and kept at 4°C until use.

3.4 3-4, 5-dimethylthiazol-2-yl)-2, 5- diphenyl tetrazolium bromide (MTT) assay

3.4.1 Principle

The MTT assay measures metabolic activity as an indication of cell viability, proliferation and cytotoxicity. This calorimetric assay involves the conversion of yellow tetrazolium salt to purple formazan crystals by metabolically active cells (Figure 3.1). The reduction of MTT to formazan is facilitated by NAD(P)H-dependent oxidoreductases in viable cells. The coloured solution is obtained by dissolving the insoluble formazan crystals in solubilisation solution such as dimethylsulphoxide (DMSO); then absorbance is measured at 570 nm with reference wavelength 690 nm using the spectrophotometer. In the absence of cells, the MTT reagent yields a low background absorbance. The more intense the solution, the greater the number of viable, metabolically active cells (Mosmann, 1983, Riss *et al.*, 2015).

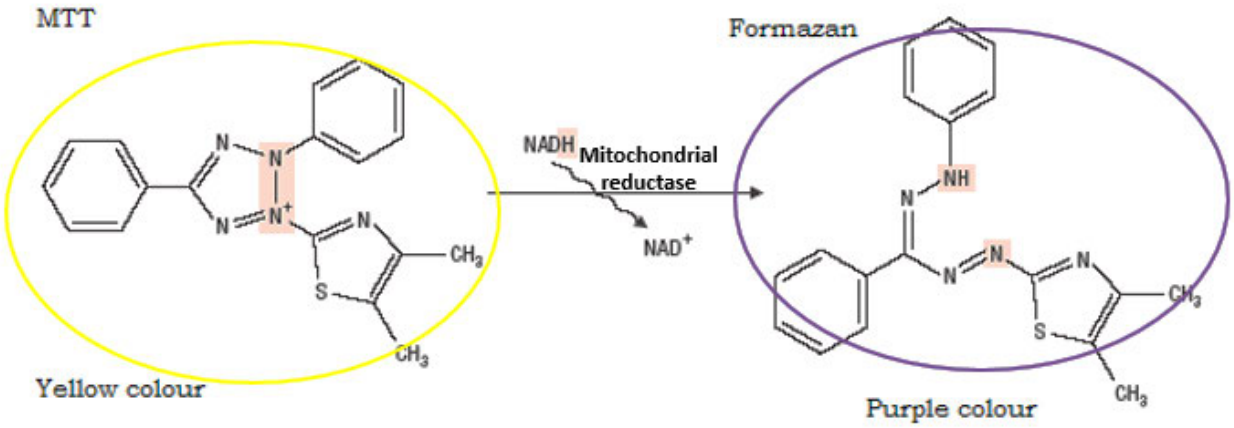

Figure 3.1: Principle of the MTT assay. Metabolism of MTT to a purple formazan salt by viable Caco-2 cells (Prepared by the Author).

3.4.2 Protocol

The MTT calorimetric assay was used to determine *A. afra* crude leaf extract's cytotoxicity on Caco-2 and Hek293 cells. The cells were seeded (20 000 cell/well in 300 µl CCM) in triplicate into a 96-well microtitre plate at (37°C, 5% CO_2), incubated to adhere overnight and treated with a range (0-5 mg/ml) of the *A. afra* extracts in CCM for 48 hours (37°C, 5% CO_2). Following incubation, the

treatment was discarded and replaced with 20 µl MTT salt solution (5 mg/ml in 0.1 M phosphate buffered saline (PBS) (pH 7.4) and 100 µl of CCM dispensed into each well and incubated (4 hours). The MTT solution was then discarded and 100 µl of DMSO was added into the wells followed by incubation for 1 hour. The absorbance was read at 570 nm with reference wavelength 690 nm on a BioTek® µQuant™ microplate reader (Winooski, Vermont, USA). The absorbance was used to calculate cell viability:

$$\text{Cell viability} = \left(\frac{Absorbance\ of\ treated\ cells}{Absorbance\ of\ control\ cells}\right) \times 100$$

GraphPad Prism V5 software (GraphPad software Software Inc. La Jolla, California, USA) was used to determine the half-maximum inhibitory concentration (IC_{50}) by plotting a concentration-response curve. The extrapolated IC_{50} value was used in subsequent assays. Untreated cells served as the control.

3.5 Lactate dehydrogenase assay

3.5.1 Principle

Lactate dehydrogenase (LDH) is an oxidoreductase found in the cytoplasm of all cells. Due to loss of membrane integrity following cellular damage, cell death and inflammation, the LDH may escape the cell's confines and be extruded into the plasma or cell media. The LDH assay quantifies the amount of enzyme released by damaged cells. The LDH activity is indirectly quantifiable; NADH produced during the conversion of lactate to pyruvate interacts with a specific probe to produce a coloured formazan product that can be measured with a spectrophotometer at 450nm (Figure 3.2) (Watanabe *et al.*, 1995, Fiume *et al.*, 2014).

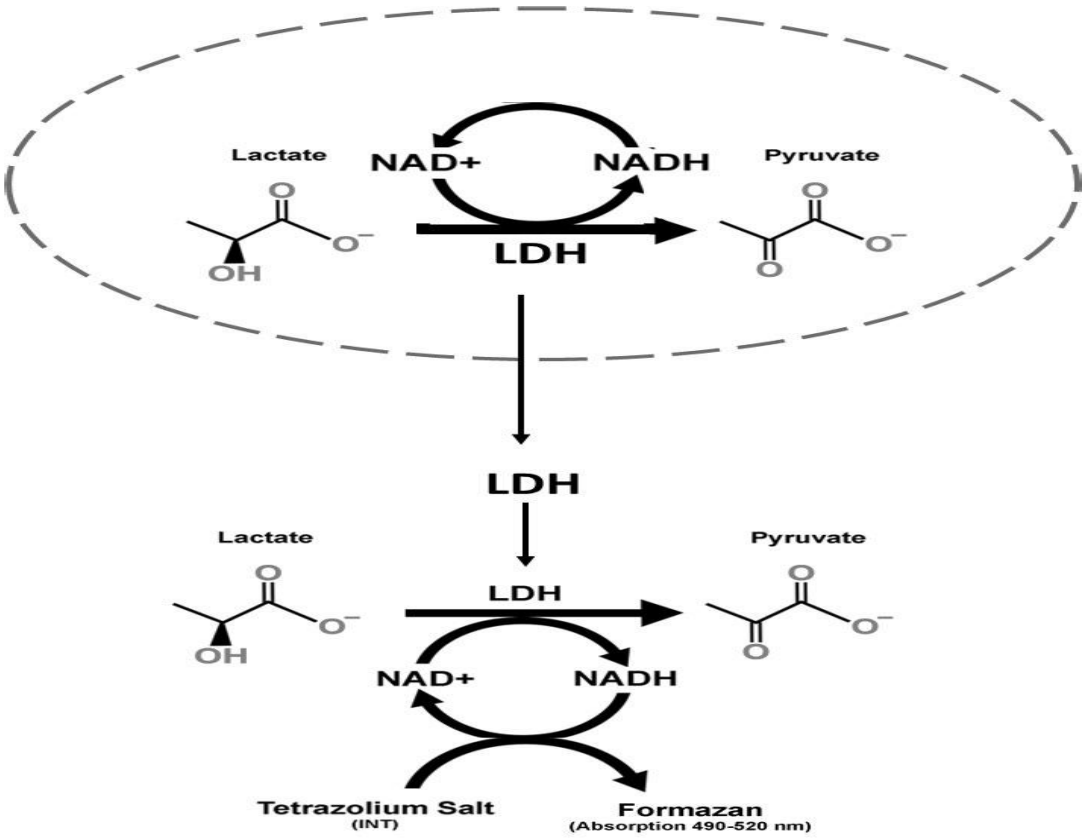

Figure 3.2: Quantification principle for extracellular LDH. Release of LDH from a damaged cell quantified using a tetrazolium-based spectrophotometric assay (Forest *et al.*, 2015).

3.5.2 Protocol

The LDH cytotoxicity detection kit (04744926001) that detects the amount of LDH released by damaged cells was used to quantify LDH levels in the treated cell media. The relevant treatment media (control and IC_{50}) and blank (negative control with CCM only) was added in triplicate into the 96-well microtitre plate (50 µl per well). This was followed by addition of 25 µl of the LDH reagent (buffer and catalyst) and incubated in the dark for 30 minutes at room temperature (RT). Thereafter, 12.5 µl stop solution was added and absorbance was measured at 490 nm with reference wavelength 690 nm using a spectrophotometer (BioTek® µQuant^{TM} microplate spectrophotometer (Winooski, Vermont, USA)). Results were presented as the mean of the absorbance obtained.

3.6 Luminometry

Luminescence involves the emission of light from biological samples that have not been heated as in fluorescence (there is absorption of light and transmission at different wavelength) or phosphorescence (the absorption of light and transmission over a longer period). Luminescence involves two processes: (1) Chemiluminescence - emission of light through chemical reaction with

limited emission of heat (luminescence): $2H_2O$+ luminol + enhancer → $2H_2O$+ *hv* + oxidised luminol. (2) Bioluminescence is the emission of light through the production of enzyme chemical interference. The reaction involves a light emitting pigment known as luciferin and luciferase the enzyme component. The substrate luciferin reacts with oxygen and requires magnesium in the presence of ATP to produce carbon dioxide (CO_2), adenosine monophosphate (AMP) and pyrophosphate (PP) as waste products (Duellman *et al.*, 2015).

Luminescent principles were used to detect and quantify ATP, caspase activity, GSH, externalized phosphatidylserine and mitochondrial membrane potential. The Caco-2 cells were maintained until 80% confluence was reached. Culture medium was removed from the wells and treated as control and IC_{50} for 48 hours. The treated cells were washed with 0.1 M PBS, trypsinised, resuspended and counted for plating in a luminometer plate for each assay.

3.6.1 ATP quantification

3.6.1.1 Principle

The Cell Titre-Glo® assay measures intracellular ATP concentration; the assay buffer contains a lysing solution so that the intracellular ATP released is used in the reaction that converts luciferin to oxyluciferin with the concomitant emission of light (Figure 3.3) (Tahara *et al.*, 2017). The amount of emitted light is directly proportional to the concentration of ATP.

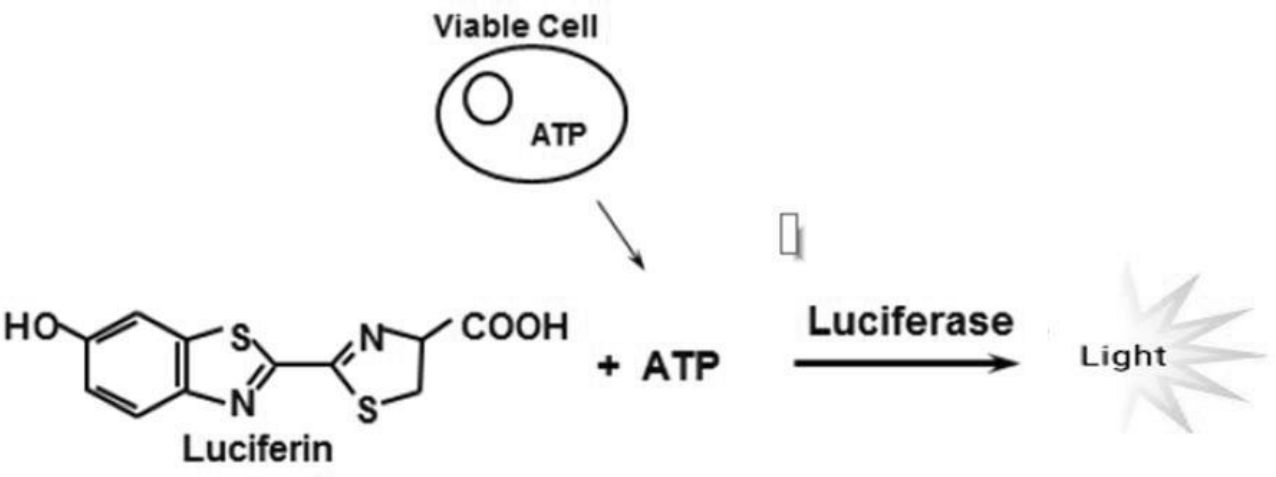

Figure 3.3: ATP quantification using the Cell Titre-Glo® assay. In the presence of ATP, magnesium, and molecular oxygen, luciferase catalyses a bioluminescent process [Adapted from (Riss *et al.*, 2015)].

3.6.1.2 Protocol

The Cell Titre-Glo® assay (CAT#G7570) prepared according to manufacturer's protocol was used to quantify ATP. Briefly, 50 µl of treated cell suspension (20000 cells/well in 0.1 M PBS) was added to an opaque luminometer plate in triplicate for each treatment. Then, 20 µl of the prepared reagent

was added into each well and incubated in the dark for 30 minutes at room temperature, allowing the luciferin-luciferase reaction to proceed. The intensity of light produced by the reaction was quantified using the Modulus™ Microplate luminometer (Turner Biosystems, Sunnyvale, USA). The level of ATP was presented as mean relative light units (RLU).

3.6.2 Caspase quantification

3.6.2.1 Principle

Each Caspase-Glo® assay contains a DEVD-aminoluciferin and a cell lysis reagent that is added to the sample. Substrate lysis will expose the luciferin substrate to the relevant caspase, which cleaves the substrate to release aminoluciferin. The aminoluciferin is subsequently cleaved in the luciferase reaction resulting in a light signal (Figure 3.4) (Sanna *et al.,* 2018). The signal produced is proportional to the caspase activity present.

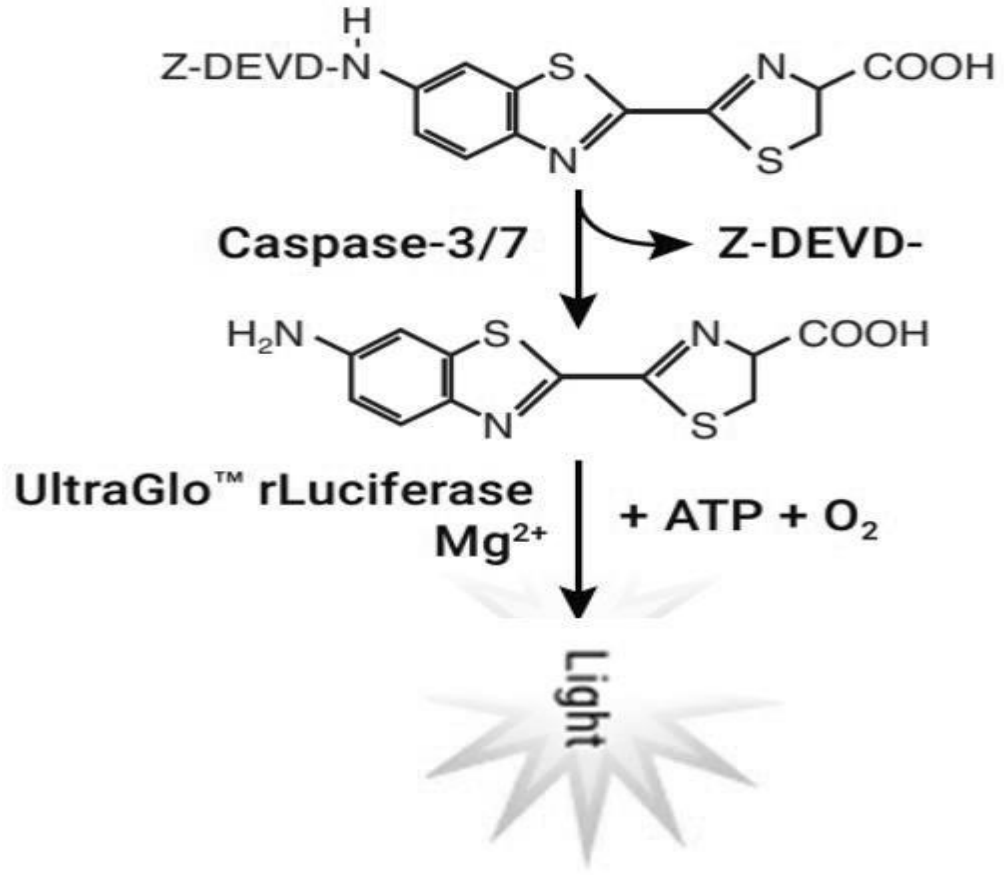

Figure 3.4: The luminescent principle for quantification of caspase activity. Luciferase utilises the aminoluciferin produced by caspase cleavage of Z-DEVD as a substrate. This reaction produces a light signal that is directly proportional to caspase activity in the presence of ATP, oxygen, and magnesium. Caspase-8, caspase-9, and caspases-3/7 activities measured using bioluminescence (worldwide.promega.com, 2019).

3.6.2.2 Protocol

Luminescence-based assay kits (Promega Caspase-Glo®, South Africa) were used to assess the activities of initiator caspase-8 (G8090) and caspase-9 (G8200), and effector caspases-3/7 (G8090) according to manufacturer's instructions. Briefly, the treated cell suspension (20000 cells/well in 50 µl 0.1 M PBS) was dispensed in triplicate in a luminometer plate. Subsequently, 25 µl of caspases-3/7, caspase-8 or caspase-9 reagents were added to respective wells and the suspension was mixed on a plate shaker. The plate was then incubated in the dark for 30 minutes (RT). Samples were analysed using the Modulus^{TM} microplate luminometer (Turner Biosystems, Sunnyvale, USA) and data was presented as mean RLU.

3.6.3 GSH quantification

3.6.3.1 Principle

The GSH-Glo^{TM} assay is based on GSH conversion of the luciferin derivative to luciferin in a reaction catalysed by glutathione-S-transferase (GST) (Murphy *et al.,* 2008). The reaction is coupled with luciferase to produce a signal (Figure 3.5) that is proportional to the amount of GSH in the sample.

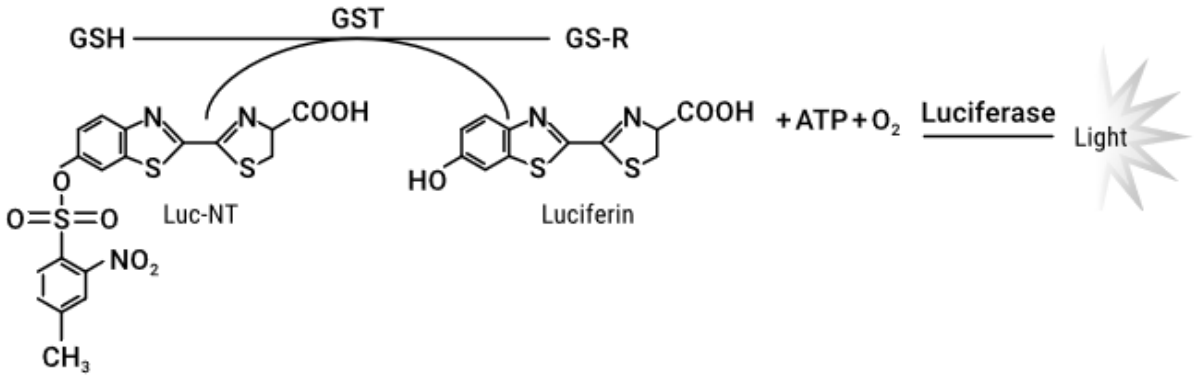

Figure 3.5: Luminescence-based principle for GSH concentration. In the presence of GST, the luminescent representation for the quantification and detection of GSH in cells, luciferin derivative, is transformed to luciferin (worldwide.promega.com, 2015).

3.6.3.2 Protocol

The GSH assay was performed according to the manufacturer's guidelines. The 96-well luminometer plate was seeded with 20000 treated cells per well in triplicate for each treatment. Thereafter, 25 µl of prepared 2X GSH-Glo reagent was added to each well and mix gently on plate shaker, followed by incubation period at RT for 30 minutes in the dark, then 50 µl of Luciferin Detection Reagent was added to each well and mixed on a plate shaker. After a further 15-minutes incubation, the

luminescence was read on a Modulus™ microplate luminometer (Turner Biosystems, Sunnyvale, USA). Data was presented as mean RLU.

3.6.4. Phosphatidylserine (PS) quantification

3.6.4.1 Principle

Phosphatidylserine (PS) exposure on the cell membrane's outer surface is a robust, well-validated method of determining apoptosis, and necrotic cells can be distinguished from apoptotic cells using propidium iodide (PI), which penetrates and intercalates with DNA in dead or non-viable cells (Figure 3.6) (Crowley *et al.*, 2016). The RealTime-Glo™ Annexin V Apoptosis and Necrosis Assay detects Annexin V binding to externalised PS using a simple luminescence signal, and a fluorescence signal created following PI attachment identifies necrotic cells (Crowley *et al.*, 2016).

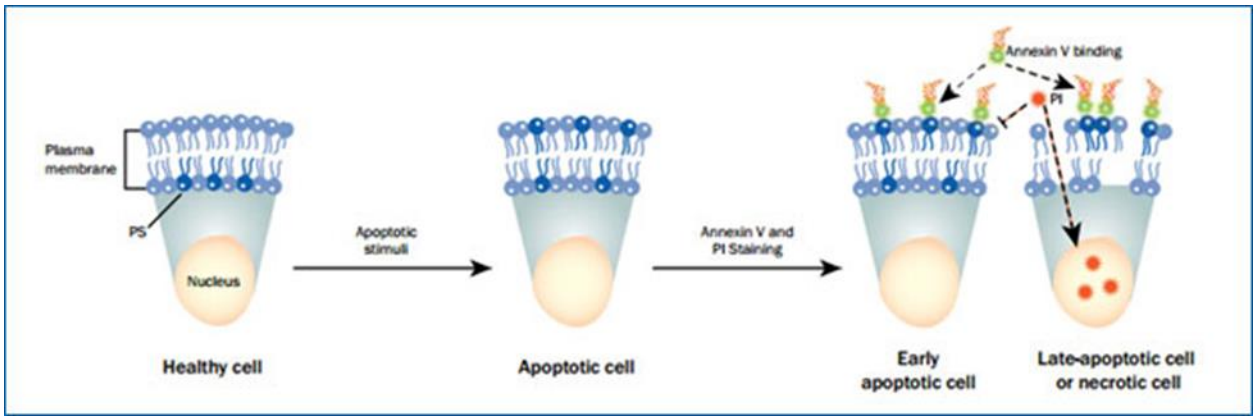

Figure 3.6: Differentiation of apoptotic and necrotic cells using the RealTime-GloTM Annexin V Apoptosis and Necrosis Assay. Propidium iodide attaches to DNA in non-viable cells and creates a detectable fluorescence, whereas Annexin V binds to externalised phosphatidylserine to discriminate early apoptotic cells (Novus, 2021).

3.6.4.2 Protocol

For each treatment, Caco-2 cell suspension was seeded in triplicate into a white, opaque 96-well luminometer plate at a density of 20000 cells/well for 24 hours at 37°C. The cells were treated with 300 µl of each of the following treatments: Untreated cells (C) and treated cells by with IC_{50} were incubated for 48 hours at 37°C. Apoptosis and necrosis was determined in treated cells using the RealTime-Glo™ Annexin V Apoptosis and Necrosis Assay (JA1011, Promega, USA). The 2X Detection Reagent components were thawed at room temperature, and the 2X Detection Reagent was made in a 1 ml microfuge tube by a 500-fold dilution with 0.1 M PBS (pH 7.4). The Annexin V NanoBiT® substrate (1 µl) was added into a 1 ml microfuge tube containing 500 µl of 0.1 M PBS (pH 7.4) and vortexed immediately. Thereafter, 1 µl $CaCl_2$ was added and vortexed followed by the

addition of 1 µl Necrosis Detection Reagent. The mixture was vortexed, then 1 µl Annexin-V SmBiT and Annexin-V LgBiT (1 µl) were added, which were then inverted and stored on ice until needed. Each well was filled with 2X Detection Reagents (25 µl/well) and incubated for 30 minutes at room temperature. The Annexin-V apoptosis luminescence signal was measured using the Modulus™ microplate luminometer (Turner Biosystems, Sunnyvale, California, USA) and reported as RLU.

3.6.5 JC-10 assay

3.6.5.1 Principle

The cationic, lipophilic dye JC-10 can be used to measure the mitochondrial membrane potential (Δψm). The JC-10 exhibits a green fluorescence when the Δψm is low whereas it also emits green-orange fluorescence when the Δψm is high (Zorova *et al.*, 2018). JC-10 monomers are measured with a blue filter (excitation wavelength 488 nm, emission wavelength 529 nm) is directly proportional to the concentration fluorescence.

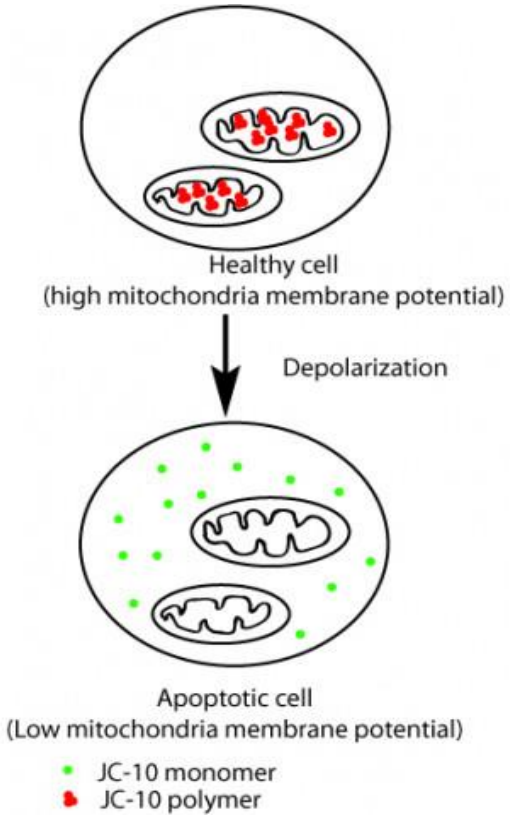

Figure 3.7: Determination of mitochondrial membrane potential using the JC-10 cationic dye. Following the JC-10 mitoscreen, different results were obtained in healthy and defective mitochondria (www.gbiosciences.com, 2022).

3.6.5.2 Protocol

The Δψm was measured using the JC-10 stain (CAT#786-1541) (Zorova *et al.*, 2018). Briefly 50 µl of treated cell suspension (20000 cells/well in 0.1 M PBS) was added to an opaque luminometer plate. Then, 25 µl of prepared reagent was added into each well and incubated in the dark for 30 minutes at RT. The intensity of fluorescence emission produced by the reaction was quantified on a Modulus™ microplate reader (Turner Biosystems, Sunnyvale, USA). The Δψm of the Caco-2 cells was expressed as the fluorescence intensity ratio of JC-10 aggregates and JC-10 monomers.

3.7 TBARS assay

3.7.1 Principle

The short half-life of most ROS makes direct quantification difficult, therefore macromolecule damage produced by oxidants is often used to assess oxidative stress. Malondialdehyde is produced when polyunsaturated fatty acids undergo lipid peroxidation and is a marker for oxidative stress. Lipid peroxidation may be assessed by the reaction of MDA with thiobarbituric acid / butylated hydroxytoluene (TBA-BHT) to form a colorimetric product proportional to the MDA present. Butylated hydroxytoluene (BHT) is used to protect the undamaged lipids from the assay's artificial peroxidation. This takes place when MDA forms a 1,2-adduct with TBA at high temperature and low pH, resulting in a pink chromogen measured at absorbance of 532 nm (Figure 3.8). A negative control accounts for the background interferences. Positive control act as a reference point of whether the experiment worked or not. Butanol was used to separate phases to distinguish between a solvent and a precipitation. The mean MDA concentration was determined by dividing the absorbance means by the absorption coefficient, 156 mM^{-1} (Fernández *et al.*, 1997, Ayala *et al.*, 2014).

$$[MDA] = \frac{Mean\ absorbance}{156\ mM^{-1}}$$

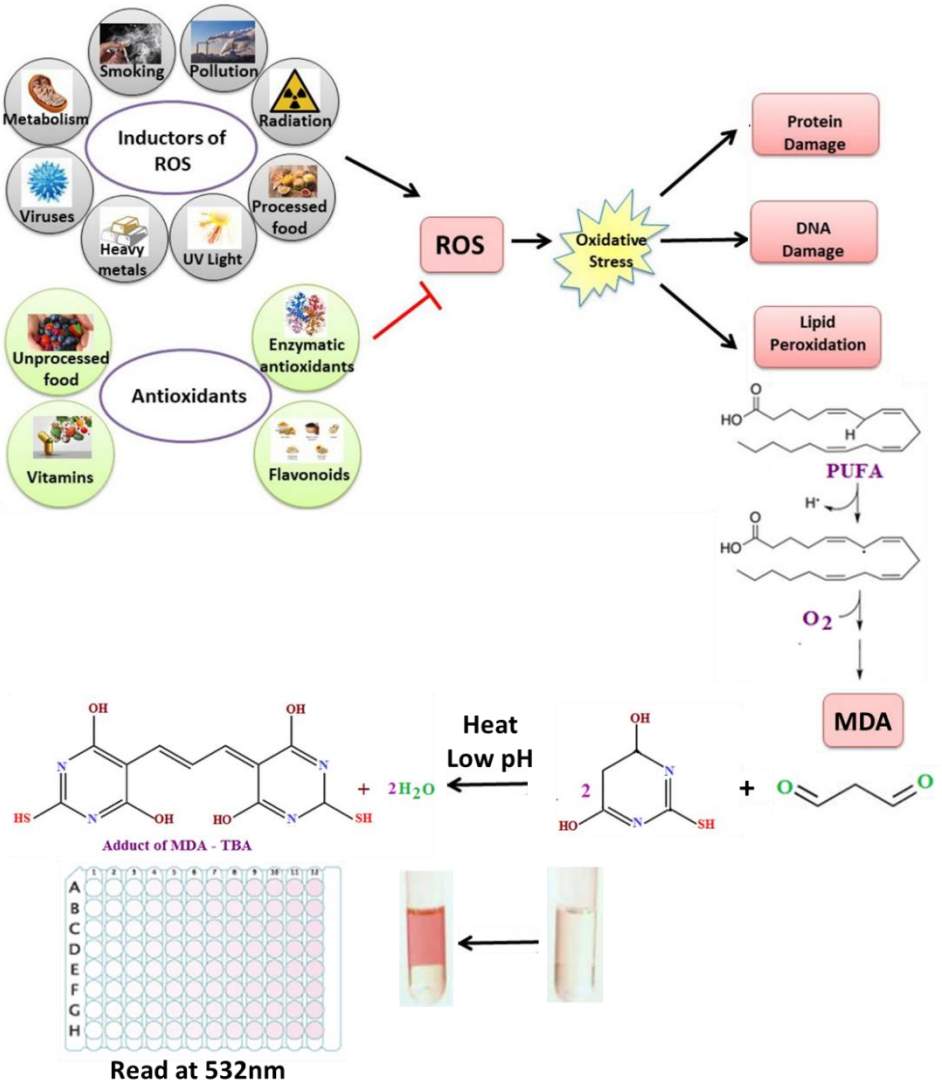

Figure 3.8: A schematic diagram shows how ROS generation leads to the formation of lipid peroxidation and how it is detected using MDA product detected at 532 nm (Modified from www.rndsystems.com and prepared by the author).

3.7.2 Protocol

Lipid peroxidation, assessed by measuring MDA concentration in the treatment medium, was used as an indication of oxidant concentration. Four glass test tubes were prepared containing 400 µl of the treatment medium (untreated control and IC_{50} respectively) and method controls (positive control containing 400 µl CCM and 1 µl MDA, and a negative control containing CCM only). A 7% phosphoric acid solution (200 µl) was added into each test tube, then 200 µl TBA/BHT solution was added to all test tubes except the negative control. The negative control tube was further supplemented with 200 µl of 3 mM HCl. The samples were vortexed to mix them properly for 1 minute each and 200 µl of 1 M HCl was added to each test tube. All samples were placed in a water bath at 100°C for 15 minutes and removed to facilitate cooling at RT. Butanol (1500 µl) was added to the cooled test tubes, then each sample was vortexed for 30 seconds to elicit separation of two phases within samples.

The upper butanol phase (500 µl) containing MDA was pipetted into microfuge tubes and 100 µl was transferred into a 96-well microtitre plate in triplicate. The absorbance was measured at 532 nm with reference of 600 nm using a BioTek® µQuant™ microplate reader (Winooski, Vermont, USA). Data was presented as MDA concentration (µM).

3.8 Nitrate assay

3.8.1 Principle

Nitric oxide plays a key role in inflammation, immunological response, and cell communication (Förstermann and Sessa, 2012). Endogenous NO is synthesised from L-arginine by NOS. Due to the short half-life of NO, nitrate and nitrite are used to indirectly assess NO concentration. For the colorimetric assay, the nitrate reduction to nitrite that is usually facilitated by the enzyme nitrate reductase in living cells is accomplished by vanadium (III) chloride (VCl_3) (Figure 3.9). The acidified nitrite reacts with sulfanilic acid (SULF) to form a complex known as diazonium ion (nitrite-sulfanilic acid) which then reacts with N-(1-naphthylethylenediamine (NEDD) to form chromaphoric azo-derivatives (Figure 3.9). The azo dye product measured at absorbance of 540 nm/690 nm indicates the presence of nitrate when it changes in colour to a pink dye (Bryan and Grisham, 2007).

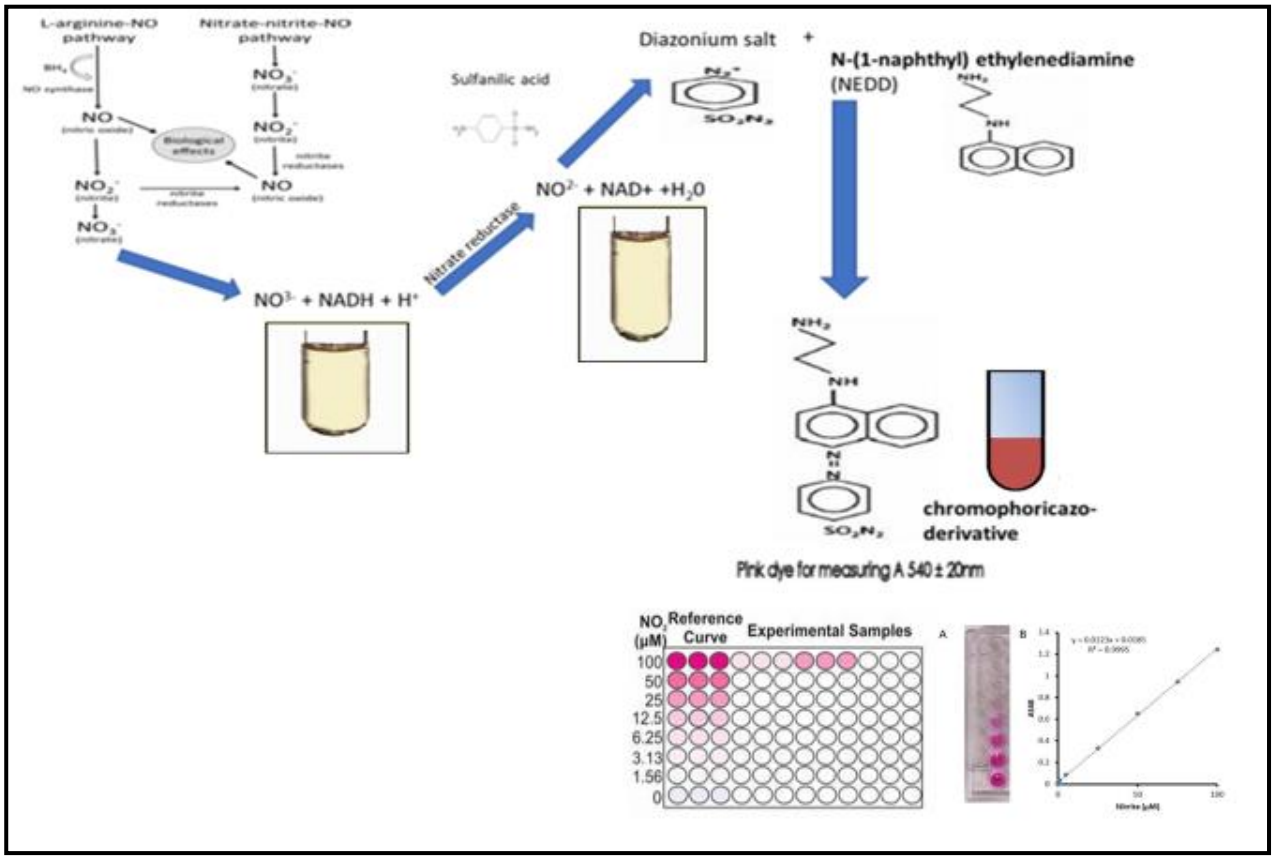

Figure 3.9: Nitrate reduction pathway resulting in the formation of chromophoric azo-derivative that is measured spectrophotometrically. Nitrates are reduced by vanadium chloride, then react with sulfanilic acid

(SULF) and N-(1-naphthyl) ethylenediamine (NEDD) in the Griess reaction to produce a pink chromagen (prepared by author).

3.8.2 Protocol

The NO concentration was indirectly assessed using the nitrate reduction assay. Standard sodium nitrate solutions (0 - 200 µM) were prepared from a 1000 µM stock, and 50 µl of each standard was added into the 96-well microtitre plate in triplicate. After adding 50 µl of each sample into the respective wells in triplicate, VCl_3 was added to each well. Then 25 µl of SULF and 50 µl of NEDD was added to each well in quick succession, and the plate was incubated for 45 minutes (dark, 37^{o}C). The absorbance was read at 540 nm (reference 600 nm) with a BioTek® µQuant^{TM} microplate reader (Winooski, Vermont, USA). Data was presented as nitrate concentration (µM) extrapolated from the standard curve.

3.9 Single cell Gel Electrophoresis (SCGE) or "Comet" assay

3.9.1 Principle

The comet assay is a technique used to assess and quantify DNA damage in individual cells (single or double strand breaks, alkali labile sites, crosslinks, base pair damage and apoptotic nuclei). The cells are fixed in low melting point agarose; these cells require lysis in non-ionic detergent to expose the negatively charged DNA fragments to alkaline conditions (Figure 3.10). The DNA supercoil unwinds under these conditions, and will migrate through the agarose gel in response to an electric field (Figure 3.10) (Singh *et al.*, 1988, Matassov *et al.*, 2004). The distance of the migration depends on the amount of DNA damage. The cells are stained with gel red to facilitate visualisation using a fluorescence microscope. Normal cells contain an intact core of DNA, while those with DNA damage will resemble a comet whose tail length is directly proportional to the amount of DNA damage (Figure 3.10) (Choucroun *et al.*, 2001, Olive and Banáth, 2006).

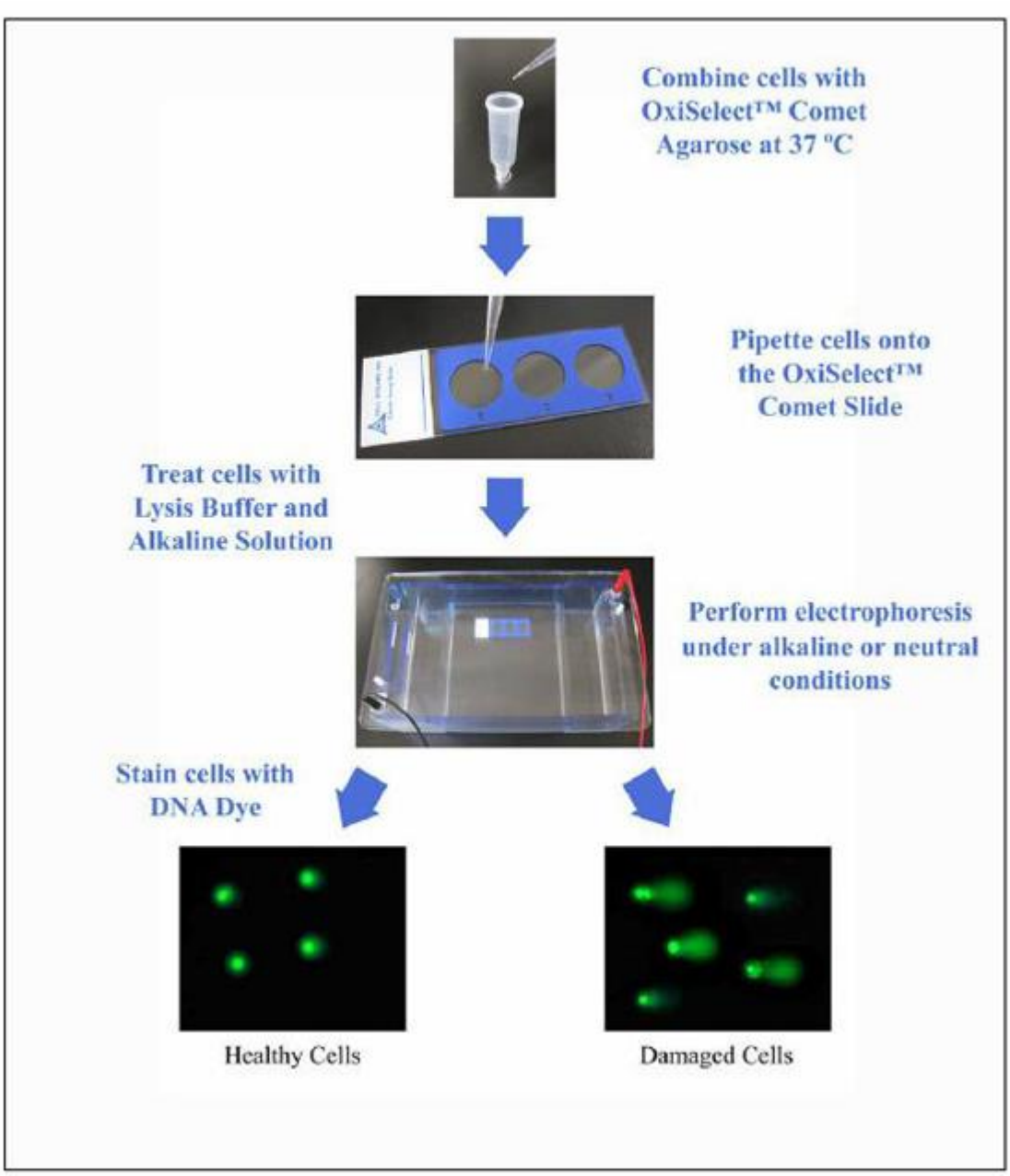

Figure 3.10: Principle of the SCGE assay: Electrophoresis under alkaline conditions results in undamaged DNA remaining tightly coiled, while fragmented DNA migrate out of the nucleus to the anode resulting in a 'comet like' structure (Ostling and Johanson, 1984, Olive and Banáth, 2006).

3.9.2 Protocol

The comet assay was used to detect damaged DNA in Caco-2 cells after treatment with *A. afra* crude aqueous leaf extract. Low melting point agarose (LMPA) was used to encapsulate the cells. Microscope slides with frosted ends per control and treatment were prepared in duplicate. The first layer contained 2% LMPA (700 µl, 37ºC) that formed a thick supporting base layer when solidified at 4ºC for 10 minutes. The second layer that included cell suspension (20000 cells in 50 µl of 0.1 M PBS), GelRed™ (#41003) nucleic acid gel stain (2 µl) and 1% LMPA (550 µl, 37ºC) was overlayed on the base and incubated for 10 minutes at 4ºC.

Subsequent addition of a third layer containing 1% LMPA (300 µl, 37ºC) set for 10 minutes at 4ºC. Permeation of fragmented DNA out of the nucleus involves cell lysing, therefore the coverslips were removed, and solidified gels were submerged into cold cell lysis buffer (100 mM EDTA, 2.5 M NaCl, 1% Triton X-100, 10% DMSO and 10 mM Tris (pH 10) and incubated for 1 hour at 4ºC in the dark. Thereafter, the slides were submerged in electrophoresis buffer [1 mM Na_2EDTA (pH 13) and 300 mM NaOH] for 20 minutes (RT) to allow equilibration before electrophoresis (300 mA, 25 V, 35 minutes) using a Bio-Rad compact power supply (Bio-Rad, Hercules, California, United States). After electrophoresis the slides were washed three times (5 minutes each) with 0.4 M Tris (pH 7.4) to remove detergents, alkali and neutralise samples. This was followed by visualisation using a fluorescence microscope (Olympus IX51 inverted microscope) which had excitation at 510-560 nm and emission at 590 nm; 50 comets were captured in each slide per control/per treatment. The length of cells and comet tails were measured using soft imaging system (Life Science Olympus soft imaging solution V5) and were reported in µM as average tail lengths.

3.10 Quantitative Polymerase Chain Reaction (qPCR) Assay

3.10.1 Principle

PCR is a sensitive, specific technique that can be used for the amplification and detection of nucleic acid sequences. In qPCR, the amplification of DNA is measured in real time, as the reaction proceeds (Garibyan and Avashia, 2013). The technique requires the following components: a DNA target sequence to be amplified; forward and reverse primers that are complementary to the 3′ ends of the forward and reverse strands of the target sequence, Taq DNA polymerase which catalyses the DNA synthesis process, deoxy nucleoside triphosphates (dNTPs) that are used to synthesise new strands of DNA and $MgCl_2$ which acts as a DNA stabiliser and is required for optimal functioning of Taq polymerase (Garibyan and Avashia, 2013). A DNA-binding dye such as SYBR green is incorporated into the qPCR reaction; the dye binds to DNA as amplification occurs and emits fluorescence as the cycle progress. In addition, a house-keeping gene is detected with the targeted gene in qPCR to provides a control by which to measure the quantity of the amplified target gene (Figure 3.11).

Since the actual PCR reaction involving denaturation, annealing and extension steps is used to amplify DNA, RNA-based PCR requires that the RNA sample is reverse-transcribed to complementary DNA (cDNA) using reverse transcriptase (Figure 3.11) (Garibyan and Avashia, 2013). To begin the PCR reaction, the temperature is raised to 95ºC so that denaturation can take place. This step ensures that the double stranded DNA (dsDNA) is “melted” into single strand DNA

(ssDNA). The annealing step involves lowering the temperature to ±55°C to allow the primers to bind to the targeted gene (Garibyan and Avashia, 2013). Primer binding provides DNA polymerase with foundation to begin copying the DNA strand. The polymerase used is Taq polymerase, from bacteria *Thermus aquaticus.* Taq polymerase is a thermostable enzyme that catalyses the synthesis of new DNA strands. However, the optimum functioning temperature for Taq polymerase is 72°C, the temperature is raised to 72°C in the extension step to facilitate DNA synthesis (Garibyan and Avashia, 2013). These three steps conclude one cycle of a PCR reaction. This cycle is repeated 30 to 40 times to achieve sound amplification of the target sequence. Computer-generated software is used to calculate relative gene expression in a qPCR reaction (Figure 3.11).

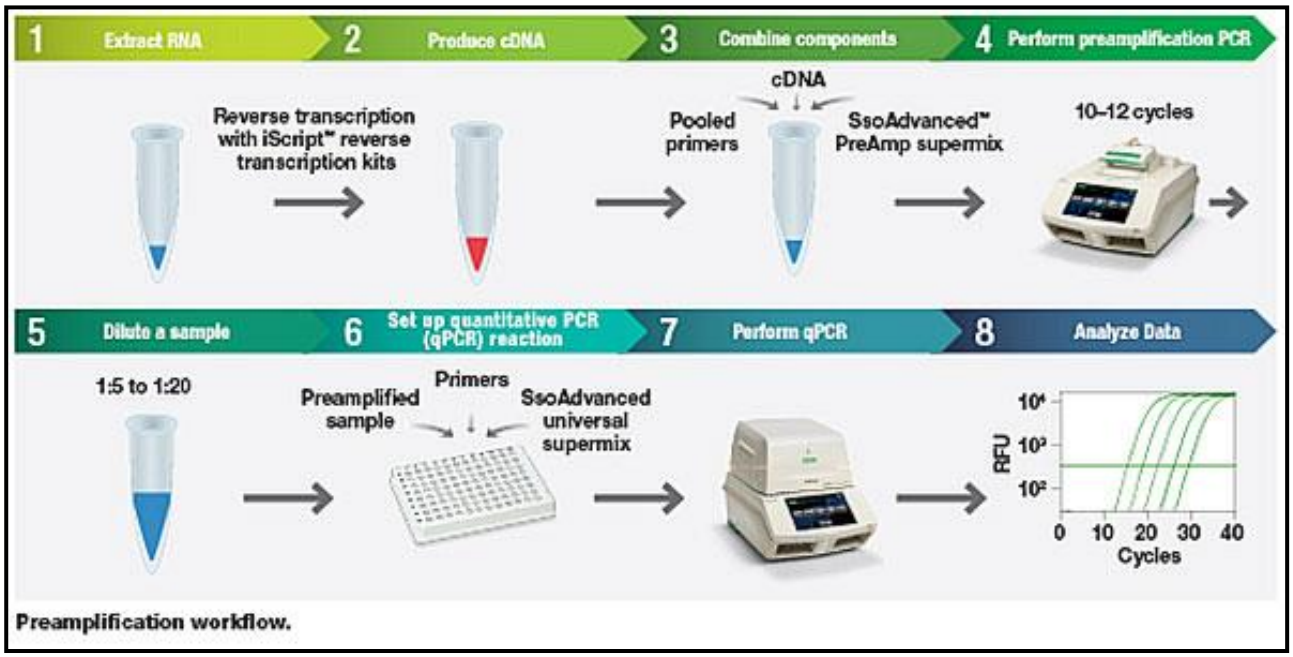

Figure 3.11: The qPCR procedure from mRNA extraction to amplified gene product (www.bio-rad.com, 2022).

qPCR allows for the amplification and simultaneous quantification of the target gene in the sample. Firstly, RNA must be isolated and synthesised single stranded complementary DNA (cDNA) by reverse transcription. This cDNA is then used for the qPCR reaction that incorporates a DNA-binding dye to facilitate quantification of the target gene expression.

3.10.2 Protocol

3.10.2.1 RNA extraction

RNA was isolated following an in-house protocol using Trizol. This is important as Trizol degrade cells without damaging the RNA. Trizol reagent (500 µl) was added to each flask and incubated (4°C, 10 minutes). Cells were removed from flasks, transferred to microfuge tubes and stored in Trizol at -

80°C overnight. Chloroform (100 µl) was added to thawed samples and incubated at RT for 3 minutes. Thereafter, cell suspensions were centrifuged (12000 x g, 4°C, 15 minutes) and the aqueous phase was removed. Thereafter, 250 µl isopropanol was added and samples were left overnight at 80°C. Samples were thawed and centrifuged (12000 x g, 4°C, 20 minutes). The supernatant was discarded, and the retained pellet was washed with 75% cold ethanol (500 µl) then centrifuged at 7400 x g (4°C, 15 minutes). Ethanol was removed and samples were allowed to air dry. The pellet was resuspended in nuclease-free water (15 µl) and incubated (RT, 3 minutes). The RNA was quantified using the Nanodrop2000 spectrometer (Thermo-Fisher Scientific) and the A_{260}/A_{280} ratio was used to assess the RNA integrity. The concentration of RNA was standardised to 1000 ng/µl and used to prepare cDNA.

3.10.2.2 cDNA synthesis

The standardised RNA was used to synthesise cDNA using the iScript cDNA synthesis Kit® (CAT#1708891) (Bio-Rad, Hercules, California, USA) as per the manufacturer's instructions. Briefly, tubes were prepared for each sample and a reaction mix (4 µl 5x iScript reaction mix, 1 µl iScript reverse transcriptase, 11 µl nuclease-free water) was prepared for each sample. After adding 4 µl of each RNA sample to the individual tubes, the tubes were transferred to a thermocycler (GeneAmp®PCR System 9700, Applied Biosciences, Waltham, Massachusetts, USA) for 35 minutes (5 minutes at 25°C, 25 minutes at 42°C and 5 minutes at 85°C). Nuclease free water (80 µl) was added to each sample, the cDNA was stored at -80°C.

3.10.2.3 qPCR

Gene expression was analysed using the iScript SYBR® Green PCR kit (CAT#1725121) (Bio-Rad, Hercules, California, USA). Each reaction volume totaled 13 µl (SYBR Green, forward primer, reverse primer, nuclease-free water and cDNA sample) following manufacturer's protocol. This assay was carried out using 3 replicates per treatment and GAPDH as a house-keeping gene. The initial denaturation occurred at 95°C (4 minutes), followed by 40 denaturation cycles (95°C, 15 seconds). An annealing step was then carried out for 40 seconds dependents on each gene's specific annealing temperatures (Table 3.1). An extension step occurred (72°C, 30 seconds), followed by a plate read of 40 cycles (CFX96 Touch™ Real-Time PCR detection System, Bio-Rad, Hercules, California, USA). The method described by Livak and Schmittgen (2001) was employed to determine the changes in relative mRNA expression, where $2^{-\Delta\Delta Ct}$ represents the fold change observed in mRNA expression (Garibyan and Avashia, 2013).

Table 3.1: Annealing temperatures of target genes

Gene	Primer sequences	Annealing temperatures
OGG1	Forward 5′GCATCGTACTCTAGCCTCCAC3′ Reverse 5′AGGACTTTGCTCCCTCCAC3′	60^{o}C
TNF-α	Forward 5′CAGAGGGAAGAGTTCCCAG3’ Reverse 5′CCTTGGTCGGTAGGAGACG3′	60^{o}C
CAT	Forward 5′TAAGACTGACCAGGGCATC-3′ Reverse 5′CAACCTTGGTGAGATCGAA3′	60^{o}C
GPx1	Forward 5′GACTACACCCAGATGAACGAGC3′ Reverse 5′CCCACCAGGAACTTCTCAAAG3′	58^{o}C
SOD2	Forward 5′GAGATGTTACACGCCCAGATAGC3′ Reverse 5′AATCCCCAGCAGTGGAATAAGG3′	57^{o}C
C-Myc	Forward 5′AGCGACTCTGAGGAGGAACAAG3′ Reverse 5′GTGGCACCTCTTGAGGACCA3′	60^{o}C
NF-κB	Forward 5′GACCTGAATGCTGTGCGGC3′ Reverse 5′ATCTTGAGCTCGGCAGTGTT3′	52.6^{o}C
NRF2	Forward 5′AGTGGATCTGCCAACTACTC3′ Reverse 5'CATCTACAAACGGGAATGTCTG3'	
GAPDH	Forward 5'TCCCTGAGCTGAACGGGAAG3' Reverse 5'GGAGGAGTGGGTGTCGCTGT3'	58^{o}C

3.11 Western blotting

3.11.1 Principle

Western blotting (protein blotting or immunoblotting) is used to analyse and detect the expressed proteins' characterisation (Roy *et al*., 2019). This is a rapid and sensitive assay based on immunochromatography where proteins are separated in the SDS-PAGE gel according to their molecular size (Figure 3.12). The isolated protein is then electrophoretically transferred onto nitrocellulose/PVDF membrane where they are detected through specific primary antibody and secondary (HRP-labelled) enzyme label antibody (Figure 3.12). The blot membrane is incubated with chemiluminescent HRP substrate and exposed to film (Figure 3.12). In this study, western blotting will be used to quantify the expression of apoptotic and antioxidant proteins.

.

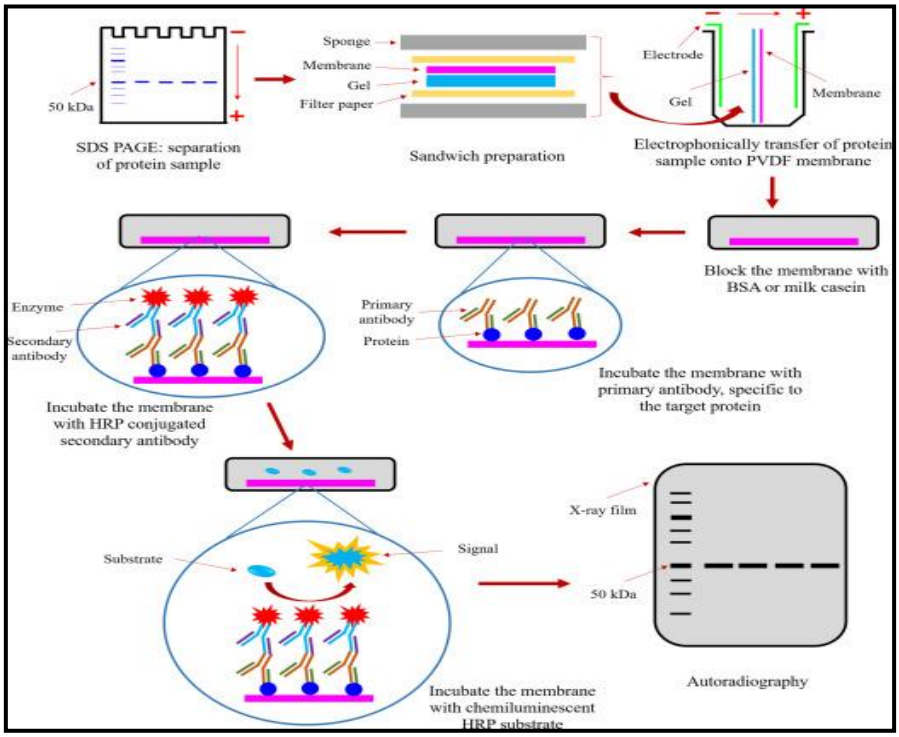

Figure 3.12: Western blotting procedure showing protein separation, transfer and immunoblotting. To quantify and analyse the expression apoptotic and oxidative associated proteins, via western blotting assay (Roy *et al.*, 2019).

3.11.2 Protocol

Western blotting was used to analyse, detect, and quantify specific proteins' expression in a homogenous sample. The quantity of proteins is relatively proportional to the bandwidth, which is expressed as a band. Confluent flasks containing Caco-2 cells were plated and treated as previously described in MTT assay. The treatment media was discarded from the flask, which were then washed with 0.1 M PBS. Briefly, 300 µl of cystobuster^{TM} (71009) containing phosphatase and protease inhibitors was added to each flask to extract total protein. A cell scraper was used, after 15 minutes on ice to scrape cells and transfer all the sample solution to a microfuge tube. The sample solution was centrifuged (4°C, 2000xg for 5 minutes) to separate the crude protein extract (supernatant).

The BCA assay was used to quantify the supernatant containing crude protein. Standards (0-1 mg/ml in PBS) of bovine serum albumin (BSA) were determined using samples' concentration. Briefly, 25 µl of model and standards were pipetted in duplicate into a 96-well microtitre plate. A 200 µl of volume BCA working solution (198 µl BCA: 4 µl $CuSO_4$ per reaction) was added to each well, followed by incubation at 37^{o}C for 30 minutes and an absorbance was measured at 562 nm using BioTek® µQuant^{TM} microplate reader. The crude protein concentration for each sample from the

standard curve was generated by OD. The samples were standardised to a 1.8 µg/ml concentration using cytobuster.

Laemmli buffer [1 M Tris (pH 7.4), glycerol, SDS, β-mercaptoethanol, bromophenol blue dye] was added to the standardised protein samples, which were then heated for 5 minutes at 100°C. The samples were cooled to RT and stored at -80°C until required. The mini-PROTEAN 3 SDS-PAGE apparatus were assembled according to the manufacturer guidelines. The gels were prepared as follows: 10% resolving gel [dH_2O, bisacrylamide, 1.5 M Tris (pH 7.4), 10% w/v SDS, 10% APS and TEMED] and 4% stacking gel [dH_2O, 0.5 M Tris (pH 7.4), 10% SDS, bisacrylamide, 10% APS and TEMED]. The electrophoretic tank was filled with 1X electrode buffer [dH_2O, Tris, glycine, SDS; pH 8.3] and denatured proteins (25 µl) and molecular weight marker (5 µl) were loaded per well. Electrophoresis was initiated at 150 V for 90 minutes until the tracker dye reached the gel's bottom using a Bio-Rad® compact power supplier.

The transfer buffer [25 mM Tris (pH 7.4), 192 mM glycine, 20% v/v methanol; pH 8.3] was used to equilibrate electrophoresed, nitrocellulose and blotting pads for 10 minutes. The Bio-Rad Trans-Blot® Turbo™ cassette was assembled for gel sandwich and a current (25 V, 2.5 mA) was applied for 30 minutes. The nitrocellulose membrane was transferred and blocked by 5 ml of blocking solution (5% BSA in TTBS); NaCl, KCl, Tris (pH 7.4) with Tween-20) for 2 hours at RT on a shaker. The membrane was incubated at RT for 1 hour for consistency in 5 ml of primary antibody Bax (5023), cPARP (9541), cIAP1 (7065), p-p38 MAPK (4511), HSP27 (2402), xIAP (14334), CAT (12980), Bcl-2 (15071), iNOS (13120), SOD2 (13141), p-pRb (8516), pRb (9313), pSTAT-3 (9145), STAT-3 (4904), JNK (9252), pJNK (9251), pERK (8544), ERK (4348), HSP70 (46477), Nrf2 (12721), GPx-1 (3286), c-Myc (9402), anti-rabbit IgG HRP-linked Ab (7074) and anti-mouse IgG HRP-linked (7076)] in 5% BSA in TTBS (1:1000 dilution) on a shaker for 1 h and then left overnight at 4°C. The membrane was allowed to reach RT for 1 hour on shaker and primary antibody removed, then washed with TTBS (10 ml) for 5x for consistency and then probed with secondary antibody [(anti-rabbit IgG (97074S) or anti-mouse IgG (970746)] in 5% BSA in TTBS (1:1000) for 2 hours at RT on a shaker. The membranes were washed with TTBS (10 ml) 5x and rinsed with distilled water. Chemiluminescence reagent (mixed luminol/enhancer and peroxide buffer in 1:1 ratio, each 200 µl) was added to the membrane to identify proteins of interest using a gel documentation system Molecular Image®Chemidoc^{TM}XRS + and Bio-Rad imaging system to express bands. The bands were further analysed by Image Lab software (6.0.1) by Bio-Rad. The expressed protein was quantified and normalised with β-actin (abd1214), the housekeeping protein that served as a loading control.

The membrane was stripped and washed with 10 ml distilled water (dH_2O) for 1 minute and the water was discarded, followed by quenching by 5 ml of hydrogen peroxide (H_2O_2) and incubated at 37ºC for 30 minutes. The H_2O_2 was then decanted, and the membrane was washed with 10 ml dH_2O for 1 minute. Thus, dH_2O was discarded and 10 ml TTBS buffer added for 1 minute. The buffer was removed followed by blocking the stripped membrane with 5 ml of 5% BSA/TTBS for 1 hour, then probed with HRP-conjugated β-actin (Sigma, Johannesburg, South Africa), a house-keeping antibody (5 ml; 1:2500 in 5% BSA/TTBS) for 30 minutes. TTBS was used to washed membrane and Molecular Image®Chemidoc^{TM}XRS + and Bio-Rad imaging system to cultivate an image. Band intensity of each protein was analysed by Bio-Rad imaging system (CA, USA) and protein bands were normalised against β-actin.

3.12 Statistical analysis

GraphPad Prism V5.0 software (GraphPad Software Inc. La Jolla, California, USA) was used to analyse the data. Each assay was performed in triplicate and repeated for verification and accuracy. One-way analysis of variance (one-way ANOVA) with 95% confidence interval and Students *t*-test with Welch's correction was used, and *p* values less than 0.05 were considered significant.

CHAPTER 4 : RESULTS

4.1 Cell viability

The MTT assay was employed to determine the cell viability of Caco-2 cells treated with 0-5000 µg/ml of *A. afra* crude aqueous leaf extract for 48 hours. There was a reduction in cell viability observed with increasing concentration of *A. afra* extract relative to the control (Figure 4.1A). The cell viability decreased by 10% and 20% at 50 µg/ml (p = 0.0060) and 125 µg/ml (p = 0.0083) respectively. Further decreases to 43% (p = 0.0273) and 19% (p = 0.0109) were recorded for 250 µg/ml and 500 µg/ml, and cell viabilities below 10% were observed for the 1000 µg/ml (p = 0.0051), 2500 µg/ml and 5000 µg/ml treatments (Figure 4.1A). The dose-response curve generated yielded an IC_{50} concentration of 250 µg/ml. The cell viability of Hek293 cells treated with the IC_{50} of *A. afra* extract did not vary significantly from the control (Figure 4.1B).

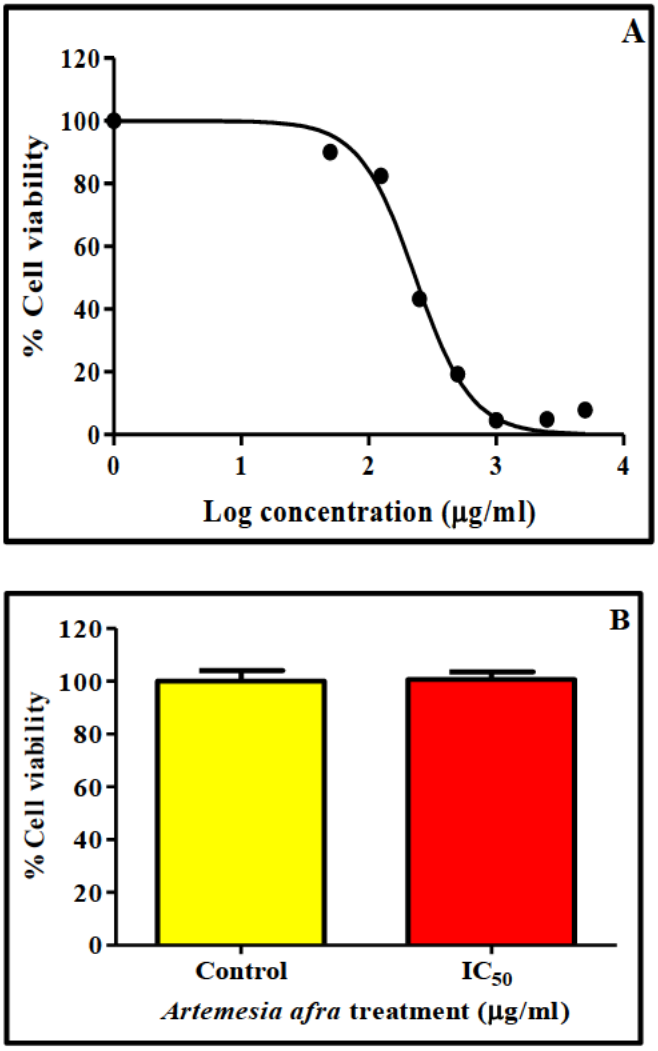

Figure 4.1: Cell viability of Caco-2 and Hek293 cells treated with *A. afra* extract for 48 hours. **A.** The dose-response reduction in Caco-2 cells viability after 48 hours was caused by treatment of *A. afra* crude aqueous leaf extract. Higher concentrations showed increased cell death. An IC_{50} concentration of 250 µg/ml was calculated. Data represented as a percentage of viable cells relative to the untreated control. **B.** The extract was not toxic to normal kidney (Hek293) cells when treated with the IC_{50} concentration.

4.2 Mitochondrial integrity

4.2.1 ATP assay

Cell Titre-Glo® assay was used to quantify intracellular ATP levels. The ATP concentration was significantly decreased from 2641000±174100 RLU in the control to 1724±35.57 RLU ($p = 0.0043$) in IC_{50}-treated cells exposed to *A. afra* (Figure 4.2).

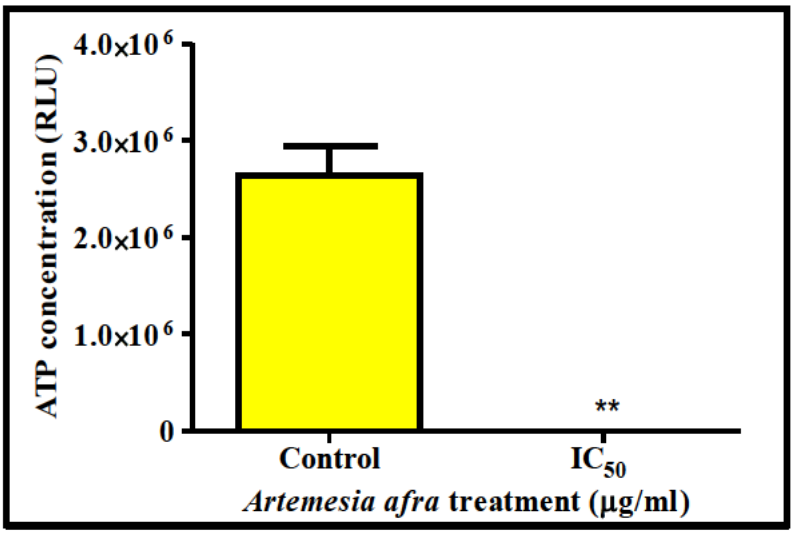

Figure 4.2: The intracellular ATP levels in treated Caco-2 cells. The ATP concentration was significantly decreased ($p = 0.0043$) in treated relative to untreated cells. [*Unpaired *t*-test with Welch`s correction; RLU: relative light units].

4.2.2 Mitochondrial membrane potential

Mitochondrial functionality can be observed by Δψm. A 40% decrease in red:green fluorescence was noted in IC_{50}-treated cells (0.8435±0.01301; $p = 0.0107$) relative to the untreated cells (1.371±0.05356) (Figure 4.3).

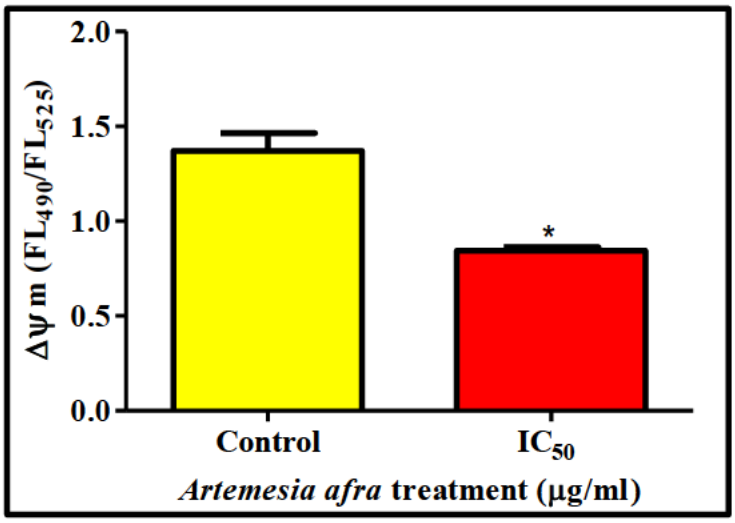

Figure 4.3: The Δψm in treated and untreated Caco-2 cells. Dissipation of the Δψm was observed in cells treated with *A. afra* crude aqueous leaf extract relative to the control ($p = 0.0026$). Δψm: mitochondrial membrane potential. [*Unpaired *t*-test with Welch`s correction].

4.3 Lactate dehydrogenase membrane integrity assay

The extracellular LDH was after the treatment of cells with *A. afra* to evaluate plasma membrane integrity. The levels of extracellular LDH were non-significantly decreased for IC_{50}-treated cells by 18% (0.6967±0.07876, $p = 0.2534$) relative to the untreated control (0.8500±0.07500) (Figure 4.4).

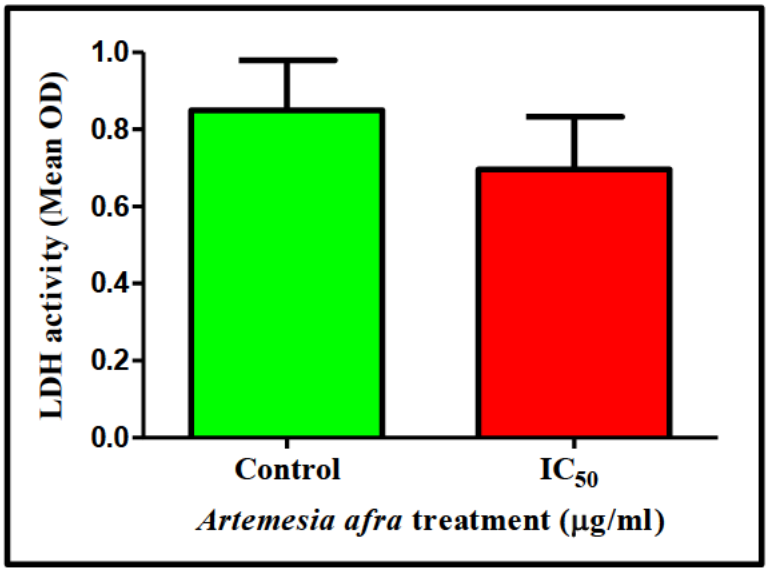

Figure 4.4: A spectrophotometric study of extracellular LDH levels in A. afra-treated and untreated Caco-2 cells. The *A. afra* treatment yielded minimal impact on the treated cells. (Unpaired students *t*-test with Welch's correction). LDH: lactate dehydrogenase results are presented as mean optical density (OD).

4.4 Free radical production

4.4.1 TBARS assay

Malondialdehyde was quantified as a marker of lipid peroxidation in Caco-2 cells treated with *A. afra*. The extracellular MDA levels were elevated by 1.92-fold from 0.01067±0.0006667 µM in the untreated cells to 0.0205±0.0025 µM in IC_{50}-treated cells ($p = 0.1638$) (Figure 4.5).

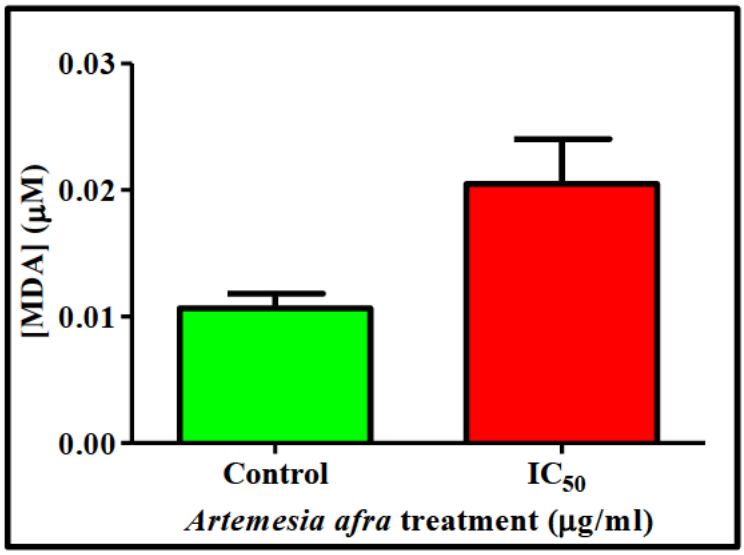

Figure 4.5: The MDA concentration in A. afra-treated Caco-2 cells. *Artemisia afra*-treated Caco-2 cells with markedly elevated extracellular MDA levels. MDA: malondialdehyde.

4.4.2 Nitrate and Nitrite

The NOS assay was employed to quantify the RNS in the treatment media of treated Caco-2 cells. Extrapolation from a standard curve calculated the concentration of nitrate and nitrite (Appendix C). Figure 4.6 shows a 3.38-fold change (6.599±0.06803 µM) of nitrate and nitrite concentration in *A. afra* IC_{50}-treated cells relative to the control (1.950±0.2974 µM; $p = 0.0043$).

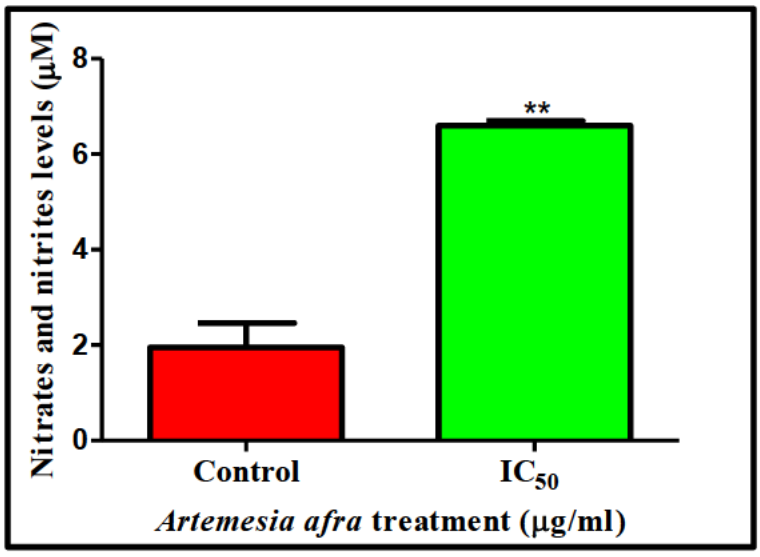

Figure 4.6: The concentration of nitrate and nitrite in Caco-2 treated cells. The nitrate and nitrite concentration was increased in Caco-2 cells following treatment with *A. afra* ($p = 0.0043$). (*Unpaired students *t*-test with Welch's correction).

4.5 Antioxidant response

4.5.1 GSH assay

Intracellular GSH levels were assessed by luminometry in Caco-2 cells to evaluate the antioxidant defense. Relative to the control (69080±11490 RLU), a 3.01-fold increase in GSH concentration to 208600±4587 RLU (p = 0.0078) was observed for IC_{50}-treated cells (Figure 4.7).

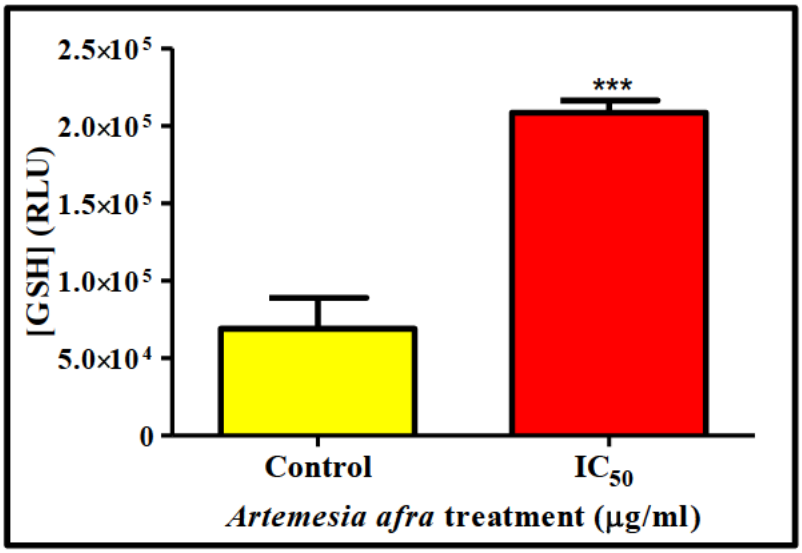

Figure 4.7: Antioxidant response to *A. afra* in Caco-2 cells. Increased levels of intracellular GSH in Caco-2 cells treated with *A. afra* (p = 0.0078). GSH: reduced glutathione. (*Unpaired students t-test with Welch's correction).

4.5.2 Antioxidant enzyme defense

The protein expression of antioxidant enzymes SOD2, GPx1 and CAT, and the master regulator Nrf2 were measured to determine the antioxidant response to free radical production. Figure 4.8A shows a significant 1.5-fold increase in Nrf2 protein expression to 0.1805±0.004402 RBI in IC_{50}-treated cells (p = 0.0068) compared to the untreated cells (0.1169±0.008405). A reduction of SOD2 protein expression from 2.015±0.01298 RBI in the control to 1.421±0.007197 RBI (p<0.0001) for the IC_{50}-treated cells was observed (Figure 4.8B). The GPx1 protein expression was upregulated for the IC_{50} treatment to 0.1615±0.003674 RBI (p = 0.00285) relative to the control (0.1292±0.003715 RBI, Figure 4.8C). Catalase protein expression (Figure 4.8D) was upregulated in IC_{50}-treated cells (0.03617±0.001118 RBI, p = 0.0025) relative to the control (0.01385±0.00008640 RBI).

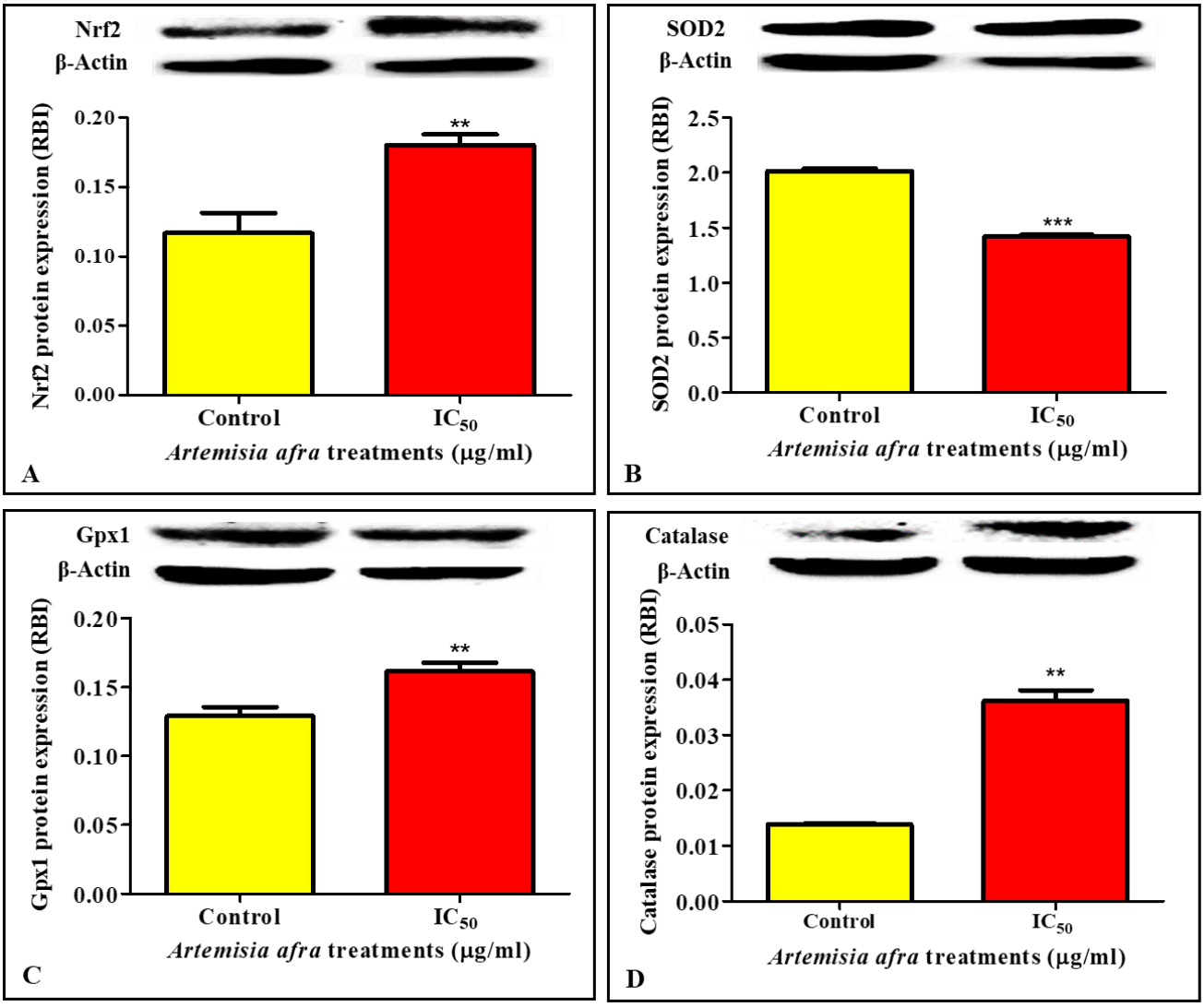

Figure 4.8: Antioxidant enzyme response in A. afra-treated and untreated Caco-2 cells. **A.** Significant upregulation in Nrf2 in IC_{50} (p = 0.0068) treated cells was noted relative to the control. **B.** SOD2 protein expression was downregulated in IC_{50} treated cells ($p < 0.0001$) **C.** Gpx1 protein expression increased after exposure to the IC_{50} of *A. afra* (p = 0.0285), **D.** Increased catalase expression was observed in *A. afra*-treated cells (p = 0.0025). (*Unpaired students *t*-test with Welch's correction)

4.5.3 Oxidative damage repair

Oxidation of DNA was determined indirectly by quantifying oxidative DNA repair using OGG1. The gene expression of OGG1 in the IC_{50}-treated cells was downregulated from 1.000±0.0000003191 in the control to 0.1683±0.04187 RLU in the untreated cell (p = 0.0025) in the treated cells (Figure 4.9).

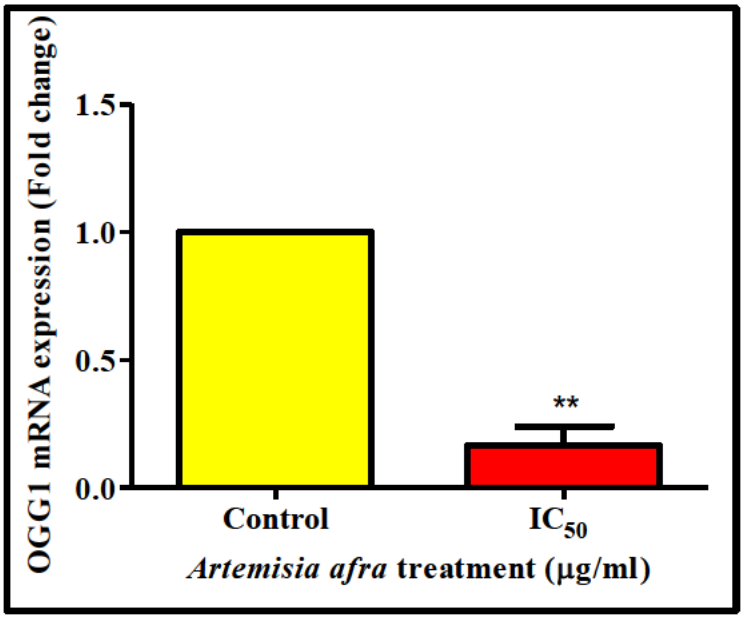

Figure 4.9: Gene expression of OGG1 in Caco-2 cells treated with A. afra extract. The OGG1 gene expression was downregulated in IC_{50}-treated cells relative to untreated Caco-2 cells ($p = 0.0025$). (*Unpaired students *t*-test with Welch's correction).

4.6 Death parameters analysis

4.6.1 Caspase analysis

Caspase activity (Figure 4.10) was used to assess the initiation (caspase-8 and caspase-9) and execution (caspases-3/7) of apoptosis. A significant downregulation of all caspases was observed in *A. afra*-treated Caco-2 cells. *A. afra* decreased the caspase-8 activity (Figure 4.10A) by 55.0-fold to 50910±2989 RLU compared to the untreated cells (2801000±426300 RLU; $p = 0.0232$), while caspase-9 activity (Figure 4.10B) was decreased 45.3-fold from 7026000±1111000 RLU in the control to 154900±25010 RLU in treated cells ($p = 0.0252$). Caspases-3/7 activity (Figure 4.10C) was similarly diminished by the *A. afra* treatment by 72.2-fold to 2026±833.6 RLU ($p = 0.0099$) relative to the control (146300±14400 RLU).

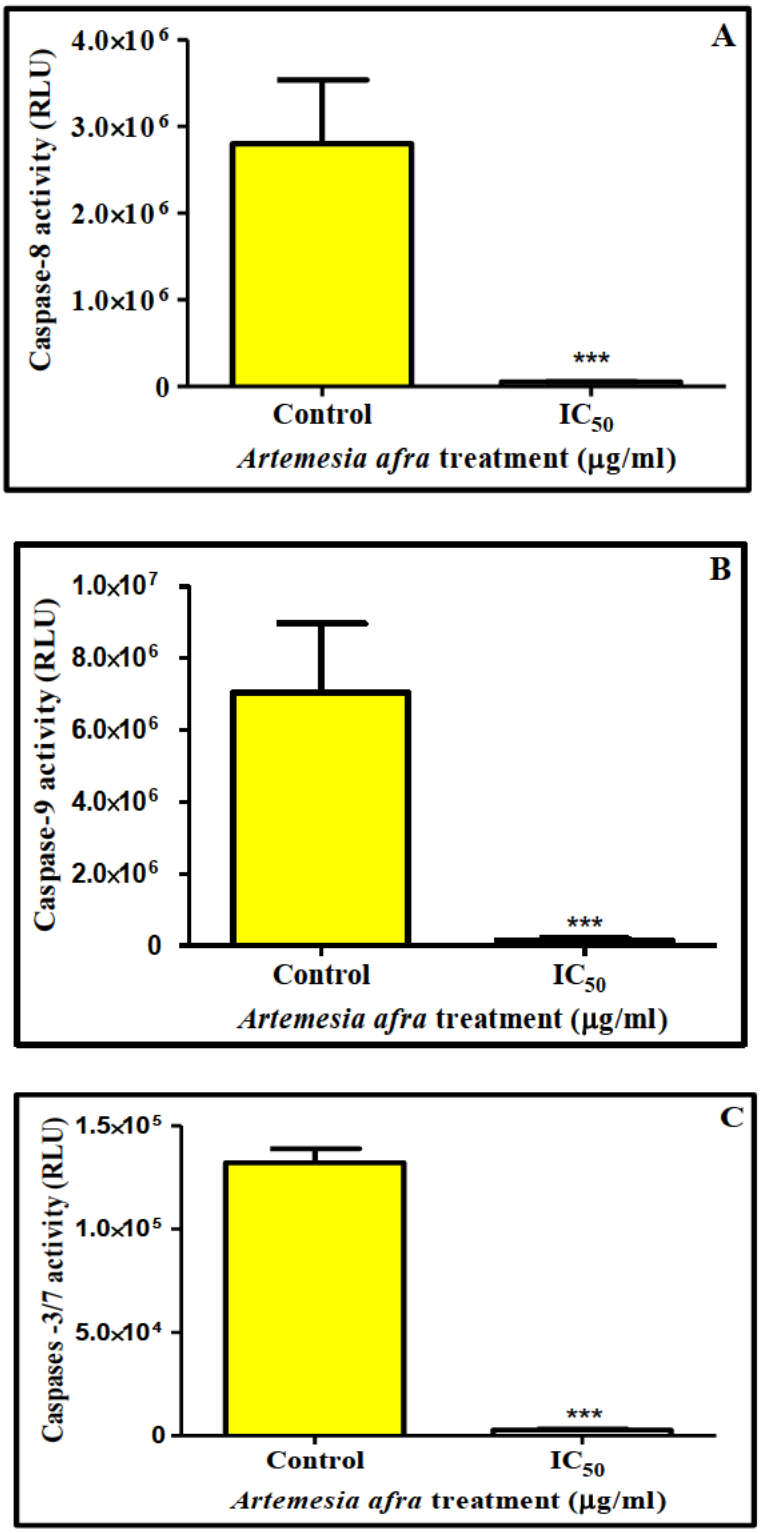

Figure 4.10: Crude aqueous leaf extract of A. afra dramatically decreased caspase activity. Initiator caspase-8 **(A)** and caspase-9 **(B)**, as well as executioner caspases-3/7 **(C)** were significantly decreased ($p = 0.0232$, $p = 0.0252$, $p = 0.0099$ respectively). (*Unpaired students *t*-test with Welch's correction).

4.6.2 Annexin-V fluorescence assay

Externalised phosphatidylserine was used as an early marker of apoptosis. *A. afra* crude aqueous leaf extract decreased the levels of externalised phosphatidylserine in IC_{50}-treated cells to 100200±5706 RLU ($p = 0.0232$) compared to the untreated control (Figure 4.11).

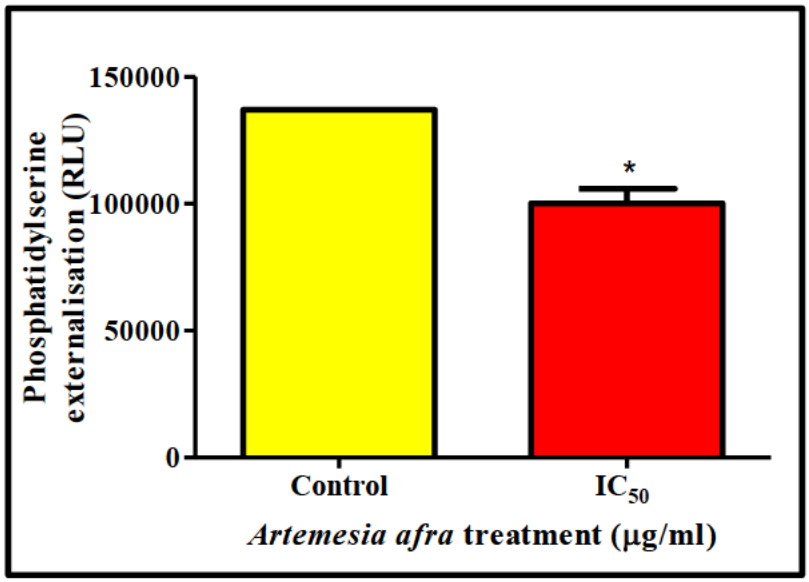

Figure 4.11: Annexin-V affinity for phosphatidylserine in *A. afra*-treated and untreated Caco-2 cells. *Artemesia. afra* significantly reduced the phosphatidylserine externalisation in treated Caco-2 cells ($p = 0.0232$). RLU: Relative Light Unit. (*Unpaired students *t*- test with Welch's correction)

4.6.3 Expression of apoptotic and anti-apoptotic proteins

Western blotting was used to evaluate the expression of pro-apoptotic and anti-apoptotic proteins, which includes Bax, Bcl-2, xIAP, cIAP1 and cPARP1. *Artemisia afra* induced an increase in the Bax/Bcl-2 ratio (Figure 4.12A) in IC_{50} treated cells compared to the control (1.114±0.00000004867 and 1.218±0.01673 respectively, $p = 0.0247$). An increase in cIAP-1 protein expression (Figure 4.12B) was observed for IC_{50}-treated cells to 0.1271±0.00000002980 RBI ($p = 0.0215$) compared to the untreated control (0.1026 ± 0.003665 RBI). A significant increase of xIAP protein expression from 0.04300±0.0008127 RBI in the control to 0.1066±0.00005667 RBI was noted in IC_{50}-treated cells (Figure 4.12C). Protein expression of cParp1 (Figure 4.12D) was upregulated when Caco-2 cells were exposed to *A. afra* treatment, with a 3.82-fold increase for the IC_{50} (4.869±0.05856 RBI) compared to the untreated control ($p = 0.0003$).

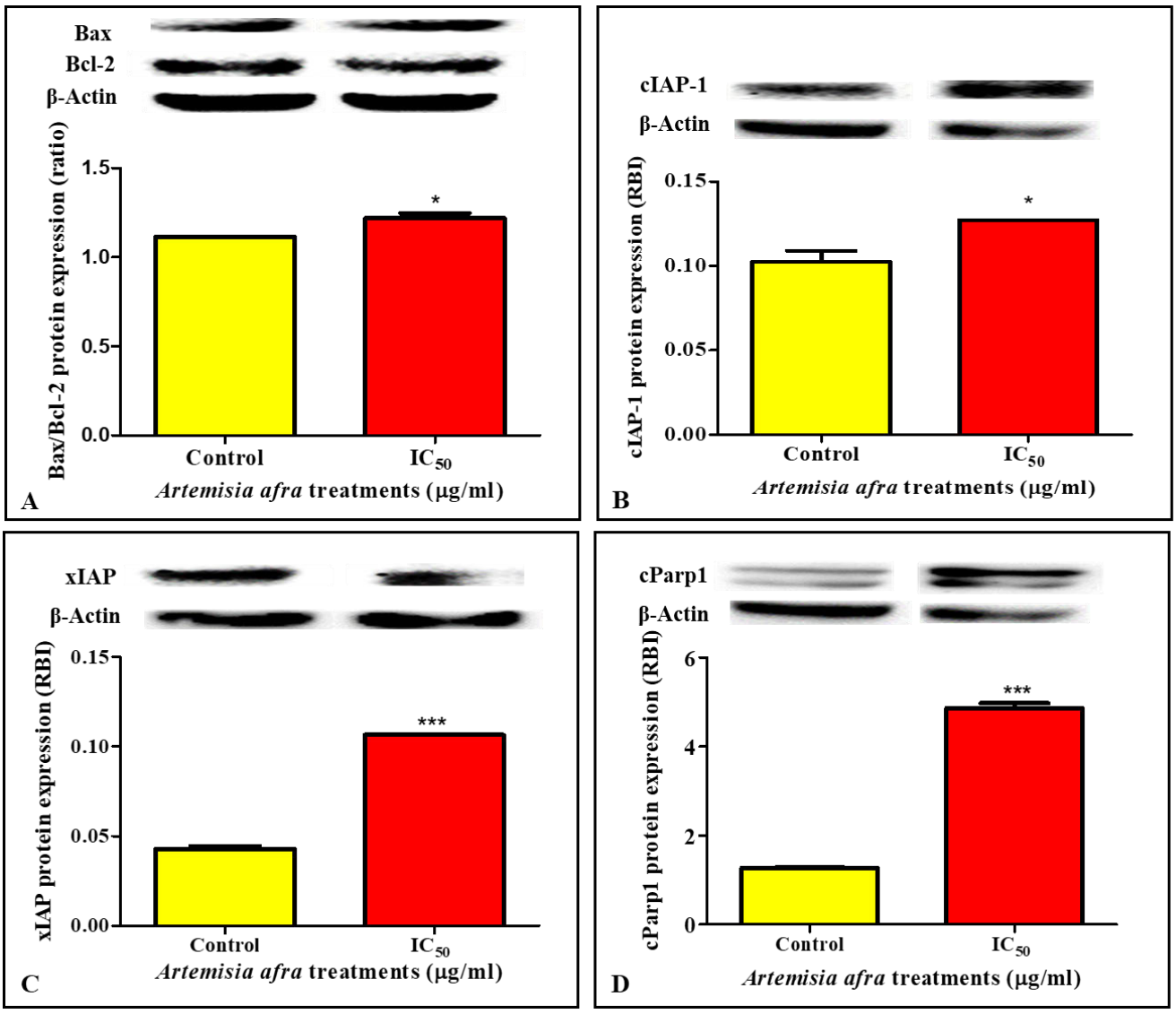

Figure 4.12: The *A. afra* extract modulated protein expression of apoptosis-associated proteins. (**A**) Bax/Bcl-2 ratio (p = 0.0247), (**B**) cIAP-1 (p = 0.0215) and (**C**) xIAP levels (p = 0.0002) and (D) cParp1 protein concentration in Caco-2 cells. (*Unpaired students *t*-test with Welch's correction).

4.7 MAPK pathway

The MAPKs were assessed because of the integral role they play in physiological responses such as cell proliferation, apoptosis and inflammatory responses. Significant upregulation of phosphorylated p38 protein levels (Figure 4.13A) were noted in IC_{50}-treated cells relative to the control (p = 0.0004). Conversely, a significant reduction in p-JNK/JNK (Figure 4.13B, $p < 0.001$) and p-ERK/ERK (Figure 4.13C, p = 0.0111) was observed in the *A. afra*-treated cells compared to the control.

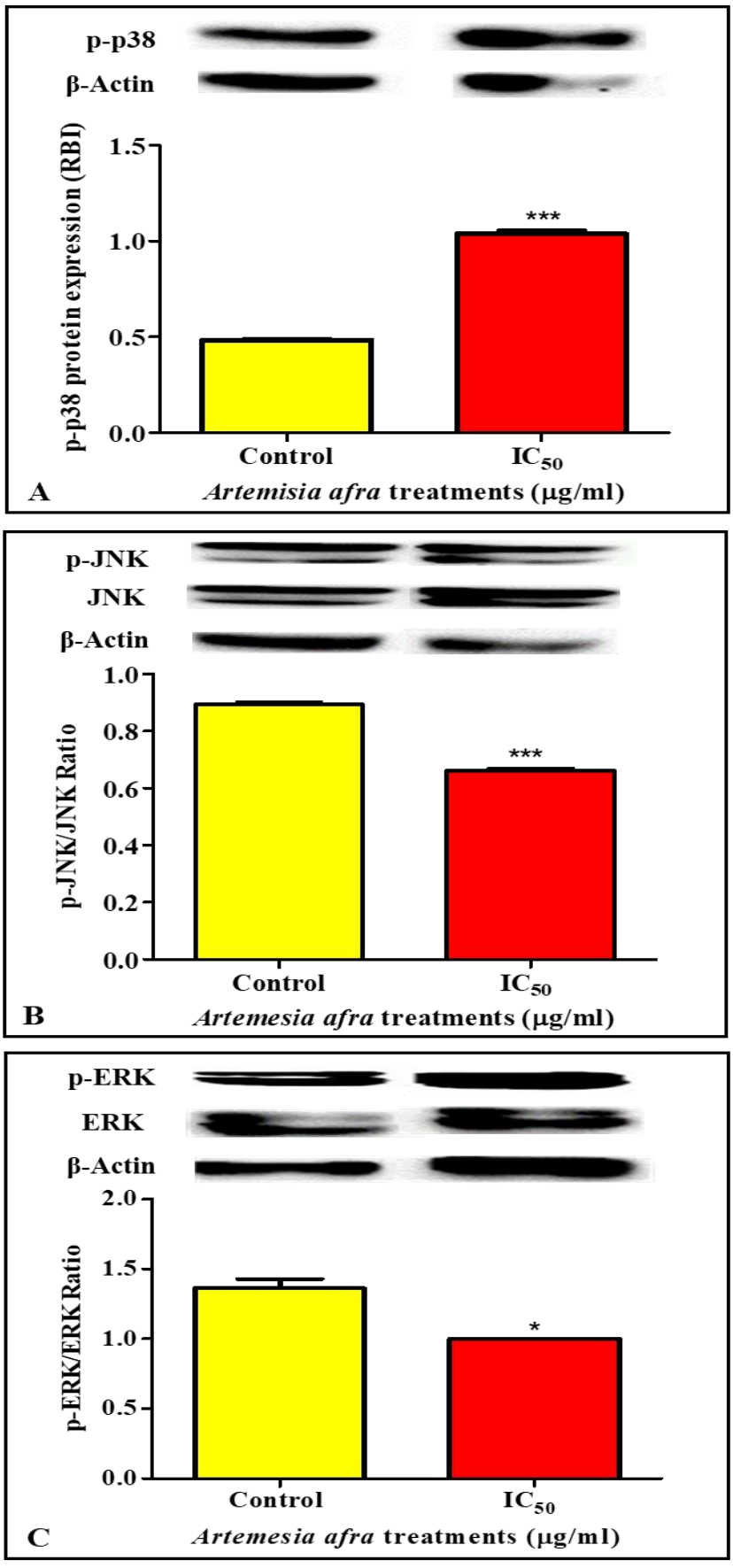

Figure 4.13: The protein expression of MAPK after *A. afra* treatment. (**A)** p-p38 (p = 0.0004), (**B**) p-JNK /JNK (p<0.0001), and **(C)** p-ERK /ERK (p<0.0001) in Caco-2 cells after treatment with the IC_{50} of *A. afra* compared to the untreated control. (*Unpaired students *t*-test with Welch's correction).

4.8 HSP response

Heat shock proteins are molecular chaperones that modulate the cell response to diverse cellular processes including oxidative stress, apoptosis and inflammation. There was an increased protein expression of HSP27 (Figure 4.14A, $p < 0.0001$) and HSP70 (Figure 4.14B, $p < 0.0001$) in Caco-2 cells treated with the IC_{50} of *A. afra* crude aqueous leaf extract.

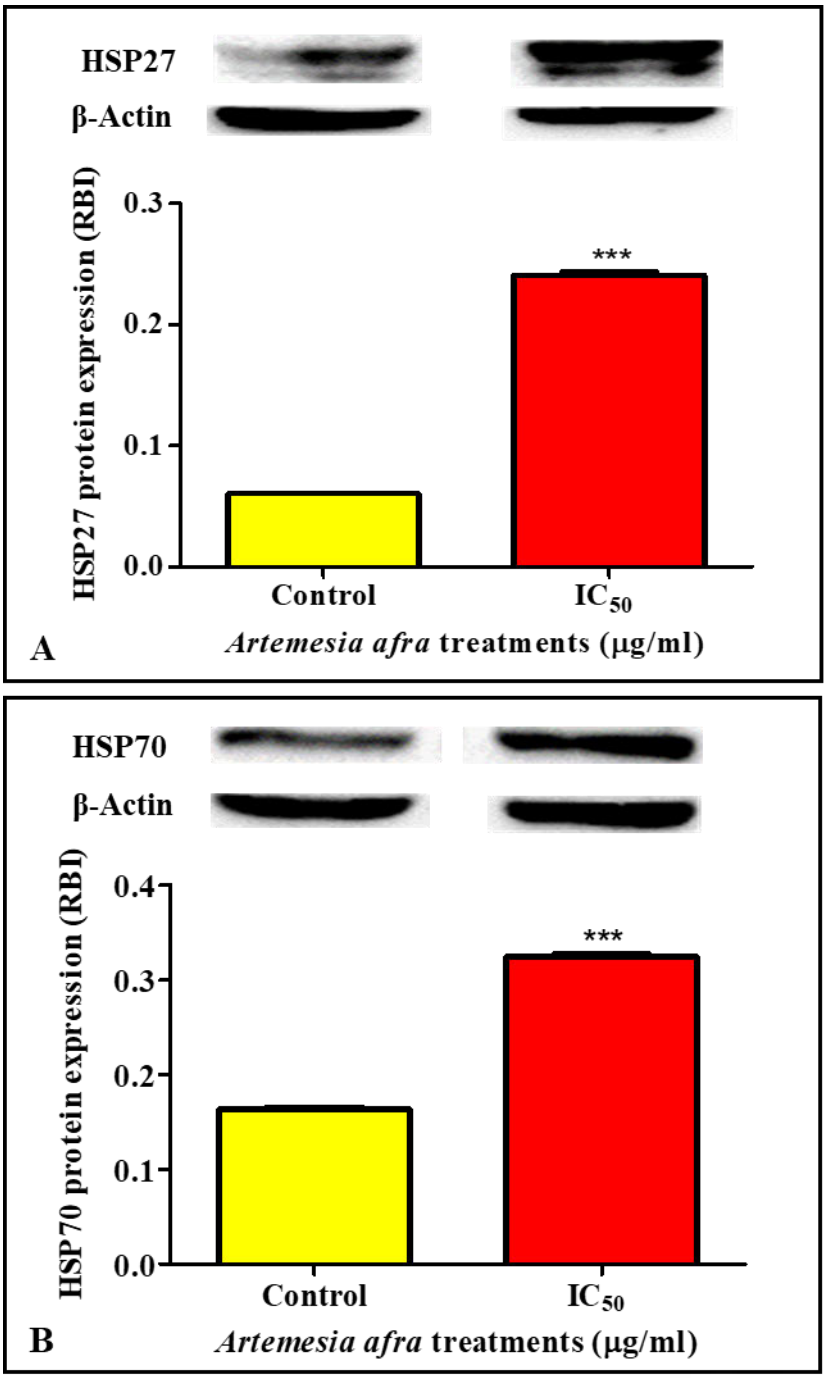

Figure 4.14: The heatshock response to *A. afra* treatment. **(A)** HSP27 ($p < 0.001$) and **(B)** HSP70 ($p < 0.0001$) in Caco-2 cells after treatment with *A. afra*. (*Unpaired students *t*-test with Welch's correction).

4.9 Comet assay

Single strand DNA breaks were measured to assess DNA integrity in *A. afra*-treated and untreated Caco-2 cells. The comet tail length (Figure 4.15) in IC_{50}-treated cells (2.943±0.07259 µM) was similar to the control (3.035±0.1776).

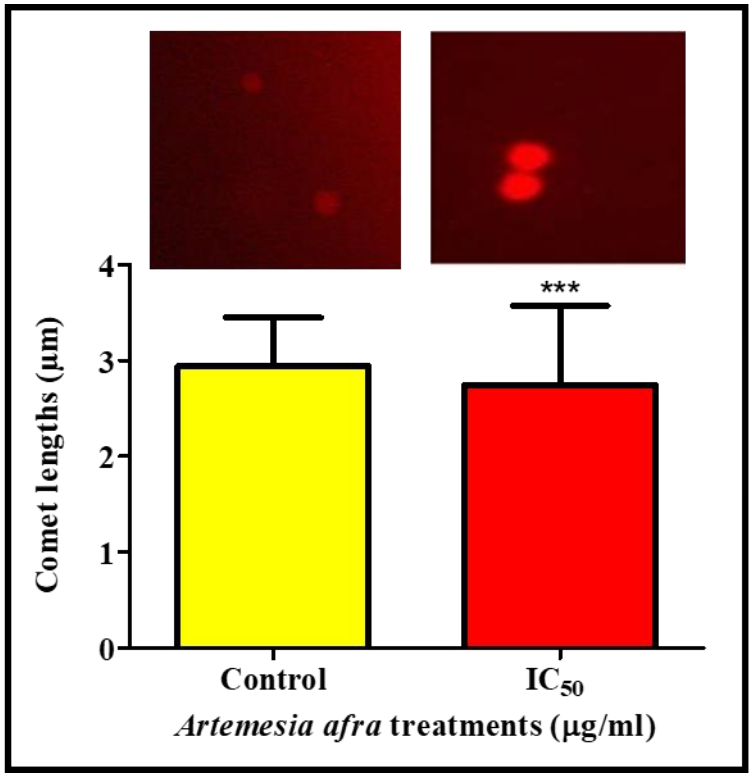

Figure 4.15: DNA fragmentation in Caco-2 cells treated with *A. afra* extract. DNA fragmentation was not induced by *A. afra* extract in treated and untreated Caco-2 cells (*$p < 0.0001$, unpaired students *t*-test with Welch's correction).

4.10 Inflammatory response invoked by the treatment with *A. afra*

The anti-inflammatory effect of *A. afra* was evaluated by deception of protein/mRNA expression of inflammatory markers including TNF-α, NF-κB and iNOS, as well as STAT3 because of its association with cancer-related inflammation. The exposure of Caco-2 cells to *A. afra* caused the non-significant activation of TNF-α gene expression relative to the control ($p = 0.1217$, Figure 4.16A), while NF-κB was significantly downregulated ($p = 0.0046$, Figure 4.16B). An increase the p-STAT3 /STAT3 ratio was observed compared to the control ($p < 0.0029$, Figure 4.16C). A 0.72-fold decrease in iNOS concentration relative to the control was observed ($p = 0.0005$, Figure 4.16D).

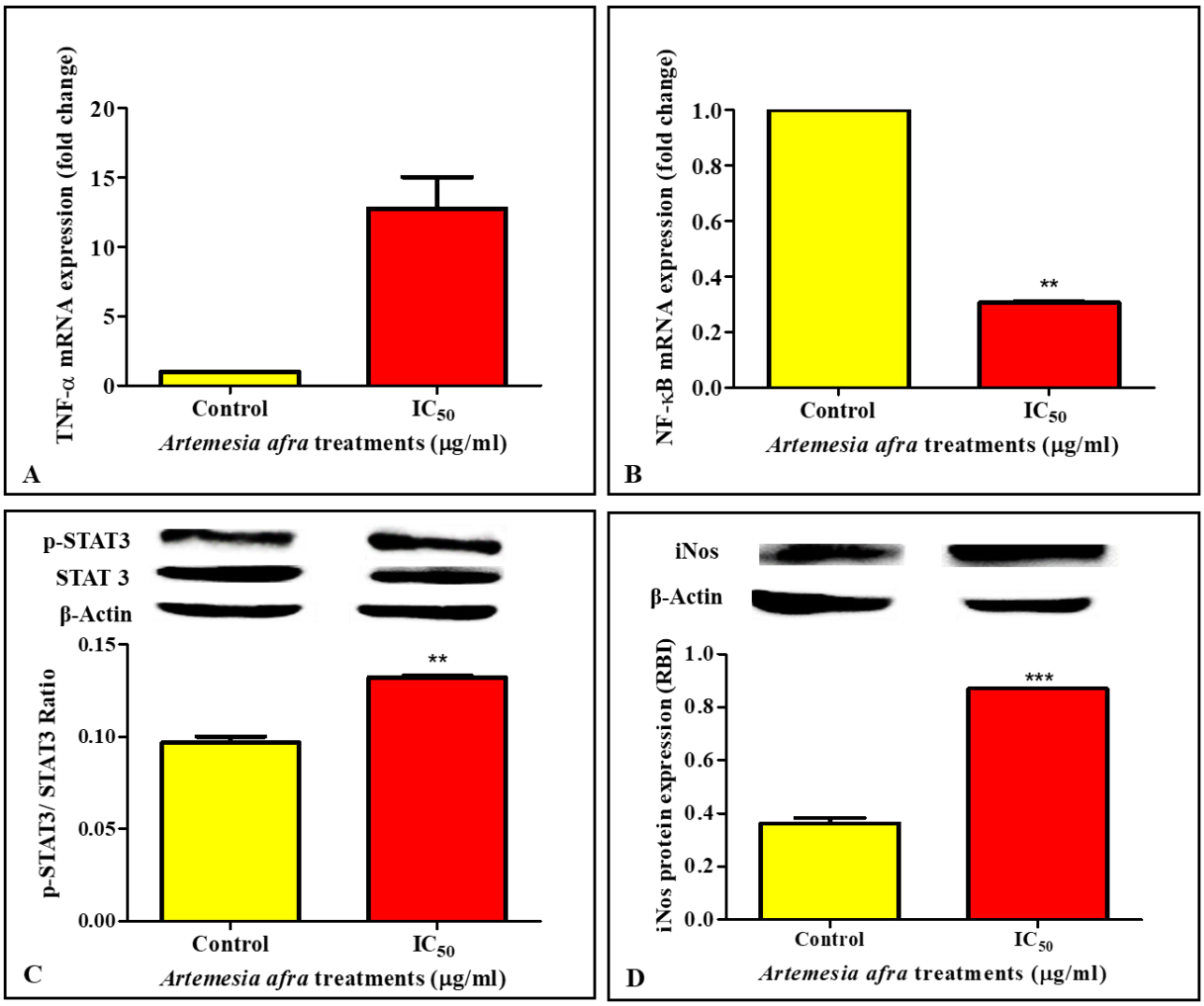

Figure 4.16: Inflammatory markers in Caco-2 cells after treatment with the IC_{50} of *A. afra*. **(A)** TNF-α mRNA was not significantly increased ($p = 0.1217$) **B.** NF-κB mRNA was decreased after treatment ($p = 0.0046$) **C.** *Artemisia afra* upregulated iNOS protein expression ($p = 0.0005$) **D.** The p-STAT3/STAT3 ratio showed increased activation by *A. afra* ($p = 0.0029$) (*Unpaired students *t*-test with Welch's correction).

4.11 Proliferation marker c-Myc and pRb

A key master regulator known as c-Myc plays a role in transcription, cellular proliferation, survival, and inhibition of apoptosis. The c-Myc gene expression was similar to the control in treated cells (Figure 4.17A); however, protein expression of c-Myc was upregulated ($p = 0.0276$, Figure 4.17B). A significant increase of p-pRb/pRb ratio was observed in *A. afra*-treated cells ($p = 0.0310$, Figure 4.17C).

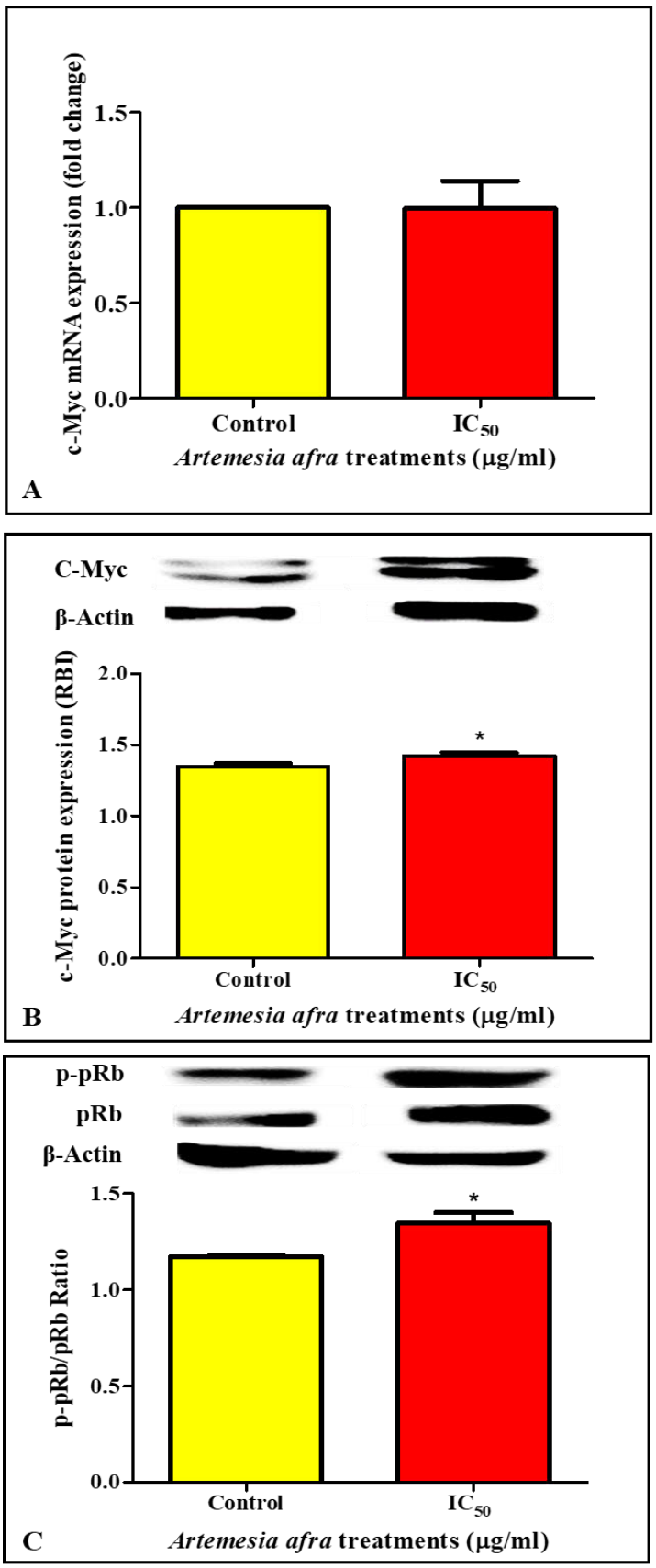

Figure 4.17: Expression of proliferation markers c-Myc and p-pRb/pRb in Caco-2 cells treated with *A. afra* extract. The gene **(A)** and protein **(B)** expression (p = 0.0276) of c-Myc in Caco-2 cells after treatment with *A. afra*. **(C)** Upregulated activity of pRb is indicated by increased ratio of p-pRb /pRb (p = 0.0310). (*Unpaired students *t*-test with Welch's correction).

CHAPTER 5 : DISCUSSION

With over 19 million cases reported annually, cancer remains a leading cause of mortality worldwide (Mathur *et al.*, 2020). In 2020 alone, almost 10 million deaths were reported, with 7 out of 10 deaths affecting developing nations including South Africa (SA) (Brand *et al.*, 2018, Mathur *et al.*, 2020). To date, CRC remains the deadliest form of cancer and the most difficult to treat (Brand *et al.*, 2018). Current therapeutic regimes available include chemotherapy, surgery, radiation and ablation. However, these anticancer treatments are often deemed too expensive, not easily accessible, require specialized well equipped medical facilities and in most cancer patients, these drugs exert debilitating side effect that further compromises the health of the individual (Brand *et al.*, 2018, Mathur *et al.*, 2020). For this reason, the search for new naturally derived anti-cancer agents is being extensively explored to overcome drug resistance and socioeconomic problems linked with existing therapies. In this regard, *A. afra* proved to be a good extract when screened for toxicity against various cell lines, but the mechanism by which *A. afra* extracts initiate its cytotoxic effect is not completely understood. In addition, its cytotoxic effect in human cells requires elucidation. It was hypothesised that *A. afra* induces cytotoxic effects on human CRC cancer cells upon acute exposure (48 hour).

Over the years, numerous studies have shown that natural compounds reduce cell proliferation and cause cell death in the form of apoptosis or necrosis (Abd El-Hafeez *et al.*, 2018). In this study, crude aqueous *A. afra* leaf extract decreased cell viability of the Caco-2 cell line, which demonstrated a cytotoxic effect with increasing concentrations (Figure 4.1A), whereas in a normal cell line (Hek293 cells) the extract was not toxic (Figure:4.1B). In this study, an IC_{50} of 250 µg/ml was obtained at 50% cell death with a reduction in cell viability (Figure 4.1). These findings are in coherence with previous studies. This study was in correlation with a study by Spies *et al.* (2013) which obtained an IC_{50} greater than 250 µg/ml for aqueous extract of *A. afra* in Hela and U937 cancer cells (Spies *et al.*, 2013). Although both studies showed a limited cytotoxic manifestation after 48 hour exposure to an aqueous extract of *A. afra*, slight variations may be attributed to the effects of phytochemicals which are often cell-type specific. In addition, geographical location and season of harvest may influence the phytochemical content of *A. afra* (Kane *et al.*, 2019). Cytotoxic effects on human cell lines have been shown to be induced by various *A. afra* solvent extracts. For example, the ethanol extract of *A. afra* showed 50% growth inhibition at 18.21 and 31.88 µg/ml (acute toxicity) in U937 and Hela cells respectively (Spies *et al.*, 2013). This enhanced cytotoxic effect when compared to the aqueous extracts may be related to the extraction solvent, since phytochemical constituents in the extract differ depending on solvent polarity (Kane *et al.*, 2019). The phytochemical isoalantolactone isolated from *A. afra* also demonstrated cytotoxicity at 18.15±1.16 µM in Hela cells after 24 hours (Venables *et al.*, 2016).

The MTT assay measures cell viability based on succinate dehydrogenase activity. The dose-dependent decrease in cell viability demonstrates an inhibition of succinate dehydrogenase activity at complex II of the Krebs cycle rate, which resulted in a downregulation of reducing equivalents to oxidizing equivalents such as NADH and $FADH_2$ within the cell (Mosmann, 1983). These intermediates contribute to the ETC that culminates in the production of ATP. Decreased ATP levels in IC_{50}-treated Caco-2 cells (Figure 4.2) implies that *A. afra* induced the uncoupling of oxidative phosphorylation, which may lead to the excessive generation of ROS (Adeeyo *et al.*, 2013). The highly reactive ROS molecule O_2^- can directly oxidise and inactivate iron-sulfur proteins such as NADH dehydrogenase and ATP synthase, resulting in loss of mitochondrial respiration and ATP generation, leading ultimately to mitochondrial dysfunction and decreased intracellular ATP levels (Adeeyo *et al.*, 2013).

Depolarisation of the mitochondrial membrane is a typical response to the dysregulation of mitochondrial dynamics (Domijan and Abramov, 2011). Increased ROS generation adds significantly to mitochondrial depolarization and stress. The electron transport chain has numerous sites for ROS formation and process peculiarities lead to ineffective modulation of ROS production resulting in the abnormal accumulation of ROS molecules, ultimately resulting in the onset of oxidative stress (Zorova *et al.*, 2018). As a consequence of increased ROS production, mitochondrial membrane potential and ATP synthesis are reduced (Small *et al.*, 2012). In this study upon exposure to *A. afra*, mitochondrial membrane potential is reduced (Figure 4.3) and the intracellular ATP levels decreased in all concentrations (Figure:4.2). These findings are congruent with a study by Spies and co-researchers (2013) whereby a decrease in mitochondrial membrane permeability was observed following the exposure of HeLa cells to ethanolic *A. afra* crude extract, over 48h (Spies *et al.*, 2013). Not only is the mitochondrion the primary source of ROS production but it is also a highly susceptible target for ROS molecules and their harmful effects (Stockert *et al.*, 2012). The recurrent persistence of oxidative stress, primarily O_2^- and H_2O_2, induced by overproduction of ROS, has the potential to damage cellular components and structure. ROS-induced oxidative stress combined with a decrease in the endogenous antioxidant glutathione (GSH) facilitates the oxidation of DNA and lipids. As a consequence, numerous end products such as aldehydes, more specifically MDA, are produced following lipid peroxidation (Repetto *et al.*, 2012).

The MDA concentration in this study was increased in IC_{50}-treated Caco-2 cells following exposure with crude aqueous leaf *A. afra* extract (Figure:4.5), relative to untreated cells. This result indicates increased free radical generation leading to *A. afra* acting as a potent inducer of oxidative tissue stress

as it disrupts the mitochondrial membrane of Caco-2 cells resulting in lipid peroxidation. This study is in agreement with a study conducted by Afolayan and Sunmonu (2013) where MDA concentrations was increased in liver cells of diabetic rats, indicating the possible induction of oxidative stress (Afolayan and Sunmonu, 2013). These findings support the notion that aqueous *A. afra* extract serves as a potent inducer of oxidative stress.

The principle ROS produced by mitochondria is $O_2^{\bullet-}$. The metallo-enzyme superoxide dismutase 2 (SOD) transform O_2^- to H_2O_2 (Candas and Li, 2014). In this study, mitochondrial SOD (Mn-SOD) level was reduced in IC_{50}-treated cells (Figure 4.8B), which suggests an accumulation of the O_2^- substrate and reduced concentration of the H_2O_2 product (Figure 4.6). The findings of this study does not correlate with those of Afolayan and Sunmonu (2013), who found elevated SOD2 in the liver and kidneys of diabetic rat models after oral ingestion of aqueous *A. afra* extract (Afolayan and Sunmonu, 2013). As in this study, an aqueous extract of *A. afra* was utilised for 48 hours on human epithelial cells from different organs; thus the contrast may again related to phytochemical constituents resulting from location and season of harvest (Kane *et al.*, 2019). In addition, the *in vivo* rat model may be influenced by systemic parameters not present in the current *in vitro* model.

The nitric oxide synthase (NOS) pathway produces nitric oxide (NO) from arginine, which interacts with superoxide to form RNS. This study investigated the production of RNS in response to *A. afra* exposure. A significant increase in nitrate and nitrites levels in treated Caco-2 cells was observed (Figure 4.6). This suggests that there was an increase in RNS generation. The concentration of nitrate and nitrites increased which provided favourable substrate for the production of RNS molecules. Both ROS and RNS contribute toward oxidative stress. Flavonoids content in *A. afra* functions as a potent free radical scavenger. This medicinal plant also contains Vitamin D3 and C, which are known regulators of NO production (Silbernagel *et al.*, 1990). Nitric oxide (NO) combines with O_2^- to form OON^- in states of high ROS levels, which causes lipid peroxidation (Gopi *et al.*, 2016). Therefore, oxidative stress-induced lipid peroxidation can occur as a result of RNS and ROS overproduction (Dedon and Tannenbaum, 2004). Excessive generation of NO leads to inflammation in cancer via the enzymatic activity of inducible nitric oxide synthase (iNOS) (Bogdan *et al.*, 2000, Suleria *et al.*, 2017). The NO production and peroxy-nitrite ($ONOO^-$) an oxidation product are associated with inflammatory conditions (Wang *et al.*, 2014). Reactive nitrogen species (RNS) observed in IC_{50}-treated cells is in correlation with an increase in iNOS level in IC_{50} (Figure 4.16C), suggesting the possible induction of inflammation. The results of this study were in disagreement with the findings of *Jeong* and co-researchers (2018), which stated that NOS expression induced by *Artemisia Montana* leaf crude extract was downregulated at all concentrations in LPS-stimulated Raw 264.3 cells (Jeong

et al., 2018). As in this investigation, aqueous extract of *A. afra* was utilised for 48 hours on human epithelial cells, the contrast is related to extraction solvent, chemical constituents, incubation length, and cell variation.

Haem catalase (CAT) is an enzyme that converts H_2O_2 into water and oxygen in humans along with selenium dependent glutathione peroxidase (GPx-1) (Weydert and Cullen, 2010, Davies, 2000). In IC_{50}-treated cells, CAT and GPx-1 increased (Figure: 4.8D and C), which suggests that detoxifying enzymes were active to reduce minor toxic ROS that were present. The increased GPx-1 correlated with elevated GSH expression (Figure 4.7) in this study. The substrate GSH is used in several xenobiotic elimination processes where it is a co-factor for glutathione-S-transferase, and acts as an intracellular radical scavenger (Zitka *et al.*, 2012, Milisav *et al.*, 2012). Heightened levels of GSH in IC_{50} (Figure:4.7) treated cells indicated reduced levels of oxidative stress and induces the activation of enzymes such as CAT and GPx-1 as observed in (Figure 4.8D and C). The results of this study are consistent with Afolayan and Sunmonu (2013), who reported increased GSH and Gpx-1 after oral administration of aqueous *A. afra* extract in the liver and kidneys of diabetic rat models (Afolayan and Sunmonu, 2013).

Nuclear factor-erythroid factor 2-related 2 (Nrf2) activate antioxidant transcription by binding to the antioxidant response element (ARE) as a result of intracellular increase ROS level, which causes activation of oxidative stress sensor by dissociation of Nrf2 and Kelch-like ECH-associated protein 1(KEAP1) (Ma, 2013). An upregulation of Nrf2 protein expression levels (Figure 4.8A) was observed in all treated cells. The activation of Nrf2 was necessary for the translation of detoxification enzymes and antioxidant genes to prevent oxidative stress and this was validated by GSH (Figures: 4.7). The result from this study were consistent with the upregulation of Nrf2 in neurons when induced by *Artemisia amydalina* to protect against oxidative stress in Alzheimer diseases (Sajjad *et al.*, 2019). The difference may also be attributed to variation in cell and tissue type (Tomasetti and Vogelstein, 2015).

Stress response proteins protects biomolecules from harm by inhibiting enhancing survival and proliferation (Ikwegbue *et al.*, 2018). It also enhances the translocation of precursor proteins into mitochondria while modifying regulatory proteins, in addition to the characteristics. An increase of intracellular protein expression of HSP70 and HSP27 in treated cells was observed (Figure 4.14A and B). In literature, HSP27 binds to cytochrome c thereby disrupting the process of apoptosis by interrupting and blocking downstream caspase activation (Figure 4.14A). In this study, the activation of Bax was decreased (Figure 4.12A). This study further indicates that elevated HSP70 (Figure

4.14B) may have prevented apoptosis at a pre-mitochondrial level by inhibiting the stress signal. Thus, Bax homo- and hetero-dimerisation was prevented and downstream events that follow mitochondrial outer membrane permeabilisation and cytochrome c did not occur. Consequently, the interaction of cytochrome c with Apaf-1 that results in caspase activation was impeded preventing apoptosis. Furthermore, the formation of death-inducing signaling complexes (DISC) was also inhibited (Garrido *et al.*, 2006).

Activation of death receptors is mediated by caspase-8 whereas the intrinsic pathway is activated by DNA damage through the mobilization of Bax protein (Yan and Shi, 2005). Bax protein facilitate the opening of the mitochondrial membrane pores, allowing cytochrome c to be released and caspase activation (Yan and Shi, 2005). Activation of initiator caspase-8 and caspase-9 triggers caspases-3/7 to be active, which executes apoptosis. There are various protein which inhibit apoptosis from occurring which include inhibitor of apoptosis protein (IAPs) members of the Bcl-2 family of antiapoptotic proteins that converge on the mitochondria-mediated pathway to inhibit caspase activity. Bcl-2 family of antiapoptotic also plays a role by inhibiting pro-apoptotic protein (Kale *et al.*, 2018).

In this study, caspases-8, -9 and -3/7 (initiators and executioner of apoptosis) were significantly downregulated in IC_{50}-treated cells (Figure 4.10 A, B and C). These findings indicate that caspases and apoptosis were not the primary cause of cytotoxic effect. Furthermore, activation of cIAP-1 and xIAP at the IC_{50} concentration correlated with the decreased of caspase activities (Figure 4.10); since these inhibitors bind activated caspases to prevent initiation and execution of apoptosis (Figure 4.12B and C), their elevation verifies that apoptosis had no role in this study. Our data revealed increased HSP70 levels in all treated cells implying prevention of cell death in conditions where caspase activation is inhibited by exogenous caspase inhibitors (HSP70), or in cells where Apaf-1 or caspase-9 are genetically inactivated, indicating that the cytochrome c/Apaf-1/caspase pathway had no role in this study (Garrido *et al.*, 2006). The data obtained is clearly in contradiction with the study by Spies and co-researcher's (2013) which showed induction of caspases-3/7 and caspase-8 elevation following exposure of HeLa and U937 cells to ethanolic *A. afra* crude extract after 24 hours and 48 hours exposure. Since the extract induced extrinsic apoptosis in cervical and myeloid, but intestinal cells are resistant to this effect, this data suggests cell-type specific effects of the aqueous extract of *A. afra*. The differential effects may occur due to additional phytochemical constituents extracted with solvent that may not be present in the aqueous extract; seasonal and location differences may also contribute to this observation (Kane *et al.*, 2019).

Proliferation, migration, differentiation, and death of cells are controlled by MAPK activation (Lavoie *et al.*, 2020). Phosphorylation of BH3-only family of Bcl2 proteins involved JNK, which inhibits Bcl-2 or Bcl-antiapoptotic XL's action (Koff *et al.*, 2015). In our study, JNK-P/JNK ratio was significantly reduced in IC_{50}-treated cells (Figure 4.13B). Hence, downregulation correlated with the production of anti-apoptotic proteins (Bcl-2) and NF-κB in this study (Figure 4.12Aand 4.16B).The P-ERK/ERK activity is linked to the overexpression of proapoptotic Bcl-2-family such as Bax (Koff *et al.*, 2015, Dhanasekaran and Reddy, 2008). Our data suggests that the reduction in ERK-P/ERK ratio (Figure 4.13C) observed in IC_{50}-treated cells relative to the untreated cells were, in coordination with the downregulation of proapoptotic protein in this study (Figure 4.12A). The findings of this study were consistent with the results obtained by Tan and co-researchers (2014) which stated an ethyl acetate extract of *Artemisia anomala S. Moore* also reduced the activation of MAPK signaling pathways such as JNK, ERK, and NF-κB signaling pathway (Tan *et al.*, 2014).

A multi-tasking kinase (p38 MAPK) that interacts with a variety of substrates to regulate a variety of cellular activities, including cell proliferation, differentiation, stress response, apoptosis, and cell migration and survival, among others (Martínez-Limón *et al.*, 2020). Many transcriptional regulators that coordinate specific gene expression programs are phosphorylated when p38 is activated which include JNK and ERK (Martínez-Limón *et al.*, 2020). In this study, a significant increase of p-p38 MAPK protein expression (Figure 4.13A) was observed in all treated cells relative to the untreated cells. This demonstrated that activated p38 MAPK phosphorylated and activated MAPKAP kinase 2 (Martínez-Limón *et al.*, 2020), as well as the transcription factors. Our data coordinated with the increase of HSP27 and HSP70 expression (Figure 4.14A and B) which are phosphorylated by p38 MAPK in this study. In addition, p-p38 was consistent with TNF-α from this study (Figure 4.16A); although the upregulation of TNF-α by the *A. afra* extract was not significant, it was sufficient to induce the activation of p-p38 MAPK (Cruceriu *et al.*, 2020).

Leakage of intracellular contents into the extracellular component of a cell due to plasma breakdown results in cell death. Cytoplasmic enzyme, LDH leaks from damaged perforated cells and is often associated with this toxic process. Cell membrane integrity is evaluated by measuring extracellular LDH levels found within the cytoplasm (Watanabe *et al.*, 1995). In this study, *A. afra* affected the Caco-2 cell membrane integrity causing LDH leakage from the cytosol of the cell. As seen in Figure 4.4, a reduction of extracellular levels of LDH in in IC_{50}-treated cells was observed thus indicating intact cell membrane. Phosphatidylserine is retained in the cytosolic portion of the cell membrane but when cells undergoes apoptosis, the phosphatidylserine becomes externalized, rendering it a

biomarker for early apoptosis (Li *et al.*, 2003). In this study, the results showed decreased in the affinity of Annexin-V to bind externalised phosphatidylserine in all treated cell relative to the untreated cells (Figure:4.11). This finding suggests that early apoptosis was not induced in IC_{50}-treated cells, the results further supported the detain Figure: 4.10, thus validating apoptosis was not induced. The current findings of this study are in contrast to those produced by Spies *et al.* (2013) in which observed heighten levels of affinity-V to bind in phosphatidylserine induced by ethanol *A. afra* extract for 24h and 48h in Hela cell (Spies *et al.*, 2013). The contrast in findings may be attributed to differences in extraction solvent, incubation period and cell variation.

A DNA damage-activated nuclear enzyme, PARP-1, is involved in DNA repair, transcription control, DNA replication, cell differentiation, proliferation, and cell death (Perry *et al.*, 1997, Erener *et al.*, 2012, Langelier *et al.*, 2012). Cell death can occur via a death pathway that requires no Bcl/Bax and caspase activity which is caused by excessive influx of Ca^{2+} that result in poly (ADP-ribose) polymerase (PARP) overactivation or initiated by inflammation. Peroxy-nitrite induced hyperactivation of PARP resulting in depletion of NAD^+ and ATP culminating cell dysfunction (Hong *et al.*, 2006). PARP-1 becomes overactivated during DNA damage causing poly ADP-ribosylation of numerous nuclear proteins using NAD^+ as a substrate. The death process that occurs from PARP-1 overactivation is due to the rapid energy depletion that occurs (Hong *et al.*, 2006). In this study, upregulation of cleave PARP-1 was observed (Figure 4.12D) in all treated cells relative to the control. These finding suggest that there was DNA repair response activated in response to DNA damage induced by *A. afra*, and cleavage of PARP-1 signifies genotoxic potential of the extract to result in cellular dysfunction. Hence this correlated with RNS production (Figure 4.6) in this study. As reported by Ko and Ren (2012), DNA repair serves importance during occurrences of DNA damage (Ko and Ren, 2012).

Caco-2 cell following exposure to *A. afra* extract was observed to have intact DNA as shown by the DNA fragmentation assay (Figure 4.15). Despite the fact that there was no evidence of apoptosis, the comet assay revealed that slightly DNA fragmentation was present in IC_{50} (Figure 4.15) treated cells which explains the rise of cPARP-1 expression as it responds to single stranded DNA (Figure 4.12D). Fragmentation of DNA observed in IC_{50}-treated cells correlated with the facts that apoptosis did not occur as the DNA remain intact. When DNA is damaged, the cell activates DNA repair enzymes such as OGG1, a DNA glycosylate enzyme that eliminates 8-oxoguanine base lesions that could cause mutations and cancer if left untreated (Cooke *et al.*, 2003, Boldinova *et al.*, 2019). Exposure to *A. afra* decreased gene expression of OGG1 (Figure 4.9) and correlated with decrease of DNA tails

lengths (Figure 4.15). This suggest that OGG1 enzyme activity was not compromised and consequently, base lesions continue to amplify promoting carcinogenesis.

Failure of the DNA repair mechanisms may result in chronic inflammation that activates cytokines and growth factors to promote cell proliferation. Cytokines such as TNF-α initiate and amplify the inflammatory response (Fiers, 1991, Chung *et al.*, 2017, Cruceriu *et al.*, 2020). In addition to its role as an inflammatory mediator, TNF-α fulfils a range of functions in immune homeostasis and host defense, and is a known regulator for ROS production (Roitt and Delves, 1992, Makamure *et al.*, 2016). This study observed heightened levels of TNF-α in treated cells compared to the control (Figure 4.16A) suggesting that inflammatory response might have been activated at this concentration. The current findings validated that in IC_{50}-treated cells there was an inflammatory response initiated, and it correlated with heightened iNOS levels at this concentration (Figure 4.16C). Hence, TNF-α is proposed to trigger the cascade signaling which consist of STAT-3 activation (Parameswaran and Patial, 2010).

Signal transducer and activator of transcription 3 is a crucial mediator controlling signal transduction to the nucleus and triggering the transcription of proliferation-related genes (Yu *et al.*, 2009, Wang *et al.*, 2011). Phosphorylation of STAT3 has been linked to aberrant oncogenic activities in CRC, including initiation, proliferation, angiogenesis, and progression (Silva *et al.*, 2015, Rozovski *et al.*, 2016). Extract of *A. afra* induced a significant increase in protein expression of p-STAT-3/STAT-3 ratio (Figure 4.16D) in IC_{50}-treated cells equivalent to the untreated cells. These findings verified that activation of STAT-3 had a role in inflammatory response through its activation in IC_{5O} -treated cells. The findings of this study are in coherence with data *Eungyeong Jang* and co-investigators which found the extract *Artemisia capillaris* inhibited STAT3 in hepatocellular carcinoma (Jang *et al.*, 2017).

Expression of STAT-3 is known to be the key mediator of the cell cycle progression which include c-Myc protein (Barré *et al.*, 2005). Versatile transcription factor (c-Myc) that controls the expression of genes with anti-proliferative effects while activating the many synthetic process required for fast cell division. The findings of this study showed an upregulated c-Myc level (Figure:4.17A) which were consistent with gene expression of c-Myc (Figure 4.17B). Controls the cell cycle via pRb is through phosphorylation-dependent interactions with the E2F family of transcription factors2: in early and mid G1, the protein complex D-type cyclins/CDK4,6 phosphorylates pRb, whereas in late

G_1, cyclins E(A)/CDK2 gradually phosphorylate pRb (Weinberg, 1995). A heighten level occurred in IC_{50} concentrations of p-pRb/pRb ratio relative to the untreated cells. This implies cell cycle arrest at G_1 phase as this study suggest that pRb inhibit E2F transcription factor as it was ablated by *A. afra* thus inhibiting cell division (Figure:4.17C). The findings of this study suggest that *A. afra* induced c-Myc protein, which was reduced by pRb. The data from this study is in concurrence with a study by *Andrea M Steely* and co-researchers where artemisinin induce cell cycle arrest by production pRb thus inhibiting cell division (Steely *et al.*, 2017).

Nuclear Factor κB is a prominent transcription factor involved in immune response and inflammation. NF-κB target genes are associated with the regulation of cell survival as wells as apoptosis (Ben-Neriah and Karin, 2011). Expression NF-κB is regulated by ROS (Antonaki *et al.*, 2011). This study showed *A. afra* reduced the gene expression of NF-κB in all treated cells of Caco-2 cancer cells (Figure 416B). A source of ROS that predominantly activate NF-κB is H_2O_2. It can directly exert it effect or through its transformation into OH whilst in the presence of Fe^{2+} in the Fenton reaction (Ben-Neriah and Karin, 2011). These findings suggest *A. afra* did not induce ROS-mediated NF-κB transcriptional activity in Caco-2 for 48h and NF-κB is not responsible for the transcription of STAT-3 as in this study detoxifying enzyme (Figure:4.8) and antioxidant responded to H_2O_2. The findings of this study were consistent with the study of Xi Tan and co-researchers which stated an ethyl acetate extract of *Artemisia anomala S. Moore* also reduced the activation NF-κB signaling pathway (Tan *et al.*, 2014).

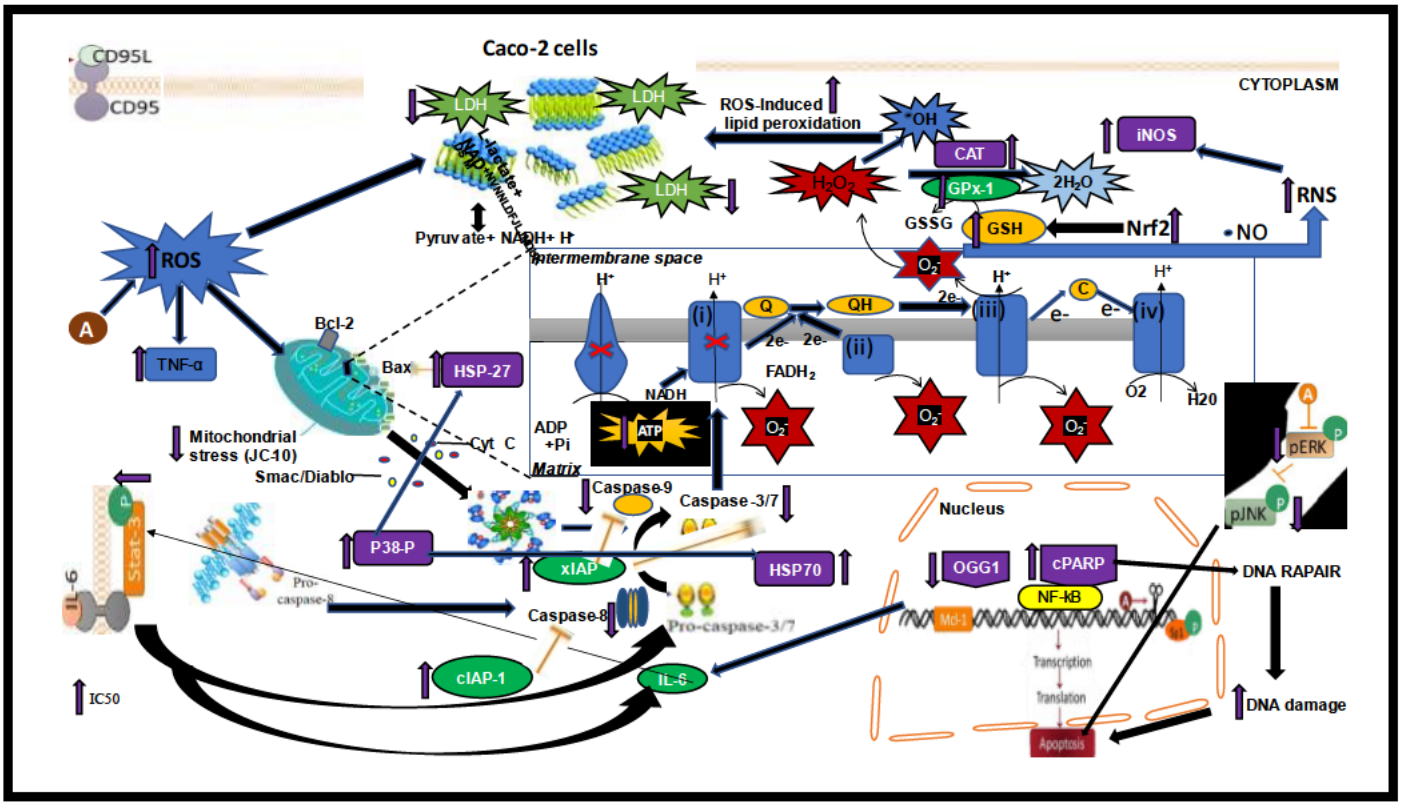

Figure 5.1: Mechanistic overview of the biochemical effects of *A. afra* on membrane and mitochondrial integrity, oxidative stress, stress response and inflammation in human cancerous Human epithelial Caco-2 cells (Prepared by Author).

CHAPTER 6 : CONCLUSION

A widely popular plant *A. afra*, is used to alleviate diseases worldwide. It characterised many medicinal properties and is associated with pharmacological activities that may aid in the development of new anticancer treatment modalities. However, the mechanism by which *A. afra* causes cytotoxicity in human CRC has not yet been investigated and established. In this study, the cytotoxic effects of CRC on the Caco-2 cell line following 48 hours exposure was determined (Figure 5.1).

The results from the study showed reduced mitochondrial viability, ATP depletion. Altered mitochondrial energetics may predispose to ROS production. Although not significant, *A. afra* induced ROS-mediated lipid peroxidation and DNA damage to a certain degree. *A. afra* did not act via the typical NF-κB inflammatory pathway but instead induced transcriptional activity of inflammation biomarkers through elevation of ROS levels thus triggering the STAT3 pathway. This led to the activation of the antioxidant response and a response of DNA repair mechanism via PARP-1and OGG1 ultimately resulting amelioration of DNA damage. Both c-Myc and pRb promoted cell cycle continuation. Stress response protein preserved proteins from damage by restricting apoptosis. Taken together, *A. afra* is an anti-proliferative, cytotoxic and genotoxic agent in human Caco-2 cancer cells. Understanding the underlying biochemical mechanism of toxicity of *A. afra* on Caco-2 cells may aid in the development of new promising therapeutic treatments for CRC.

Phytochemical analysis of the bioactive compounds present in CRC is further recommended for future studies. It would be of interest to identify the compounds responsible for the cytotoxicity of CRC seen in the epithelial cell line. Further studies are also required to determine the effect of CRC on normal cell lines and an *in-vivo* model.

REFERENCES

Uncategorized References

ABD EL-HAFEEZ, A. A., FUJIMURA, T., KAMEI, R., HIRAKAWA, N., BABA, K., ONO, K. & KAWAMOTO, S. 2018. Synergistic tumor suppression by a Perilla frutescens-derived methoxyflavanone and anti-cancer tyrosine kinase inhibitors in A549 human lung adenocarcinoma. *Cytotechnology,* 70**,** 913-919.

ABDEL-AZIZ, S. M., AERON, A. & KAHIL, T. A. 2016. Health benefits and possible risks of herbal medicine. *Microbes in Food and Health.* Springer.

ACHANTA, G. & HUANG, P. 2004. Role of p53 in sensing oxidative DNA damage in response to reactive oxygen species-generating agents. *Cancer research,* 64**,** 6233-6239.

ADEEYO, A., ADEFULE, A., OFUSORI, D., ADERINOLA, A. & CAXTON-MARTINS, E. 2013. Antihyperglycemic effects of aqueous leaf extracts of mistletoe and Moringa oleifera in streptozotocin-induced diabetes Wistar rats. *Diabetologia Croatica,* 42.

AFOLAYAN, A. J. & SUNMONU, T. O. 2013. Protective role of Artemisia afra aqueous extract on tissue antioxidant defense systems in streptozotocin-induced diabetic rats. *African Journal of Traditional, Complementary and Alternative Medicines,* 10**,** 15-20.

AHMAD, M. & KAHWAJI, C. I. 2018. Biochemistry, Electron Transport Chain.

ALBENSI, B. C. 2019. What is nuclear factor kappa B (NF-κB) doing in and to the mitochondrion? *Frontiers in cell and developmental biology,* 7**,** 154.

ALFONSO-PRIETO, M., VIDOSSICH, P. & ROVIRA, C. 2012. The reaction mechanisms of heme catalases: an atomistic view by ab initio molecular dynamics. *Archives of biochemistry and biophysics,* 525**,** 121-130.

ANAVI, S. & TIROSH, O. 2020. iNOS as a metabolic enzyme under stress conditions. *Free Radical Biology and Medicine,* 146**,** 16-35.

ANTONAKI, A., DEMETRIADES, C., POLYZOS, A., BANOS, A., VATSELLAS, G., LAVIGNE, M. D., APOSTOLOU, E., MANTOUVALOU, E., PAPADOPOULOU, D. & MOSIALOS, G. 2011. Genomic analysis reveals a novel nuclear factor-κB (NF-κB)-binding site in Alu-repetitive elements. *Journal of Biological Chemistry,* 286**,** 38768-38782.

ARMAGHANY, T., WILSON, J. D., CHU, Q. & MILLS, G. 2012. Genetic alterations in colorectal cancer. *Gastrointestinal cancer research: GCR,* 5**,** 19.

AUYANG, Y. S. 2006. Cancer causes and cancer research on many levels of complexity.

AYALA, A., MUÑOZ, M. F. & ARGÜELLES, S. 2014. Lipid peroxidation: production, metabolism, and signaling mechanisms of malondialdehyde and 4-hydroxy-2-nonenal. *Oxidative medicine and cellular longevity,* 2014.

AZZOUZ, L. L. & SHARMA, S. 2018. Physiology, large intestine.

BAIRD, L. & DINKOVA-KOSTOVA, A. T. 2011. The cytoprotective role of the Keap1–Nrf2 pathway. *Archives of toxicology,* 85**,** 241-272.

BALIGA, B. & KUMAR, S. 2003. Apaf-1/cytochrome c apoptosome: an essential initiator of caspase activation or just a sideshow? *Cell death and differentiation,* 10**,** 16-18.

BARRÉ, B., VIGNERON, A. & COQUERET, O. 2005. The STAT3 transcription factor is a target for the Myc and riboblastoma proteins on the Cdc25A promoter. *Journal of Biological Chemistry,* 280**,** 15673-15681.

BEINKE, S. & LEY, S. C. 2004. Functions of NF-κB1 and NF-κB2 in immune cell biology. *Biochemical Journal,* 382**,** 393-409.

BEN-NERIAH, Y. & KARIN, M. 2011. Inflammation meets cancer, with NF-κB as the matchmaker. *Nature immunology,* 12**,** 715-723.

BETTERIDGE, D. J. 2000. What is oxidative stress? *Metabolism-Clinical and Experimental,* 49**,** 3-8.

BISHAYEE, A. 2014. The inflammation and liver cancer. *Inflammation and cancer***,** 401-435.

BOGDAN, C., RÖLLINGHOFF, M. & DIEFENBACH, A. 2000. The role of nitric oxide in innate immunity. *Immunological reviews,* 173**,** 17-26.
BOLDINOVA, E. O., KHAIRULLIN, R. F., MAKAROVA, A. V. & ZHARKOV, D. O. 2019. Isoforms of Base Excision Repair Enzymes Produced by Alternative Splicing. *International journal of molecular sciences,* 20**,** 3279.
BRAND, M., GAYLARD, P. & RAMOS, J. 2018. Colorectal cancer in South Africa: An assessment of disease presentation, treatment pathways and 5-year survival. *South African Medical Journal,* 108**,** 118-122.
BRATTON, S. B. & SALVESEN, G. S. 2010. Regulation of the Apaf-1–caspase-9 apoptosome. *Journal of cell science,* 123**,** 3209-3214.
BRAÜNLICH, P. M., INNGJERDINGEN, K. T., INNGJERDINGEN, M., JOHNSON, Q., PAULSEN, B. S. & MABUSELA, W. 2018a. Polysaccharides from the South African medicinal plant Artemisia afra: Structure and activity studies. *Fitoterapia,* 124**,** 182-187.
BRAÜNLICH, P. M., INNGJERDINGEN, K. T., INNGJERDINGEN, M., JOHNSON, Q., PAULSEN, B. S. & MABUSELA, W. J. F. 2018b. Polysaccharides from the South African medicinal plant Artemisia afra: Structure and activity studies. 124**,** 182-187.
BRAY, F., FERLAY, J., SOERJOMATARAM, I., SIEGEL, R. L., TORRE, L. A. & JEMAL, A. 2018. Global cancer statistics 2018: GLOBOCAN estimates of incidence and mortality worldwide for 36 cancers in 185 countries. *CA: a cancer journal for clinicians,* 68**,** 394-424.
BRYAN, N. S. & GRISHAM, M. B. 2007. Methods to detect nitric oxide and its metabolites in biological samples. *Free Radical Biology and Medicine,* 43**,** 645-657.
BURITS, M., ASRES, K. & BUCAR, F. 2001. The antioxidant activity of the essential oils of Artemisia afra, Artemisia abyssinica and Juniperus procera. *Phytotherapy Research,* 15**,** 103-108.
CAMPBELL, K. J. & TAIT, S. W. 2018. Targeting BCL-2 regulated apoptosis in cancer. *Open biology,* 8**,** 180002.
CANDAS, D. & LI, J. J. 2014. MnSOD in oxidative stress response-potential regulation via mitochondrial protein influx. *Antioxidants & redox signaling,* 20**,** 1599-1617.
CARGNELLO, M. & ROUX, P. P. 2011. Activation and function of the MAPKs and their substrates, the MAPK-activated protein kinases. *Microbiology and molecular biology reviews,* 75**,** 50-83.
CHABNER, B. A. & LONGO, D. L. 2011. *Cancer chemotherapy and biotherapy: principles and practice,* Lippincott Williams & Wilkins.
CHAN, A. & MURIN, S. 2011. Up in smoke: the fallacy of the harmless Hookah. *Chest,* 139**,** 737-738.
CHANG, H. Y. & YANG, X. 2000. Proteases for cell suicide: functions and regulation of caspases. *Microbiol. Mol. Biol. Rev.,* 64**,** 821-846.
CHENG, X., PEUCKERT, C. & WÖLFL, S. 2017. Essential role of mitochondrial Stat3 in p38 MAPK mediated apoptosis under oxidative stress. *Scientific reports,* 7**,** 1-11.
CHOI, T. G. & KIM, S. S. 2019. Physiological Functions of Mitochondrial Reactive Oxygen Species. *Free Radical Medicine and Biology.* IntechOpen.
CHOUCROUN, P., GILLET, D., DORANGE, G., SAWICKI, B. & DEWITTE, J. 2001. Comet assay and early apoptosis. *Mutation Research/Fundamental and Molecular Mechanisms of Mutagenesis,* 478**,** 89-96.
CHUNG, S. S., WU, Y., OKOBI, Q., ADEKOYA, D., ATEFI, M., CLARKE, O., DUTTA, P. & VADGAMA, J. V. 2017. Proinflammatory cytokines IL-6 and TNF-α increased telomerase activity through NF-κB/STAT1/STAT3 activation, and withaferin A inhibited the signaling in colorectal cancer cells. *Mediators of inflammation,* 2017.
CLICK, B. & REGUEIRO, M. 2019. The inflammatory bowel disease medical home: from patients to populations. *Inflammatory bowel diseases,* 25**,** 1881-1885.
COLLIN, F. 2019. Chemical basis of reactive oxygen species reactivity and involvement in neurodegenerative diseases. *International journal of molecular sciences,* 20**,** 2407.

COOKE, M. S., EVANS, M. D., DIZDAROGLU, M. & LUNEC, J. 2003. Oxidative DNA damage: mechanisms, mutation, and disease. *The FASEB Journal,* 17**,** 1195-1214.
COOPER, G. & HAUSMAN, R. 2000. The cell: a molecular approach. Sinauer Associates. *Sunderland, MA*.
COPE, F. O. & TOMEI, L. D. 1991. *Apoptosis: the molecular basis of cell death*.
CORY, S. & ADAMS, J. M. 2002. The Bcl2 family: regulators of the cellular life-or-death switch. *Nature Reviews Cancer,* 2**,** 647-656.
CROWLEY, L. C., MARFELL, B. J., SCOTT, A. P. & WATERHOUSE, N. J. 2016. Quantitation of apoptosis and necrosis by annexin V binding, propidium iodide uptake, and flow cytometry. *Cold Spring Harbor Protocols,* 2016**,** pdb. prot087288.
CRUCERIU, D., BALDASICI, O., BALACESCU, O. & BERINDAN-NEAGOE, I. 2020. The dual role of tumor necrosis factor-alpha (TNF-α) in breast cancer: molecular insights and therapeutic approaches. *Cellular Oncology,* 43**,** 1-18.
DAHER, S., MASSARWA, M., BENSON, A. A., KHOURY, T. J. J. O. C. & HEPATOLOGY, T. 2018. Current and future treatment of hepatocellular carcinoma: an updated comprehensive review. 6**,** 69.
DANIAL, N. N. & HOCKENBERY, D. M. 2018. Cell death. *Hematology*. Elsevier.
DAVIES, K. J. 2000. Oxidative stress, antioxidant defenses, and damage removal, repair, and replacement systems. *IUBMB life,* 50**,** 279-289.
DEAVALL, D., MARTIN, E., HORNER, J. & ROBERTS, R. 2012. Drug-induced oxidative stress and toxicity. J Toxicol 2012: 13.
DEDON, P. C. & TANNENBAUM, S. R. 2004. Reactive nitrogen species in the chemical biology of inflammation. *Archives of biochemistry and biophysics,* 423**,** 12-22.
DEWSON, G., KRATINA, T., CZABOTAR, P., DAY, C. L., ADAMS, J. M. & KLUCK, R. M. 2009. Bak activation for apoptosis involves oligomerization of dimers via their α6 helices. *Molecular cell,* 36**,** 696-703.
DHANASEKARAN, D. N. & REDDY, E. P. 2008. JNK signaling in apoptosis. *Oncogene,* 27**,** 6245-6251.
DOMIJAN, A.-M. & ABRAMOV, A. Y. 2011. Fumonisin B1 inhibits mitochondrial respiration and deregulates calcium homeostasis—implication to mechanism of cell toxicity. *The international journal of biochemistry & cell biology,* 43**,** 897-904.
DU TOIT, A. & VAN DER KOOY, F. 2019a. Artemisia afra, a controversial herbal remedy or a treasure trove of new drugs? *Journal of ethnopharmacology***,** 112127.
DU TOIT, A. & VAN DER KOOY, F. J. J. O. E. 2019b. Artemisia afra, a controversial herbal remedy or a treasure trove of new drugs? **,** 112127.
DUELLMAN, S. J., ZHOU, W., MEISENHEIMER, P., VIDUGIRIS, G., CALI, J. J., GAUTAM, P., WENNERBERG, K. & VIDUGIRIENE, J. 2015. Bioluminescent, nonlytic, real-time cell viability assay and use in inhibitor screening. *Assay and drug development technologies,* 13**,** 456-465.
EDGE, S. B., BYRD, D. R., CARDUCCI, M. A., COMPTON, C. C., FRITZ, A. & GREENE, F. 2010. *AJCC cancer staging manual,* Springer New York.
ELMORE, S. 2007. Apoptosis: a review of programmed cell death. *Toxicologic pathology,* 35**,** 495-516.
ERENER, S., PÉTRILLI, V., KASSNER, I., MINOTTI, R., CASTILLO, R., SANTORO, R., HASSA, P. O., TSCHOPP, J. & HOTTIGER, M. O. 2012. Inflammasome-activated caspase 7 cleaves PARP1 to enhance the expression of a subset of NF-κB target genes. *Molecular cell,* 46**,** 200-211.
FERNÁNDEZ, J., PÉREZ-ÁLVAREZ, J. A. & FERNÁNDEZ-LÓPEZ, J. A. 1997. Thiobarbituric acid test for monitoring lipid oxidation in meat. *Food chemistry,* 59**,** 345-353.
FESTJENS, N., CORNELIS, S., LAMKANFI, M. & VANDENABEELE, P. J. B. C. 2006. Caspase-containing complexes in the regulation of cell death and inflammation. 387**,** 1005-1016.

FIERS, W. 1991. Tumor necrosis factor characterization at the molecular, cellular and in vivo level. *FEBS letters,* 285**,** 199-212.
FIUME, L., MANERBA, M., VETTRAINO, M. & DI STEFANO, G. 2014. Inhibition of lactate dehydrogenase activity as an approach to cancer therapy. *Future medicinal chemistry,* 6**,** 429-445.
FOREST, V., FIGAROL, A., BOUDARD, D., COTTIER, M., GROSSEAU, P. & POURCHEZ, J. 2015. Adsorption of lactate dehydrogenase enzyme on carbon nanotubes: How to get accurate results for the cytotoxicity of these nanomaterials. *Langmuir,* 31**,** 3635-3643.
FÖRSTERMANN, U. & SESSA, W. C. 2012. Nitric oxide synthases: regulation and function. *European heart journal,* 33**,** 829-837.
FRANCO, R., SÁNCHEZ-OLEA, R., REYES-REYES, E. M., PANAYIOTIDIS, M. I. J. M. R. G. T. & MUTAGENESIS, E. 2009. Environmental toxicity, oxidative stress and apoptosis: menage a trois. 674**,** 3-22.
GARIBYAN, L. & AVASHIA, N. 2013. Research techniques made simple: polymerase chain reaction (PCR). *The Journal of investigative dermatology,* 133**,** e6.
GARRIDO, C., BRUNET, M., DIDELOT, C., ZERMATI, Y., SCHMITT, E. & KROEMER, G. 2006. Heat shock proteins 27 and 70: anti-apoptotic proteins with tumorigenic properties. *Cell cycle,* 5**,** 2592-2601.
GELLER, D. A., LOWENSTEIN, C. J., SHAPIRO, R. A., NUSSLER, A. K., DI SILVIO, M., WANG, S. C., NAKAYAMA, D. K., SIMMONS, R. L., SNYDER, S. H. & BILLIAR, T. R. 1993. Molecular cloning and expression of inducible nitric oxide synthase from human hepatocytes. *Proceedings of the National Academy of Sciences,* 90**,** 3491-3495.
GIBSON, S. B. 2004. Epidermal growth factor and trail interactions in epithelial-derived cells. *Vitamins & Hormones.* Elsevier.
GILL, S. S., HEUMAN, D. M. & MIHAS, A. A. 2001. Small intestinal neoplasms. *Journal of clinical gastroenterology,* 33**,** 267-282.
GOLDSTEIN, J. C., WATERHOUSE, N. J., JUIN, P., EVAN, G. I. & GREEN, D. R. 2000. The coordinate release of cytochrome c during apoptosis is rapid, complete and kinetically invariant. *Nature cell biology,* 2**,** 156-162.
GOPI, S., VARMA, K., JUDE, S. & DIVYA, M. 2016. A study on the nitric oxide (NO) enhancing ability of a natural phytochemical formulation. *Asian Journal of Pharmaceutical Technology & Innovation,* 4**,** 1-6.
GRAVEN, E., DEAN, S., SVOBODA, K. P., MAVI, S. & GUNDIDZA, M. G. 1992. Antimicrobial and antioxidative properties of the volatile (essential) oil of Artemisia afra Jacq. *Flavour and Fragrance journal,* 7**,** 121-123.
GREEN, D. R. & LLAMBI, F. 2015. Cell death signaling. *Cold Spring Harbor perspectives in biology,* 7**,** a006080.
GREEN, D. R. J. C. 2019. The coming decade of cell death research: five riddles. 177**,** 1094-1107.
GREENWELL, M. & RAHMAN, P. 2015. Medicinal plants: their use in anticancer treatment. *International journal of pharmaceutical sciences and research,* 6**,** 4103.
GRETEN, F. R. & GRIVENNIKOV, S. I. 2019. Inflammation and cancer: triggers, mechanisms, and consequences. *Immunity,* 51**,** 27-41.
GRIVENNIKOV, S. I., GRETEN, F. R. & KARIN, M. 2010. Immunity, inflammation, and cancer. *Cell,* 140**,** 883-899.
GUANTAI, A. & ADDAE-MENSAH, I. 1999. Cardiovascular effect of Artemisia afra and its constituents. *Pharmaceutical biology,* 37**,** 351-356.
GUTTERIDGE, J. 1995. Lipid peroxidation and antioxidants as biomarkers of tissue damage. *Clinical chemistry,* 41**,** 1819-1828.
HALLIWELL, B. & CHIRICO, S. 1993. Lipid peroxidation: its mechanism, measurement, and significance. *The American journal of clinical nutrition,* 57**,** 715S-725S.
HALLIWELL, B. & GUTTERIDGE, J. 1989. Free radicals in biology and medicine. Clarendon. Oxford.

HARRIS, M. & THOMPSON, C. 2000. The role of the Bcl-2 family in the regulation of outer mitochondrial membrane permeability. *Cell Death & Differentiation,* 7**,** 1182-1191.
HASSAN, M., WATARI, H., ABUALMAATY, A., OHBA, Y. & SAKURAGI, N. 2014. Apoptosis and molecular targeting therapy in cancer. *BioMed research international,* 2014.
HERMES-LIMA, M. 2004. Oxygen in biology and biochemistry: role of free radicals. *Functional metabolism: Regulation and adaptation,* 1**,** 319-66.
HIDALGO, I. J., RAUB, T. J. & BORCHARDT, R. T. 1989. Characterization of the human colon carcinoma cell line (Caco-2) as a model system for intestinal epithelial permeability. *Gastroenterology,* 96**,** 736-749.
HILLIARD, O. M. 1977. *Compositae in natal,* University of Natal Press.
HONG, S. J., DAWSON, T. M. & DAWSON, V. L. 2006. PARP and the release of apoptosis-inducing factor from mitochondria. *Poly (ADP-Ribosyl) ation.* Springer.
HUGHES, L. A., SIMONS, C. C., VAN DEN BRANDT, P. A., VAN ENGELAND, M. & WEIJENBERG, M. P. 2017. Lifestyle, diet, and colorectal cancer risk according to (epi) genetic instability: current evidence and future directions of molecular pathological epidemiology. *Current colorectal cancer reports,* 13**,** 455-469.
HUSSEIN, R. A. & EL-ANSSARY, A. A. 2018. Plants secondary metabolites: the key drivers of the pharmacological actions of medicinal plants. *Herbal Medicine.*
IKWEGBUE, P. C., MASAMBA, P., OYINLOYE, B. E. & KAPPO, A. P. 2018. Roles of heat shock proteins in apoptosis, oxidative stress, human inflammatory diseases, and cancer. *Pharmaceuticals,* 11**,** 2.
JAISWAL, A. K. 2004. Nrf2 signaling in coordinated activation of antioxidant gene expression. *Free Radical Biology and Medicine,* 36**,** 1199-1207.
JAISWAL, M., LARUSSO, N. F., NISHIOKA, N., NAKABEPPU, Y. & GORES, G. J. 2001. Human Ogg1, a protein involved in the repair of 8-oxoguanine, is inhibited by nitric oxide. *Cancer research,* 61**,** 6388-6393.
JAKUPOVIC, J., KLEMEYER, H., BOHLMANN, F. & GRAVEN, E. 1988. Glaucolides and guaianolides from Artemisia afra. *Phytochemistry,* 27**,** 1129-1133.
JANG, E., KIM, S.-Y., LEE, N.-R., YI, C.-M., HONG, D.-R., LEE, W. S., KIM, J.-H., LEE, K.-T., KIM, B.-J. & LEE, J.-H. 2017. Evaluation of antitumor activity of Artemisia capillaris extract against hepatocellular carcinoma through the inhibition of IL-6/STAT3 signaling axis. *Oncology reports,* 37**,** 526-532.
JEONG, S. H., KIM, J. & MIN, H. 2018. In vitro anti-inflammatory activity of the Artemisia montana leaf ethanol extract in macrophage RAW 264.7 cells. *Food and Agricultural Immunology,* 29**,** 688-698.
JIANG, W. G., SANDERS, A. J., KATOH, M., UNGEFROREN, H., GIESELER, F., PRINCE, M., THOMPSON, S., ZOLLO, M., SPANO, D. & DHAWAN, P. Tissue invasion and metastasis: Molecular, biological and clinical perspectives. Seminars in cancer biology, 2015. Elsevier, S244-S275.
JIN, Z. & EL-DEIRY, W. S. 2005. Overview of cell death signaling pathways. *Cancer biology & therapy,* 4**,** 147-171.
JULIEN, O., WELLS, J. A. J. C. D. & DIFFERENTIATION 2017. Caspases and their substrates. 24**,** 1380-1389.
KALE, J., OSTERLUND, E. J. & ANDREWS, D. W. 2018. BCL-2 family proteins: changing partners in the dance towards death. *Cell Death & Differentiation,* 25**,** 65-80.
KANE, N. F., KYAMA, M. C., NGANGA, J. K., HASSANALI, A., DIALLO, M. & KIMANI, F. T. 2019. Comparison of phytochemical profiles and antimalarial activities of Artemisia afra plant collected from five countries in Africa. *South African Journal of Botany,* 125**,** 126-133.
KAUFMANN, S. H., DESNOYERS, S., OTTAVIANO, Y., DAVIDSON, N. E. & POIRIER, G. G. 1993. Specific proteolytic cleavage of poly (ADP-ribose) polymerase: an early marker of chemotherapy-induced apoptosis. *Cancer research,* 53**,** 3976-3985.

KEHRER, J. P. 2000. The Haber–Weiss reaction and mechanisms of toxicity. *Toxicology,* 149**,** 43-50.
KERR, J. F., WYLLIE, A. H. & CURRIE, A. R. J. B. J. O. C. 1972. Apoptosis: a basic biological phenomenon with wideranging implications in tissue kinetics. 26**,** 239-257.
KO, H. L. & REN, E. C. 2012. Functional aspects of PARP1 in DNA repair and transcription. *Biomolecules,* 2**,** 524-548.
KOFF, J. L., RAMACHANDIRAN, S. & BERNAL-MIZRACHI, L. 2015. A time to kill: targeting apoptosis in cancer. *International journal of molecular sciences,* 16**,** 2942-2955.
KONISHI, T., SHIMADA, Y., NAGAO, T., OKABE, H. & KONOSHIMA, T. 2002. Antiproliferative sesquiterpene lactones from the roots of Inula helenium. *Biological and Pharmaceutical Bulletin,* 25**,** 1370-1372.
KOWALTOWSKI, A. J. & VERCESI, A. E. 1999. Mitochondrial damage induced by conditions of oxidative stress. *Free Radical Biology and Medicine,* 26**,** 463-471.
KRÖNCKE, K., FEHSEL, K. & KOLB-BACHOFEN, V. 1998. Inducible nitric oxide synthase in human diseases. *Clinical and experimental immunology,* 113**,** 147.
KRUMOVA, K. & COSA, G. 2016. Overview of reactive oxygen species.
KULINSKY, V. 2007. Biochemical aspects of inflammation. *Biochemistry (Moscow),* 72**,** 595-607.
KUPKA, S., REICHERT, M., DRABER, P. & WALCZAK, H. 2016. Formation and removal of poly-ubiquitin chains in the regulation of tumor necrosis factor-induced gene activation and cell death. *The FEBS journal,* 283**,** 2626-2639.
KURUTAS, E. B. 2015. The importance of antioxidants which play the role in cellular response against oxidative/nitrosative stress: current state. *Nutrition journal,* 15**,** 1-22.
LANGELIER, M.-F., PLANCK, J. L., ROY, S. & PASCAL, J. M. 2012. Structural basis for DNA damage–dependent poly (ADP-ribosyl) ation by human PARP-1. *Science,* 336**,** 728-732.
LAVOIE, H., GAGNON, J. & THERRIEN, M. 2020. ERK signalling: a master regulator of cell behaviour, life and fate. *Nature Reviews Molecular Cell Biology,* 21**,** 607-632.
LEA, T. 2015. Caco-2 Cell Line. *In:* VERHOECKX, K., COTTER, P., LÓPEZ-EXPÓSITO, I., KLEIVELAND, C., LEA, T., MACKIE, A., REQUENA, T., SWIATECKA, D. & WICHERS, H. (eds.) *The Impact of Food Bioactives on Health: in vitro and ex vivo models.* Cham: Springer International Publishing.
LI-WEBER, M. 2013. Targeting apoptosis pathways in cancer by Chinese medicine. *Cancer letters,* 332**,** 304-312.
LI, M. O., SARKISIAN, M. R., MEHAL, W. Z., RAKIC, P. & FLAVELL, R. A. 2003. Phosphatidylserine receptor is required for clearance of apoptotic cells. *Science,* 302**,** 1560-1563.
LIN, J. L., NAKAGAWA, A., SKEEN-GAAR, R., YANG, W.-Z., ZHAO, P., ZHANG, Z., GE, X., MITANI, S., XUE, D. & YUAN, H. S. 2016. Oxidative stress impairs cell death by repressing the nuclease activity of mitochondrial endonuclease G. *Cell reports,* 16**,** 279-287.
LIN, M. V., KING, L. Y. & CHUNG, R. T. 2015. Hepatitis C virus–associated cancer. *Annual Review of Pathology: Mechanisms of Disease,* 10**,** 345-370.
LIN, Y., DEVIN, A., RODRIGUEZ, Y. & LIU, Z.-G. 1999. Cleavage of the death domain kinase RIP by caspase-8 prompts TNF-induced apoptosis. *Genes & development,* 13**,** 2514-2526.
LIU, N., VAN DER KOOY, F. & VERPOORTE, R. 2009. Artemisia afra: a potential flagship for African medicinal plants? *South African Journal of Botany,* 75**,** 185-195.
LIU, T., ZHANG, L., JOO, D. & SUN, S.-C. 2017a. NF-κB signaling in inflammation. *Signal transduction and targeted therapy,* 2**,** 1-9.
LIU, T., ZHANG, L., JOO, D. & SUN, S.-C. 2017b. NF-κB signaling in inflammation. *Signal transduction and targeted therapy,* 2**,** 17023.
LIU, Y. & WANG, W. 2016. Aflatoxin B1 impairs mitochondrial functions, activates ROS generation, induces apoptosis and involves Nrf2 signal pathway in primary broiler hepatocytes. *Animal Science Journal,* 87**,** 1490-1500.

LLOYD, R. V., HANNA, P. M. & MASON, R. P. 1997. The origin of the hydroxyl radical oxygen in the Fenton reaction. *Free radical biology and medicine,* 22**,** 885-888.
LOBO, V., PATIL, A., PHATAK, A. & CHANDRA, N. 2010. Free radicals, antioxidants and functional foods: Impact on human health. *Pharmacognosy reviews,* 4**,** 118.
LONG, J. & RYAN, K. 2012. New frontiers in promoting tumour cell death: targeting apoptosis, necroptosis and autophagy. *Oncogene,* 31**,** 5045-5060.
MA, Q. 2013. Role of nrf2 in oxidative stress and toxicity. *Annual review of pharmacology and toxicology,* 53**,** 401-426.
MAGALHÃES, P. J., CARVALHO, D. O., CRUZ, J. M., GUIDO, L. F. & BARROS, A. A. 2009. Fundamentals and health benefits of xanthohumol, a natural product derived from hops and beer. *Natural product communications,* 4**,** 1934578X0900400501.
MAHMOOD, N., NAZIR, R., KHAN, M., IQBAL, R., ADNAN, M., ULLAH, M. & YANG, H. J. P. 2019. Phytochemical Screening, Antibacterial Activity and Heavy Metal Analysis of Ethnomedicinal Recipes and Their Sources Used Against Infectious Diseases. 8**,** 454.
MAHOMOODALLY, M. F. 2013. Traditional medicines in Africa: an appraisal of ten potent African medicinal plants. *Evidence-Based Complementary and Alternative Medicine,* 2013.
MAHOP, T. & MAYET, M. J. A. J. O. B. 2007. Enroute to biopiracy? Ethnobotanical research on antidiabetic medicinal plants in the Eastern Cape Province, South Africa. 6**,** 2945-2952.
MAK, D., SENGAYI, M., CHEN, W. C., DE VILLIERS, C. B., SINGH, E. & KRAMVIS, A. 2018. Liver cancer mortality trends in South Africa: 1999–2015. *BMC cancer,* 18**,** 798.
MAKAMURE, M. T., REDDY, P., CHUTURGOON, A. A., NAIDOO, R. N., MENTZ, G., BATTERMAN, S. & ROBINS, T. G. 2016. Tumour necrosis factor α polymorphism (TNF-308α G/A) in association with asthma related phenotypes and air pollutants among children in KwaZulu-Natal. *Asian Pacific journal of allergy and immunology*.
MARTÍNEZ-LIMÓN, A., JOAQUIN, M., CABALLERO, M., POSAS, F. & DE NADAL, E. 2020. The p38 pathway: from biology to cancer therapy. *International journal of molecular sciences,* 21**,** 1913.
MARTÍNEZ-VALVERDE, I., PERIAGO, M. J. & ROS, G. 2000. Nutritional importance of phenolic compounds in the diet. *Archivos latinoamericanos de nutricion,* 50**,** 5-18.
MATASSOV, D., KAGAN, T., LEBLANC, J., SIKORSKA, M. & ZAKERI, Z. 2004. Measurement of apoptosis by DNA fragmentation. *Apoptosis Methods and Protocols.* Springer.
MATHUR, P., SATHISHKUMAR, K., CHATURVEDI, M., DAS, P., SUDARSHAN, K. L., SANTHAPPAN, S., NALLASAMY, V., JOHN, A., NARASIMHAN, S. & ROSELIND, F. S. 2020. Cancer statistics, 2020: report from national cancer registry programme, India. *JCO Global Oncology,* 6**,** 1063-1075.
MATIVANDLELA, S. P. N., MEYER, J. J. M., HUSSEIN, A. A., HOUGHTON, P. J., HAMILTON, C. J., LALL, N. J. P. R. A. I. J. D. T. P. & DERIVATIVES, T. E. O. N. P. 2008. Activity against Mycobacterium smegmatis and M. tuberculosis by extract of South African medicinal plants. 22**,** 841-845.
MCCABE, M., PERNER, Y., MAGOBO, R., MIRZA, S. & PENNY, C. 2019. Descriptive epidemiological study of South African colorectal cancer patients at a Johannesburg Hospital Academic institution. *JGH Open*.
MCGAW, L. J. & ELOFF, J. N. J. J. O. E. 2008. Ethnoveterinary use of southern African plants and scientific evaluation of their medicinal properties. 119**,** 559-574.
MILISAV, I., POLJSAK, B. & ŠUPUT, D. 2012. Adaptive response, evidence of cross-resistance and its potential clinical use. *International journal of molecular sciences,* 13**,** 10771-10806.
MILLER, A., HOOGSTRATEN, B., STAQUET, M. & WINKLER, A. J. C. 1981. Reporting results of cancer treatment. 47**,** 207-214.
MODING, E. J., KASTAN, M. B. & KIRSCH, D. G. 2013. Strategies for optimizing the response of cancer and normal tissues to radiation. *Nature reviews Drug discovery,* 12**,** 526-542.
MOKDAD, A. A., SINGAL, A. G. & YOPP, A. C. J. J. 2015. Liver Cancer. 314**,** 2701-2701.

MORE, G., LALL, N., HUSSEIN, A. & TSHIKALANGE, T. E. 2012. Antimicrobial constituents of Artemisia afra Jacq. ex Willd. against periodontal pathogens. *Evidence-Based Complementary and Alternative Medicine,* 2012.
MOSMANN, T. 1983. Rapid colorimetric assay for cellular growth and survival: application to proliferation and cytotoxicity assays. *Journal of immunological methods,* 65**,** 55-63.
MOTHIBE, M. E. & SIBANDA, M. 2019. African traditional medicine: south african perspective. *Traditional and Complementary Medicine.* IntechOpen.
MOTSUKU, L., CHEN, W. C., MUCHENGETI, M. M., NAIDOO, M., MAC QUENE, T., KELLETT, P., MOHLALA, M. I., CHU, K. M. & SINGH, E. 2021. Colorectal cancer incidence and mortality trends by sex and population group in South Africa: 2002–2014. *BMC cancer,* 21**,** 1-11.
MOYO, P., KUNYANE, P., SELEPE, M. A., ELOFF, J. N., NIEMAND, J., LOUW, A. I., MAHARAJ, V. J. & BIRKHOLTZ, L.-M. 2019a. Bioassay-guided isolation and identification of gametocytocidal compounds from Artemisia afra (Asteraceae). *Malaria journal,* 18**,** 65.
MOYO, P., KUNYANE, P., SELEPE, M. A., ELOFF, J. N., NIEMAND, J., LOUW, A. I., MAHARAJ, V. J. & BIRKHOLTZ, L.-M. 2019b. Bioassay-guided isolation and identification of gametocytocidal compounds from Artemisia afra (Asteraceae). *Malaria journal,* 18**,** 1-11.
MUKINDA, J. T. 2005. *Acute and chronic toxicity of the flavonoid-containing plant, Artemisia afra in rodents.* University of the Western Cape.
MURPHY, K., RANGANATHAN, V., FARNSWORTH, M., KAVALLARIS, M. & LOCK, R. B. 2000. Bcl-2 inhibits Bax translocation from cytosol to mitochondria during drug-induced apoptosis of human tumor cells. *Cell Death & Differentiation,* 7**,** 102-111.
NAIDOO, V., MCGAW, L. J., BISSCHOP, S., DUNCAN, N. & ELOFF, J. N. 2008. The value of plant extracts with antioxidant activity in attenuating coccidiosis in broiler chickens. *Veterinary parasitology,* 153**,** 214-219.
NGUYEN, T., NIOI, P. & PICKETT, C. B. 2009. The Nrf2-antioxidant response element signaling pathway and its activation by oxidative stress. *Journal of biological chemistry,* 284**,** 13291-13295.
NIELSEN, N. D., SANDAGER, M., STAFFORD, G. I., VAN STADEN, J. & JÄGER, A. K. J. J. O. E. 2004. Screening of indigenous plants from South Africa for affinity to the serotonin reuptake transport protein. 94**,** 159-163.
NOVUS, B. 2021. *Phosphatidylserine Externalization in Apoptosis* [Online]. Available: https://www.novusbio.com/research-topics/apoptosis/phosphatidylserine-externalization [Accessed 15 March 2021].
NOWSHEEN, S. & YANG, E. 2012. The intersection between DNA damage response and cell death pathways. *Experimental oncology,* 34**,** 243.
OLIVE, P. L. & BANÁTH, J. P. 2006. The comet assay: a method to measure DNA damage in individual cells. *Nature protocols,* 1**,** 23.
ORGANIZATION, W. H. 2015. *Guidelines for the prevention care and treatment of persons with chronic hepatitis B infection: Mar-15*, World Health Organization.
ORGANIZATION, W. H. 2019. *WHO global report on traditional and complementary medicine 2019*, World Health Organization.
OSTLING, O. & JOHANSON, K. J. 1984. Microelectrophoretic study of radiation-induced DNA damages in individual mammalian cells. *Biochemical and biophysical research communications,* 123**,** 291-298.
PARAMESWARAN, N. & PATIAL, S. 2010. Tumor necrosis factor-α signaling in macrophages. *Critical Reviews™ in Eukaryotic Gene Expression,* 20.
PATIL, G., DASS, S. & CHANDRA, R. 2011. Artemisia afraand Modern Diseases. *J Pharmacogenom Pharmacoproteomics,* 2**,** 2153-0645.1000105.

PERRY, D. K., SMYTH, M. J., STENNICKE, H. R., SALVESEN, G. S., DURIEZ, P., POIRIER, G. G. & HANNUN, Y. A. 1997. Zinc is a potent inhibitor of the apoptotic protease, caspase-3 a novel target for zinc in the inhibition of apoptosis. *Journal of Biological Chemistry,* 272**,** 18530-18533.

PICARD, M., TAIVASSALO, T., GOUSPILLOU, G. & HEPPLE, R. T. 2011. Mitochondria: isolation, structure and function. *The Journal of physiology,* 589**,** 4413-4421.

POLJSAK, B., ŠUPUT, D. & MILISAV, I. 2013. Achieving the balance between ROS and antioxidants: when to use the synthetic antioxidants. *Oxidative medicine and cellular longevity,* 2013.

RABE, T. & VAN STADEN, J. 1997. Antibacterial activity of South African plants used for medicinal purposes. *Journal of ethnopharmacology,* 56**,** 81-87.

RADI, R. 2018. Oxygen radicals, nitric oxide, and peroxynitrite: Redox pathways in molecular medicine. *Proceedings of the National Academy of Sciences,* 115**,** 5839-5848.

RAHAL, A., KUMAR, A., SINGH, V., YADAV, B., TIWARI, R., CHAKRABORTY, S. & DHAMA, K. 2014. Oxidative stress, prooxidants, and antioxidants: the interplay. *BioMed research international,* 2014.

RAMAN, M., CHEN, W. & COBB, M. 2007. Differential regulation and properties of MAPKs. *Oncogene,* 26**,** 3100-3112.

RASUL, A., KHAN, M., ALI, M., LI, J. & LI, X. 2013. Targeting apoptosis pathways in cancer with alantolactone and isoalantolactone. *The Scientific World Journal,* 2013.

RAWLA, P., SUNKARA, T. & BARSOUK, A. 2019. Epidemiology of colorectal cancer: Incidence, mortality, survival, and risk factors. *Przegląd Gastroenterologiczny,* 14**,** 89.

REED, J. C. 1999. Dysregulation of apoptosis in cancer. *Journal of clinical oncology,* 17**,** 2941-2941.

REITER, R. J., MELCHIORRI, D., SEWERYNEK, E., POEGGELER, B., BARLOW-WALDEN, L., CHUANG, J., ORTIZ, G. G. & ACUÑACASTROVIEJO, D. 1995. A review of the evidence supporting melatonin's role as an antioxidant. *Journal of pineal research,* 18**,** 1-11.

RENAULT, T. T., FLOROS, K. V. & CHIPUK, J. E. 2013. BAK/BAX activation and cytochrome c release assays using isolated mitochondria. *Methods,* 61**,** 146-155.

REPETTO, M., SEMPRINE, J. & BOVERIS, A. 2012. Lipid peroxidation: chemical mechanism, biological implications and analytical determination. *Lipid peroxidation,* 1**,** 3-30.

RISS, T. L., MORAVEC, R. A., NILES, A. L., DUELLMAN, S., BENINK, H., WORZELLA, T. & MINOR, L. 2015. Cell Viability Assays. Eli Lilly & Company and the National Center for Advancing Translational Sciences.

ROITT, I. M. & DELVES, P. J. 1992. *Encyclopedia of immunology,* Academic Press.

ROMANI, A. M. 2018. Physiology and Pathology of Mitochondrial Dehydrogenases. *Secondary Metabolites: Sources and Applications***,** 125.

ROY, J., JAIN, N., SINGH, G., DAS, B. & MALLICK, B. 2019. Small RNA proteome as disease biomarker: An incognito treasure of clinical utility. *AGO-Driven Non-Coding RNAs.* Elsevier.

ROZOVSKI, U., HARRIS, D. M., LI, P., LIU, Z., WU, J. Y., GRGUREVIC, S., FADERL, S., FERRAJOLI, A., WIERDA, W. G. & MARTINEZ, M. 2016. At high levels, constitutively activated STAT3 induces apoptosis of chronic lymphocytic leukemia cells. *The Journal of Immunology,* 196**,** 4400-4409.

SAJJAD, N., WANI, A., SHARMA, A., ALI, R., HASSAN, S., HAMID, R., HABIB, H. & GANAI, B. A. 2019. Artemisia amygdalina upregulates Nrf2 and protects neurons against oxidative stress in Alzheimer disease. *Cellular and molecular neurobiology,* 39**,** 387-399.

SAK, K. 2012. Chemotherapy and dietary phytochemical agents. *Chemotherapy research and practice,* 2012.

SALVESEN, G. S. 2010. Caspases: cell signaling by proteolysis. *Handbook of Cell Signaling.* Elsevier.

SARASTE, A. & PULKKI, K. J. C. R. 2000. Morphologic and biochemical hallmarks of apoptosis. 45**,** 528-537.
SCHIEBER, M. & CHANDEL, N. S. 2014. ROS function in redox signaling and oxidative stress. *Current biology,* 24**,** R453-R462.
SCHMIDT-ARRAS, D. & ROSE-JOHN, S. 2016. IL-6 pathway in the liver: from physiopathology to therapy. *Journal of hepatology,* 64**,** 1403-1415.
SCHNEIDER, P. & TSCHOPP, J. 2000. Apoptosis induced by death receptors. *Pharmacochemistry Library.* Elsevier.
SHADAD, A. K., SULLIVAN, F. J., MARTIN, J. D. & EGAN, L. J. 2013. Gastrointestinal radiation injury: symptoms, risk factors and mechanisms. *World journal of gastroenterology: WJG,* 19**,** 185.
SHAMAS-DIN, A., KALE, J., LEBER, B. & ANDREWS, D. W. 2013. Mechanisms of action of Bcl-2 family proteins. *Cold Spring Harbor perspectives in biology,* 5**,** a008714.
SHARIFI-RAD, M., ANIL KUMAR, N. V., ZUCCA, P., VARONI, E. M., DINI, L., PANZARINI, E., RAJKOVIC, J., TSOUH FOKOU, P. V., AZZINI, E., PELUSO, I., PRAKASH MISHRA, A., NIGAM, M., EL RAYESS, Y., BEYROUTHY, M. E., POLITO, L., IRITI, M., MARTINS, N., MARTORELL, M., DOCEA, A. O., SETZER, W. N., CALINA, D., CHO, W. C. & SHARIFI-RAD, J. 2020. Lifestyle, Oxidative Stress, and Antioxidants: Back and Forth in the Pathophysiology of Chronic Diseases. *Front Physiol,* 11**,** 694.
SHARMA, P., JHA, A. B., DUBEY, R. S. & PESSARAKLI, M. 2012. Reactive oxygen species, oxidative damage, and antioxidative defense mechanism in plants under stressful conditions. *Journal of botany,* 2012.
SILBERNAGEL, E., SPREITZER, H. & BUCHBAUER, G. 1990. NONVOLATILE CONSTITUENTS OF ARTEMISIA-AFRA. SPRINGER-VERLAG WIEN SACHSENPLATZ 4-6, PO BOX 89, A-1201 VIENNA, AUSTRIA.
SILVA, K. A. S., DONG, J., DONG, Y., DONG, Y., SCHOR, N., TWEARDY, D. J., ZHANG, L. & MITCH, W. E. 2015. Inhibition of Stat3 activation suppresses caspase-3 and the ubiquitin-proteasome system, leading to preservation of muscle mass in cancer cachexia. *Journal of Biological Chemistry,* 290**,** 11177-11187.
SIMON, K. 2016. Colorectal cancer development and advances in screening. *Clinical interventions in aging,* 11**,** 967.
SINGH, N. P., MCCOY, M. T., TICE, R. R. & SCHNEIDER, E. L. 1988. A simple technique for quantitation of low levels of DNA damage in individual cells. *Experimental cell research,* 175**,** 184-191.
SKEEL, R. T. & KHLEIF, S. N. 2011. *Handbook of cancer chemotherapy,* Lippincott Williams & Wilkins.
SMALL, D. M., COOMBES, J. S., BENNETT, N., JOHNSON, D. W. & GOBE, G. C. 2012. Oxidative stress, anti-oxidant therapies and chronic kidney disease. *Nephrology,* 17**,** 311-321.
SNEZHKINA, A. V., KUDRYAVTSEVA, A. V., KARDYMON, O. L., SAVVATEEVA, M. V., MELNIKOVA, N. V., KRASNOV, G. S. & DMITRIEV, A. A. 2019. ROS Generation and antioxidant defense systems in normal and malignant cells. *Oxidative medicine and cellular longevity,* 2019.
SOARES-SILVA, M., DINIZ, F. F., GOMES, G. N. & BAHIA, D. 2016. The mitogen-activated protein kinase (MAPK) pathway: role in immune evasion by trypanosomatids. *Frontiers in microbiology,* 7**,** 183.
SPIES, L., KOEKEMOER, T., SOWEMIMO, A., GOOSEN, E. & VAN DE VENTER, M. 2013. Caspase-dependent apoptosis is induced by Artemisia afra Jacq. ex Willd in a mitochondria-dependent manner after G2/M arrest. *South African Journal of Botany,* 84**,** 104-109.
STEELY, A. M., WILLOUGHBY, J. A., SUNDAR, S. N., AIVALIOTIS, V. I. & FIRESTONE, G. L. 2017. Artemisinin disrupts androgen responsiveness of human prostate cancer cells by

stimulating the 26S proteasome-mediated degradation of the androgen receptor protein. *Anti-cancer drugs,* 28**,** 1018-1031.
STOCKERT, J. C., BLÁZQUEZ-CASTRO, A., CAÑETE, M., HOROBIN, R. W. & VILLANUEVA, Á. 2012. MTT assay for cell viability: Intracellular localization of the formazan product is in lipid droplets. *Acta histochemica,* 114**,** 785-796.
STUEHR, D. J. 2004. Enzymes of the L-arginine to nitric oxide pathway. *The Journal of nutrition,* 134**,** 2748S-2751S.
SULAIMAN, S. & MARCIANI, L. 2019. MRI of the Colon in the Pharmaceutical Field: The Future before us. *Pharmaceutics,* 11**,** 146.
SULERIA, H. A. R., ADDEPALLI, R., MASCI, P., GOBE, G. & OSBORNE, S. A. 2017. In vitro anti-inflammatory activities of blacklip abalone (Haliotis rubra) in RAW 264.7 macrophages. *Food and agricultural immunology,* 28**,** 711-724.
SULIMAN, S., VAN VUUREN, S. & VILJOEN, A. 2010. Validating the in vitro antimicrobial activity of Artemisia afra in polyherbal combinations to treat respiratory infections. *South African Journal of Botany,* 76**,** 655-661.
SUNG, H., FERLAY, J., SIEGEL, R. L., LAVERSANNE, M., SOERJOMATARAM, I., JEMAL, A. & BRAY, F. 2021. Global cancer statistics 2020: GLOBOCAN estimates of incidence and mortality worldwide for 36 cancers in 185 countries. *CA: a cancer journal for clinicians,* 71**,** 209-249.
SURJANA, D., HALLIDAY, G. M. & DAMIAN, D. L. 2010. Role of nicotinamide in DNA damage, mutagenesis, and DNA repair. *Journal of nucleic acids,* 2010.
TAN, X., WANG, Y.-L., YANG, X.-L. & ZHANG, D.-D. 2014. Ethyl acetate extract of Artemisia anomala S. moore displays potent anti-inflammatory effect. *Evidence-Based Complementary and Alternative Medicine,* 2014.
THANAN, R., OIKAWA, S., HIRAKU, Y., OHNISHI, S., MA, N., PINLAOR, S., YONGVANIT, P., KAWANISHI, S. & MURATA, M. 2015. Oxidative stress and its significant roles in neurodegenerative diseases and cancer. *International journal of molecular sciences,* 16**,** 193-217.
THRING, T. & WEITZ, F. 2006. Medicinal plant use in the Bredasdorp/Elim region of the Southern Overberg in the Western Cape Province of South Africa. *Journal of ethnopharmacology,* 103**,** 261-275.
TOHME, S., SIMMONS, R. L. & TSUNG, A. 2017. Surgery for cancer: a trigger for metastases. *Cancer research,* 77**,** 1548-1552.
TOMASETTI, C. & VOGELSTEIN, B. 2015. Variation in cancer risk among tissues can be explained by the number of stem cell divisions. *Science,* 347**,** 78-81.
TORGOVNICK, A. & SCHUMACHER, B. 2015. DNA repair mechanisms in cancer development and therapy. *Frontiers in genetics,* 6**,** 157.
TSAI, W.-T., LO, Y.-C., WU, M.-S., LI, C.-Y., KUO, Y.-P., LAI, Y.-H., TSAI, Y., CHEN, K.-C., CHUANG, T.-H. & YAO, C.-H. 2016. Mycotoxin patulin suppresses innate immune responses by mitochondrial dysfunction and p62/sequestosome-1-dependent mitophagy. *Journal of biological chemistry,* 291**,** 19299-19311.
TSUJIMOTO, Y. 1997. Apoptosis and necrosis: intracellular ATP level as a determinant for cell death modes. *Cell Death & Differentiation,* 4**,** 429-434.
TURRENS, J. F. 2003. Mitochondrial formation of reactive oxygen species. *The Journal of physiology,* 552**,** 335-344.
UEDA, T., SHIMADA, E. & URAKAWA, T. 1994. Serum levels of cytokines in patients with colorectal cancer: possible involvement of interleukin-6 and interleukin-8 in hematogenous metastasis. *Journal of gastroenterology,* 29**,** 423-429.
VALDERRAMA-TREVIÑO, A. I., BARRERA-MERA, B., CEBALLOS-VILLALVA, J. C. & MONTALVO-JAVÉ, E. E. 2017. Hepatic metastasis from colorectal cancer. *Euroasian journal of hepato-gastroenterology,* 7**,** 166.

VAN CRUCHTEN, S. & VAN DEN BROECK, W. 2002. Morphological and biochemical aspects of apoptosis, oncosis and necrosis. *Anatomia, histologia, embryologia,* 31**,** 214-223.
VAN WYK, B.-E. 2011. The potential of South African plants in the development of new medicinal products. *South African Journal of Botany,* 77**,** 812-829.
VAN WYK, B.-E., OUDTSHOORN, B. V. & GERICKE, N. 1997. *Medicinal Plants of South Africa,* Briza.
VENABLES, L., KOEKEMOER, T., VAN DE VENTER, M. & GOOSEN, E. 2016. Isoalantolactone, a sesquiterpene lactone from Artemisia afra Jacq. ex Willd and its in vitro mechanism of induced cell death in HeLa cells. *South African Journal of Botany,* 103**,** 216-221.
VILJOEN, A. M., VAN VUUREN, S. F., GWEBU, T., DEMIRCI, B. & BAŞER, K. H. C. 2006. The geographical variation and antimicrobial activity of African wormwood (Artemisia afra Jacq.) essential oil. *Journal of Essential Oil Research,* 18**,** 19-25.
VRINGER, E. & TAIT, S. W. G. 2019. Mitochondria and Inflammation: Cell Death Heats Up. *Frontiers in Cell and Developmental Biology,* 7.
WALLACE, K. B. & STARKOV, A. 2000. Mitochondrial targets of drug toxicity. *Annual review of pharmacology and toxicology,* 40**,** 353-388.
WANG, H., LAFDIL, F., WANG, L., PARK, O., YIN, S., NIU, J., MILLER, A. M., SUN, Z. & GAO, B. 2011. Hepatoprotective versus oncogenic functions of STAT3 in liver tumorigenesis. *The American journal of pathology,* 179**,** 714-724.
WANG, X., WANG, W., LI, L., PERRY, G., LEE, H.-G. & ZHU, X. 2014. Oxidative stress and mitochondrial dysfunction in Alzheimer's disease. *Biochimica et Biophysica Acta (BBA)-Molecular Basis of Disease,* 1842**,** 1240-1247.
WATANABE, W., SUDO, K., ASAWA, S., KONNO, K., YOKOTA, T. & SHIGETA, S. 1995. Use of lactate dehydrogenase to evaluate the anti-viral activity against influenza A virus. *Journal of virological methods,* 51**,** 185-191.
WATT, J. M. & BREYER-BRANDWIJK, M. G. 1962. The Medicinal and Poisonous Plants of Southern and Eastern Africa being an Account of their Medicinal and other Uses, Chemical Composition, Pharmacological Effects and Toxicology in Man and Animal. *The Medicinal and Poisonous Plants of Southern and Eastern Africa being an Account of their Medicinal and other Uses, Chemical Composition, Pharmacological Effects and Toxicology in Man and Animal.*
WEI, M. C., ZONG, W.-X., CHENG, E. H.-Y., LINDSTEN, T., PANOUTSAKOPOULOU, V., ROSS, A. J., ROTH, K. A., MACGREGOR, G. R., THOMPSON, C. B. & KORSMEYER, S. J. 2001. Proapoptotic BAX and BAK: a requisite gateway to mitochondrial dysfunction and death. *Science,* 292**,** 727-730.
WEINBERG, R. A. 1995. The retinoblastoma protein and cell cycle control. *Cell,* 81**,** 323-330.
WEYDERT, C. J. & CULLEN, J. J. 2010. Measurement of superoxide dismutase, catalase and glutathione peroxidase in cultured cells and tissue. *Nature protocols,* 5**,** 51.
WORLDWIDE.PROMEGA.COM. 2015. *The GSH-Glo™ Glutathione Assay* [Online]. Available: https://worldwide.promega.com/products/cell-health-assays/oxidative-stress-assays/gsh_glo-glutathione-assay/?catNum=V6911#protocols [Accessed March 2021].
WORLDWIDE.PROMEGA.COM. 2019. *Homogeneous Assay Measures Caspase-3/7 Activity* [Online]. Available: https://worldwide.promega.com/products/cell-health-assays/apoptosis-assays/caspase_glo-3_7-assay-systems/?catNum=G8090 [Accessed March 2021].
WWW.BIO-RAD.COM. 2022. *Preamplification-supermix* [Online]. Available: https://www.bio-rad.com/en-za/product/preamplification-supermix?ID=NVENAUMNI [Accessed January 2022].
WWW.GBIOSCIENCES.COM. 2022. *JC-10 Mitochondrial Membrane Potential Assay* [Online]. Available: https://www.gbiosciences.com/Bioassays/Cell_Health_Assay/Apoptosis-Assays-Accessories/JC-10_Mitochondrial_Membrane_Potential_Assay [Accessed 3 January 2022].

XIANG, Y., GUO, Z., ZHU, P., CHEN, J. & HUANG, Y. 2019. Traditional Chinese medicine as a cancer treatment: Modern perspectives of ancient but advanced science. *Cancer medicine,* 8**,** 1958-1975.

YAN, N. & SHI, Y. 2005. Mechanisms of apoptosis through structural biology. *Annu. Rev. Cell Dev. Biol.,* 21**,** 35-56.

YAN, T., LU, L., XIE, C., CHEN, J., PENG, X., ZHU, L., WANG, Y., LI, Q., SHI, J. & ZHOU, F. 2015. Severely impaired and dysregulated cytochrome P450 expression and activities in hepatocellular carcinoma: implications for personalized treatment in patients. *Molecular cancer therapeutics,* 14**,** 2874-2886.

YU, H., PARDOLL, D. & JOVE, R. 2009. STATs in cancer inflammation and immunity: a leading role for STAT3. *Nature reviews cancer,* 9**,** 798-809.

YUAN, S. & AKEY, C. W. 2013. Apoptosome structure, assembly, and procaspase activation. *Structure,* 21**,** 501-515.

ZHANG, D.-W., SHAO, J., LIN, J., ZHANG, N., LU, B.-J., LIN, S.-C., DONG, M.-Q. & HAN, J. 2009. RIP3, an energy metabolism regulator that switches TNF-induced cell death from apoptosis to necrosis. *Science,* 325**,** 332-336.

ZHANG, W., XIAO, S. & AHN, D. U. 2013. Protein oxidation: basic principles and implications for meat quality. *Critical reviews in food science and nutrition,* 53**,** 1191-1201.

ZHANG, Y., CHEN, X., GUEYDAN, C. & HAN, J. 2018. Plasma membrane changes during programmed cell deaths. *Cell research,* 28**,** 9.

ZITKA, O., SKALICKOVA, S., GUMULEC, J., MASARIK, M., ADAM, V., HUBALEK, J., TRNKOVA, L., KRUSEOVA, J., ECKSCHLAGER, T. & KIZEK, R. 2012. Redox status expressed as GSH: GSSG ratio as a marker for oxidative stress in paediatric tumour patients. *Oncology letters,* 4**,** 1247-1253.

ZOROV, D. B., JUHASZOVA, M. & SOLLOTT, S. J. 2014. Mitochondrial reactive oxygen species (ROS) and ROS-induced ROS release. *Physiological reviews,* 94**,** 909-950.

ZOROVA, L. D., POPKOV, V. A., PLOTNIKOV, E. Y., SILACHEV, D. N., PEVZNER, I. B., JANKAUSKAS, S. S., BABENKO, V. A., ZOROV, S. D., BALAKIREVA, A. V. & JUHASZOVA, M. 2018. Mitochondrial membrane potential. *Analytical biochemistry,* 552**,** 50-59.

APPENDICES

APPENDIX A

Caco-2 cells were treated with a range of *A. afra* concentration (0 – 5000 µg/ml) over a 48h period. A dose-dependent decrease in Caco-2 cell viability was observed and an IC_{50} of 250 µg/ml was determined (Appendix Table A1).

Table A1: The determination of the IC_{50} using the cell viability (MTT) assay.

A.afra Concentration (µg/ml)	Average Absorbance	% Viability	Log [MOE]
0	0.945	100	
50	1.351	143	1.699
125	1.022	108	2.097
250	0.821	87	2.398
500	0.901	95	2.699
1 000	0.451	48	3.000
2 500	0.108	11	3.398
5 000	0.994	105	3.699

APPENDIX B

Table A2: Components Present in Eagles Minimum Essentials Media

COMPONENT	CONCENTRATION
Inorganic Salts	
CaCl2.2H2O	186.0
KCL	400.0
KH2PO4	60.0
MgSO4.7H2O	200.0
NaCl	8 000.0
NaHCO3	350.0
Na2HPO4.7H2O	90.0
Other Components	
Glucose Phenol	1 000.0
Red	20.0
Amino Acids	
L-Arginine-HCl	126.4
L-Cysteine	24.0
L-Histidine-HCl.H2O	42.0
L-Isoleucine	52.4
L-Leucine	52.4
L-Lysine-HCl	73.0
L-Methionine	15.0
L-Phenylalanine	33.0
L-Threonine	47.6
L-Tryptophan	10.2
L-Tyrosine L-Valine	47.6
	46.8
Vitamins	
D-Capantothenate	1.0
Choline Chloride	1.0
Folic acid	1.0
i-Inositol	2.0
Nicotinamide	1.0
Pyridoxine	1.0
Riboflavin	0.1
Thiamine-HCl	1.0

APPENDIX C

Table A3: The determination of the nitrate and nitrite standard reference curve.

Nitrite Standard Concentrations (µM)	OD1	OD2	OD3	Average OD
0	0.098	0.099	0.097	0.098
12.5	0.400	0.406	0.392	0.399
25	0.566	0.406	0.392	0.537
50	1.022	1.002	0.901	0.975
75	1.409	1.352	1.367	1.376
100	0	1.352	0	1.644
150	2.525	0	1.897	2.211
200	2.980	2.947	0	2.964

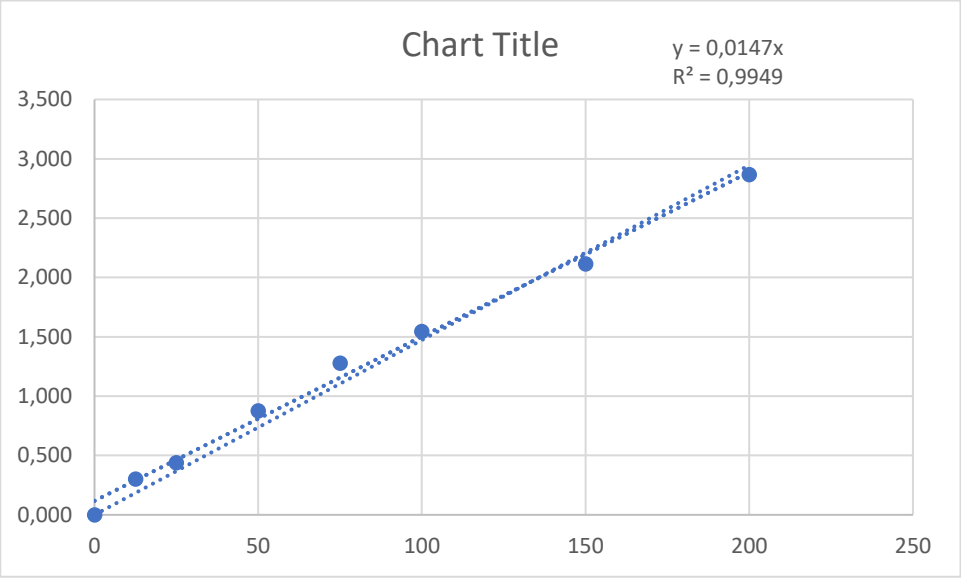

Figure A1: Nitrate and nitrite Standard reference curve used to determine nitrate and nitrite concentration in samples.

APPENDIX D

Table A4: Protein Quantification and Standardisation using Bovine Serum Albumin (BSA).

Protein Standard (mg/ml)	OD1	OD2	OD3	Average OD
0	0.11	0.127	0.131	0.123
0.2	0.287	0.291	0.276	0.285
0.4	0.458	0.440	0.418	0.439
0.6	0.440	0.574	0.584	0.533
0.8	0.418	0.731	0.769	0.639
1	0.858	0.891	0.847	0.865

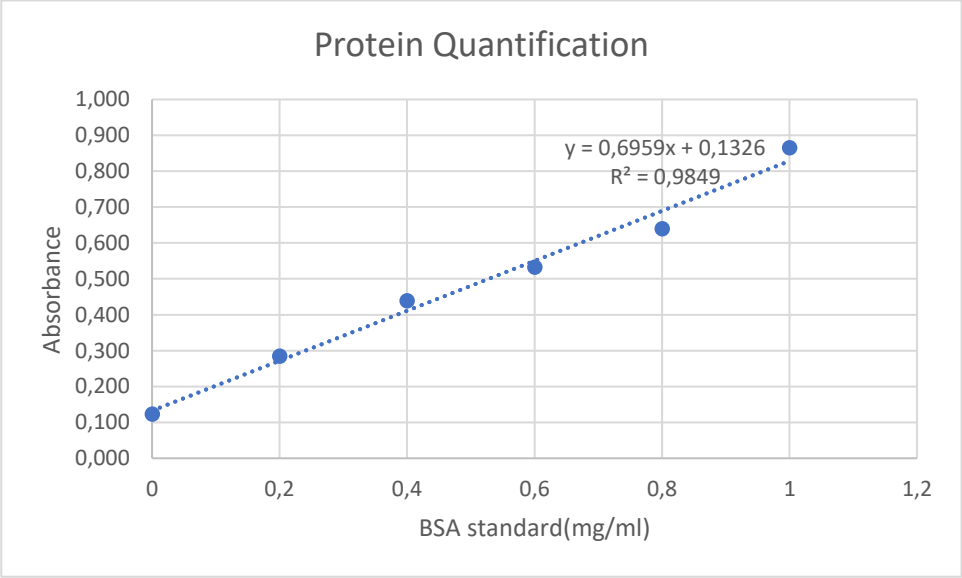

Figure A2: Standard calibration curve using a range of known bovine serum albumin concentrations for determination of sample protein concentrations using the bicinchoninic acid assay.

Table A5: Standardisation of protein using the standard calibration curve for Sodium dodecyl sulphate polyacrylamide gel electrophoresis.

	Average OD	Protein (mg/ml)	C2 (mg/ml)	V2 (µl)	V1 (µl)
Control	2.56	2.370	1.836	155	45
IC_{20}	2.32	2.128	1.836	172	28
IC_{50}	2.03	1.836	1.836	200	0

Appendix E

Table A6: Standardisation of RNA using the standard calibration curve generated by NanoDrop 2000.

	RNA (mg/ml)	C2 (mg/ml)	V2 (µl)	V1 (µl)
Control	2174.4	1055.9	5.1439	4.8560
IC_{20}	1055.9	1055.9	0	10
IC_{50}	3074.5	1055.9	6.5656	3.4343

Appendix F

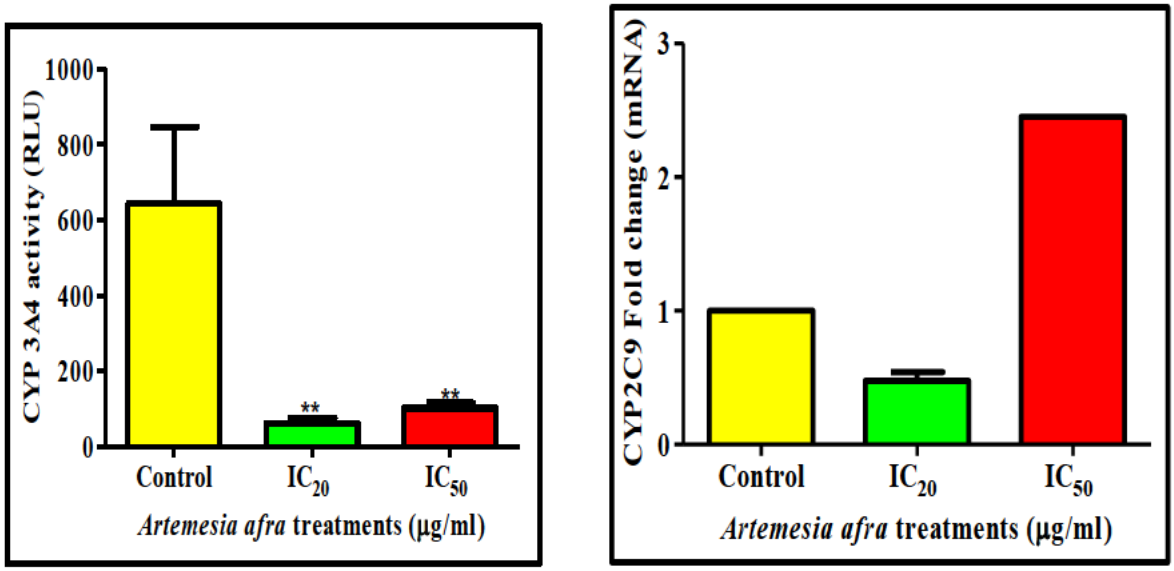

Figure A3: *A.afra* decreased CYP3A4 activity in Caco-2 cells in comparison to the control following 48h (p=0.040; p=0.0385). Gene expression of CYP2C9 activity (p=0.2255), [*Unpaired t-test with Welch`s correction; RLU: relative light units]. mRNA: messenger RNA.

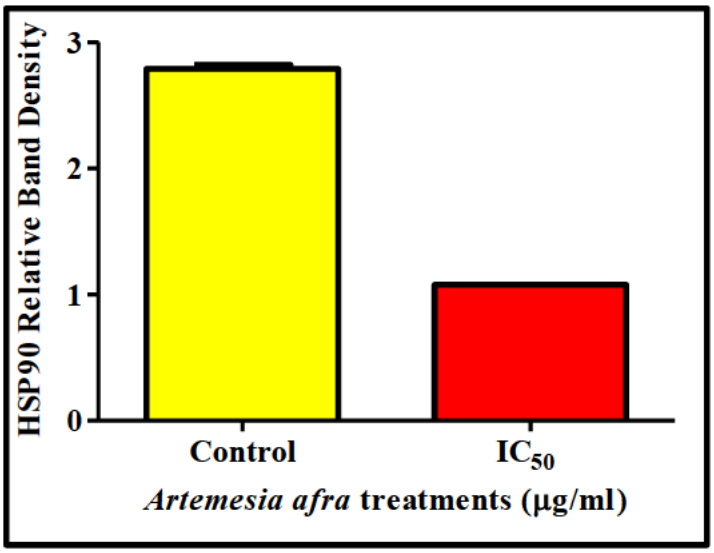

Figure A4: Exposure of *A.afra*-treated cells expression of proteins such as, HSP90 (p<0.0001) in Caco-2 cells after treatment for 48h, (One way ANOVA with Tukey's post-test).

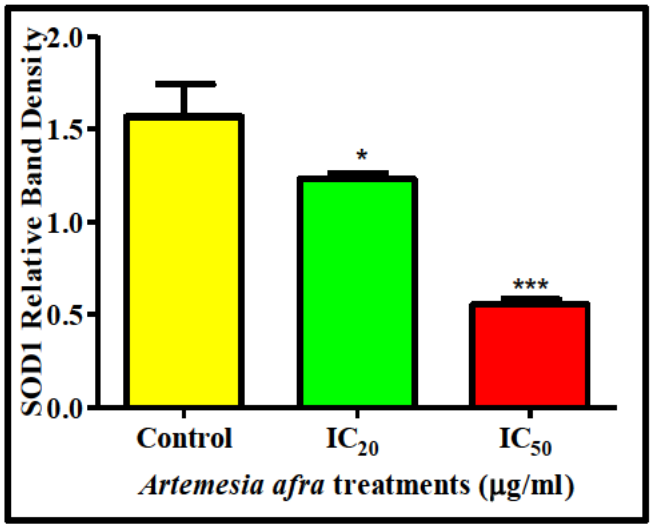

Figure A5: Treated cells of Caco-2 revealed downregulation of SOD1 (p<0.0001) protein expression after treatment for 48h, (One way ANOVA with Tukey's post-test).

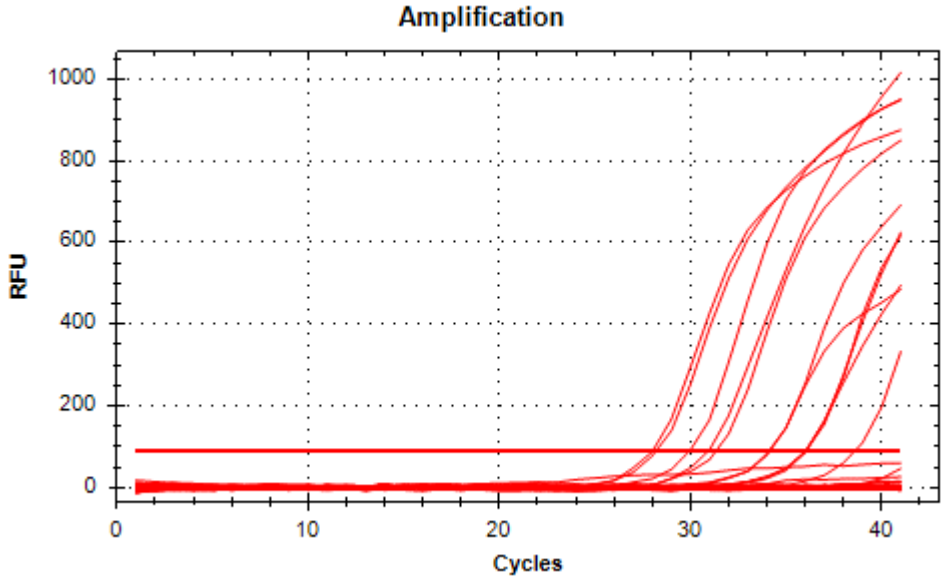

Figure A6: Melt Curve for TNF-α when *A.afra* was exposed to Caco-2 cells for 48h.

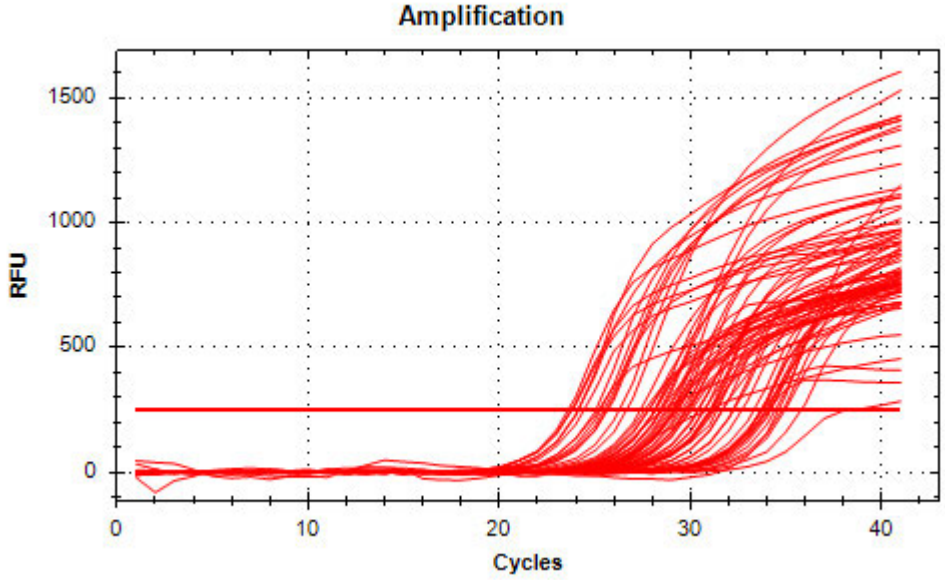

Figure A7: Melt curve for SOD2 and c-Myc when *A.afra* was exposed to Caco-2 cells for 48h.

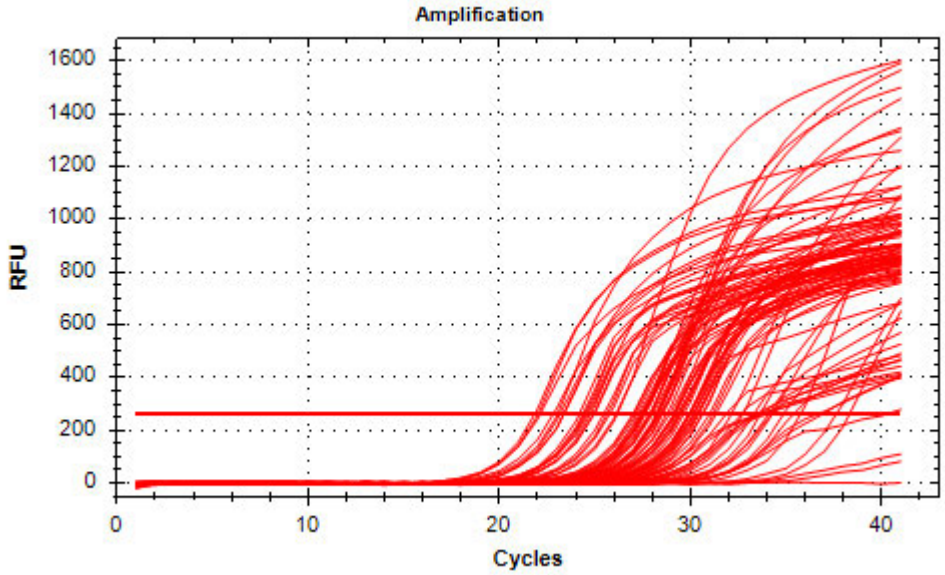

Figure A8: Melt Curve for GPx-1 and NF-κB when *A.afra* was exposed to Caco-2 cells for 48h.